



***High-Performance Advanced Methods and Experimental Investigations  
for the Safety Evaluation of Generic Small Modular Reactors***

***Research and Innovation Actions***

**Horizon 2020, Topic NFRP-2019-2020-05:  
Support for Safety Research of Small Modular Reactors**

2020 – Research and Innovation Framework Programme

Contract Number: 945063  
Start Date: 01/09/2020      Duration: 36 Months



This project has received funding from the Euratom research and training programme 20019-2020 under grant agreement No 945063.

---

**– Deliverable –**

***D3.4: State-of-the-art solutions for the transient scenarios in the four SMR cores***

---

---

**Summary**

This deliverable presents the results of the transient analysis in four SMR cores performed with the state-of-the-art nodal diffusion codes.

---

**Proprietary Rights Statement**

This document contains information which is proprietary to the McSAFER Consortium. Neither this document nor the information contained herein shall be used, duplicated or communicated by any means or any third party, in whole or in parts, except with the prior consent of the McSAFER Consortium.

**Disclaimer**

The content of this document reflects only the authors' views and the European Commission is not responsible for any use that may be made of the information it contains.

**McSAFER** – Contract Number: 945063

High-Performance Advanced Methods and Experimental Investigations for the Safety Evaluation of Generic Small Modular Reactors.




### Document Information

Document title	<b>State-of-the-art solutions for the transient scenarios in the four SMR cores</b>
Author(s)	<b>Emil Fridman (HZDR), Yurii Bilodid (HZDR), Maximiliano Dalinger (CNEA), Héctor Lestani (CNEA), Edmundo Lopasso (CNEA), Alexis Weir (CNEA), Rene Paz Zalazar (CNEA), Juan Antonio Blanco (KIT), Luigi Mercatali (KIT), Victor Sanchez (KIT), Anthime Farda (CEA), Ville Valtavirta (VTT), Ana Jambrina (VTT), AnnMarcus Seidl (PEL), David De Meyer (TLB), Radim Vocka (UJV), Havluj Frantisek (UJV)</b>
Number of pages	72
Document type	Deliverable
Work Package	WP3
Document number	D3.4
Issued by	
Date of completion	09/03/2022
Dissemination level	Public

### Document History

Rev.	Date	Comments & status	Author
0	28/02/2022	First complete draft	E. Fridman
1	09/03/2022	Final version	E. Fridman

### Document Approval

Rev.	Main author(s)	Verification	Approval
Name	Emil Fridman, HZDR	Ville Valtavirta, VTT	Victor Sanchez, KIT
Date	09/03/2022	10/03/2022	11/03/2022
Signatures			 Dr. V. Sánchez

**Distribution List**

<b>Name</b>	<b>Organisation</b>	<b>Comments</b>
Panagiotis MANOLATOS	EC DG RTD	

<b>Partner n°</b>	<b>Beneficiary short name</b>	<b>Type of beneficiary</b>	<b>Country</b>
1	KIT	University and research Centre	Germany
2	LUT	University	Finland
3	CEA	Research Centre	France
4	UJV	Private company	Czech Republic
5	HZDR	Research Centre	Germany
6	JACOBS	Private company	England
7	VTT	Research Centre	Finland
8	JRC	European Research Centre	EU
9	PEL	Utility	Germany
10	UPM	University	Spain
11	TRACTEBEL	Private company	Belgium
12	KTH	University	Sweden
13	CNEA	Research Centre	Argentina

Distribution to the partners will be through the project SharePoint.

## Table of contents

1.	Introduction .....	8
2.	CAREM .....	8
2.1.	Description of the transient scenarios.....	8
2.2.	Models (KIT) .....	10
2.3.	Models (CNEA).....	14
2.4.	Results.....	15
3.	SMART .....	22
3.1.	Description of the transient scenarios.....	22
3.2.	Models (KIT) .....	23
3.3.	Results.....	26
4.	F-SMR.....	33
4.1.	Description of the transient scenarios.....	33
4.1.1.	Initial conditions.....	33
4.1.2.	Sequence of events.....	34
4.2.	Models (CEA) .....	35
4.2.1.	Neutronics model .....	35
4.2.2.	Core thermal hydraulics model.....	36
4.2.3.	Coupling and transient calculation .....	37
4.3.	Results.....	37
5.	NuScale .....	43
5.1.	Description of the transient scenario .....	43
5.1.1.	NuScale core specifications .....	43
5.1.2.	Initial conditions for the transient.....	43
5.1.3.	Fuel rod thermal-physical properties .....	44
5.1.4.	Effective Doppler temperature for XS data.....	45
5.1.5.	Sequence of Events .....	45
5.2.	HZDR Models - Serpent/DYN3D .....	45
5.2.1.	Cross section library.....	45
5.2.2.	Nodal code modelling.....	45
5.3.	VTT Model - Serpent/ANTS.....	46
5.3.1.	Cross section library.....	46
5.3.2.	Nodal code modelling.....	46
5.4.	TBL Models - WIMS10/PANTHER .....	47
5.4.1.	Fuel & reflector model .....	47
5.4.2.	Fuel constituents .....	47
5.4.3.	Reflector constituents.....	47
5.4.4.	Core model.....	47
5.4.5.	Transient model.....	48
5.5.	PEL Models - CASMO5/SIMULATE5/S3K .....	48
5.5.1.	Cross section generation.....	48

5.5.2. Steady state calculations.....	48
5.5.3. Transient calculations.....	48
5.6. Models (UJV) .....	49
5.6.1. Cross section generation.....	49
5.6.2. Steady state calculations.....	49
5.6.3. Transient calculations.....	50
5.7. Results.....	51
6. Reference .....	55
Appendix A: Verification of PARCS-ICoCo vs. Serpent (CAREM) .....	57
Appendix B: Verification of PARCS-ICoCo vs. Serpent (SMART).....	63

## 1. Introduction

The objective of this deliverable is to summarize the state-of-the-art solutions for the transient scenarios in the four SMR cores, namely CAREM (Section 2), SMART (Section 3), F-SMR (Section 4), and NuScale (Section 5). These solutions are based on nodal diffusion codes with pin-power reconstruction capability. The presented results will serve as a reference for comparison against advanced deterministic and high-fidelity Monte Carlo based solutions.

The four reactor core designs and proposed transient scenarios are presented in the deliverable D3.1 [1]. The cross section generation methodologies, employed for the state-of-the-art transient analysis, are discussed in D3.2 [2].

## 2. CAREM

### 2.1. Description of the transient scenarios

A detailed description of the CAREM-like reactor core and the transient specifications can be found in Deliverable 3.1 [1] of this project and its addendum (which can be found at the SharePoint server of the project). A shorter description will be given here.

The CAREM-like reactor is a 32 MWe SMR, self-pressurized, natural-convection cooled light water reactor. Its global parameters are summarized in Table 1. The CRDM (Control Rod Drive Mechanisms) are inside the RPV (Reactor Pressure Vessel) avoiding the possibility of a rod ejection accident. However, provided its highly negative moderator coefficients of reactivity, any transient involving an increase in density or a decrease in temperature of the coolant are of special interest. The CAREM-like reactor core is depicted in Figure 1.

Table 1: Reactor core global parameters.

Parameter	Nominal Value
Core power	100 MWth
System pressure (core outlet)	12.25 MPa
Core flow rate	410 kg/s
Core coolant inlet temperature	~557.15 K

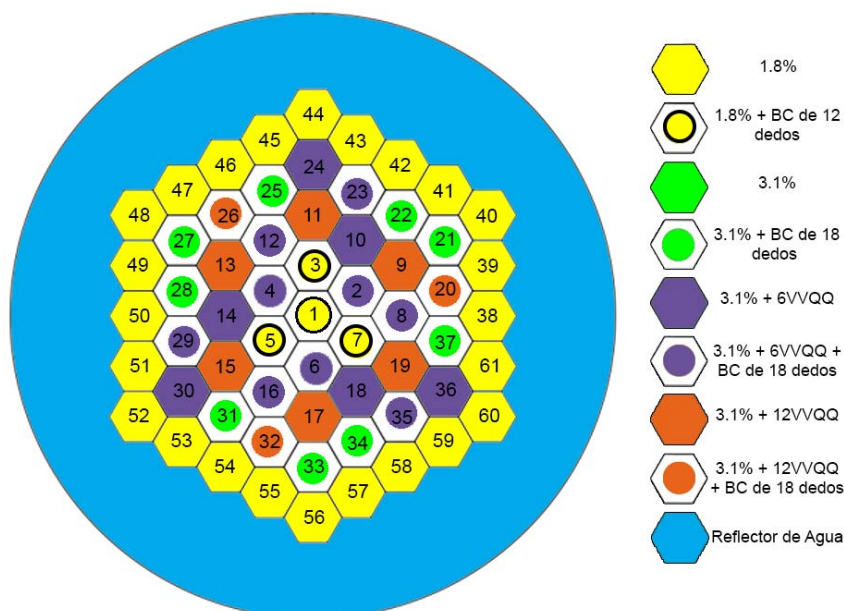


Figure 1: CAREM-like reactor core.



The transient studied here can be described as an overcooling. It consists of a cold front of coolant entering the core and producing an initial rise in power due to the positive reactivity associated with a colder and higher density coolant. The origin of this overcooling is on the secondary side and is beyond the scope of this analysis, but the physics of the secondary side is reflected on the varying border conditions imposed to the core. The border conditions are depicted in Figure 2 for the coolant inlet temperature, Figure 3 for the coolant inlet flow, and Figure 4 for the outlet pressure. The duration of the transient is 50 seconds, and variations on the border conditions begin at 2 s.

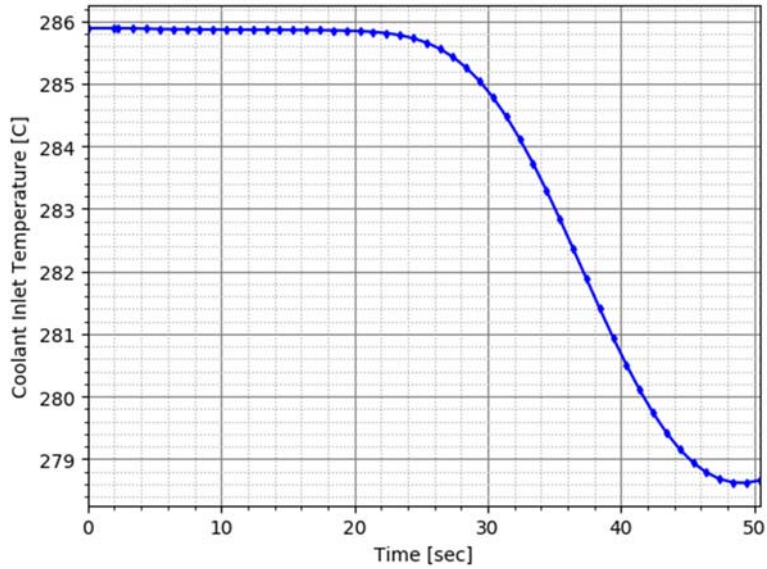


Figure 2: Border condition - Coolant inlet temperature.

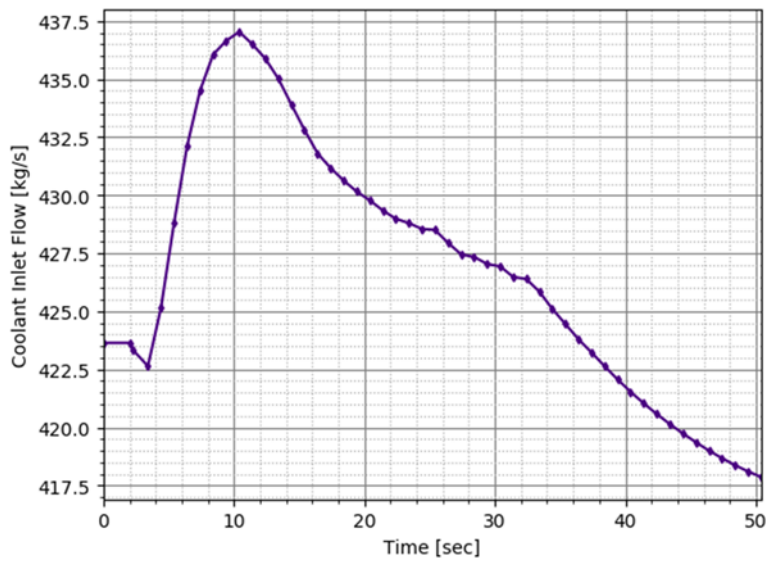


Figure 3: Border condition - Coolant inlet flow.

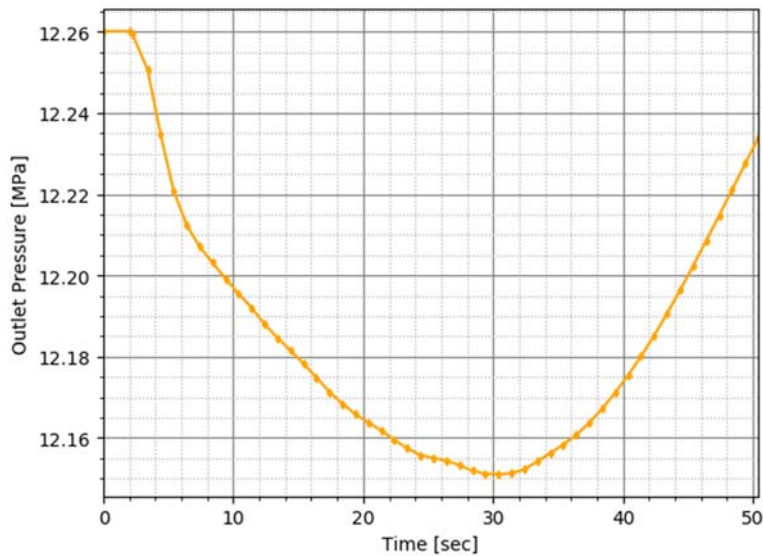


Figure 4: Border condition - Outlet pressure.

Control rod positions are fixed during the entire transient, with the bank 2 at 85.7% (1.2 m of 1.4 m inserted), the bank 9 at 67.85% (0.95 m out of 1.4 m inserted), and the central control rod is at 50%. All the other control rods are extracted. The fuels are fresh, with Xenon at equilibrium concentration.

## 2.2. Models (KIT)

The methodology employed for the CAREM-like core calculations can be observed in Figure 5. As explained in Deliverable 3.2 [2] the lattice code used for cross sections (XS) generation was SERPENT v2.1.32 [3] with JEFF3.1 nuclear data library. The output files generated by it were processed with GenPMAXS v6.2<sup>1</sup> [4] to create the PMAXS files required for the nodal code. These files were input for the nodal neutronics code PARCS v3.3.1 [5] which was coupled at KIT to the thermal hydraulics code SUBCHANFLOW v3.7.1 [6] using the CEA's ICoCo C++ API [7]. We will refer to this coupling as PARCS-SCF<sup>2</sup> which was implemented at KIT by M. Garcia.

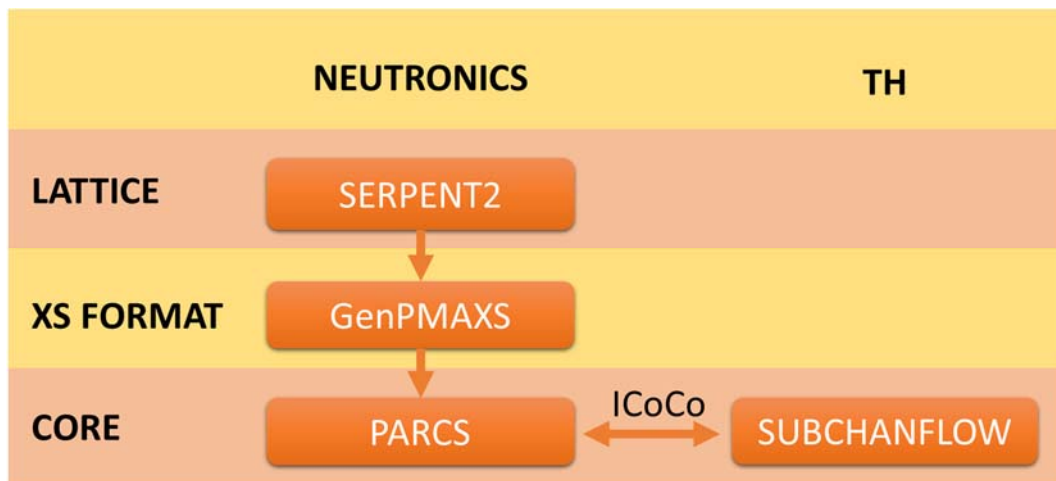


Figure 5: SERPENT2-PARCS-SCF core calculation chain

Using the lattice codes the explicit hexagonal fuel assemblies' geometry was modeled in a 2D infinite lattice with reflective Boundary Conditions (BCs). Each Fuel Assembly (FA) set of XS was condensed and homogenized using SERPENT2 capabilities. The branch structure can be observed

<sup>1</sup> Some small modifications or external scripting have been done for correct reading of DFs and CDFs. So, it will be referred to as GenPMAXS-KIT.

<sup>2</sup> PARCS v3.3.1 neutronics stand-alone calculations were also performed with the ICoCo interface for extracting fields variables. Even though its behavior is not modified it will be referred to as PARCS-ICoCo.

in Table 2. As pointed out by VTT in D3.2, the Discontinuity Factors (DFs) provided by SERPENT2 can be used when there are net-zero boundary conditions. In addition, microscopic cross sections for Xenon calculations were generated by SERPENT2 using the *set poi* card at each TH state.

*Table 2: Thermal-hydraulic states for XS branches*

<b>State</b>	<b>Fuel Temperature [K]</b>	<b>Coolant Temperature [K]</b>	<b>Coolant Density [kg/m<sup>3</sup>]</b>
<b>Nominal</b>	921	578.15	0.702
<b>FT+279.00</b>	1200	578.15	0.702
<b>FT-271.00</b>	650	578.15	0.702
<b>CT+21.85</b>	921	600.0	0.702
<b>CT-28.15</b>	921	550.0	0.702
<b>CD+98.00</b>	921	578.15	0.800
<b>CD+48.00</b>	921	578.15	0.750
<b>CD-52.00</b>	921	578.15	0.650
<b>CD-152.00</b>	921	578.15	0.550
<b>CD-252.00</b>	921	578.15	0.450
<b>CD-352.00</b>	921	578.15	0.350

In CAREM-like FAs there is a small asymmetry introduced by the instrumentation tube which would make periodic BCs a better choice. However, XS were generated for a test case with both type of BCs and differences at nodal level were non-detectable for this case. When using periodic BCs, the DFs are not correctly calculated (volume-averaged flux used for homogenous flux) but, as explained before, the asymmetry is small.

As shown by other partners in D3.2 [2], especially VTT, the number of condensed groups, leakage models, discontinuity factors, reflectors models, transport correction for reflector water, among others, can affect the results. A similar study is provided in Appendix A for neutronics stand-alone comparison against SERPENT2 full core calculations.

The axial reflector cross sections were calculated by modelling a 3D Fuel Assembly with radially reflective and axially vacuum boundary conditions.

The radial reflector cross sections were generated in a 2D full core model as shown in Figure 6. Each neighboring reflector was condensed and homogenized independently. This way, the cross sections can be calculated with a more accurate spectrum including local perturbations. The discontinuity factors for the radial reflector elements were obtained from SERPENT2. The latter produced the DFs based on the homogenous solution based in AFEN [8] (Analytic Function Expansion Nodal). This is not compatible with the core nodal code which uses TPEN [8] (Triangle-based Polynomial Expansion Nodal). Its effect was analyzed in Appendix A. The DFs between reflectors nodes was set to unity. Due to the absence of its capability in GenPMAXS, the CDFs were also obtained directly from SERPENT2, which uses an AFEN based homogeneous solution as well. For TPEN method the CDFs can improve the solution, unfortunately it also introduced instabilities and we were not able to obtain a converged solution, so they were excluded from this study.

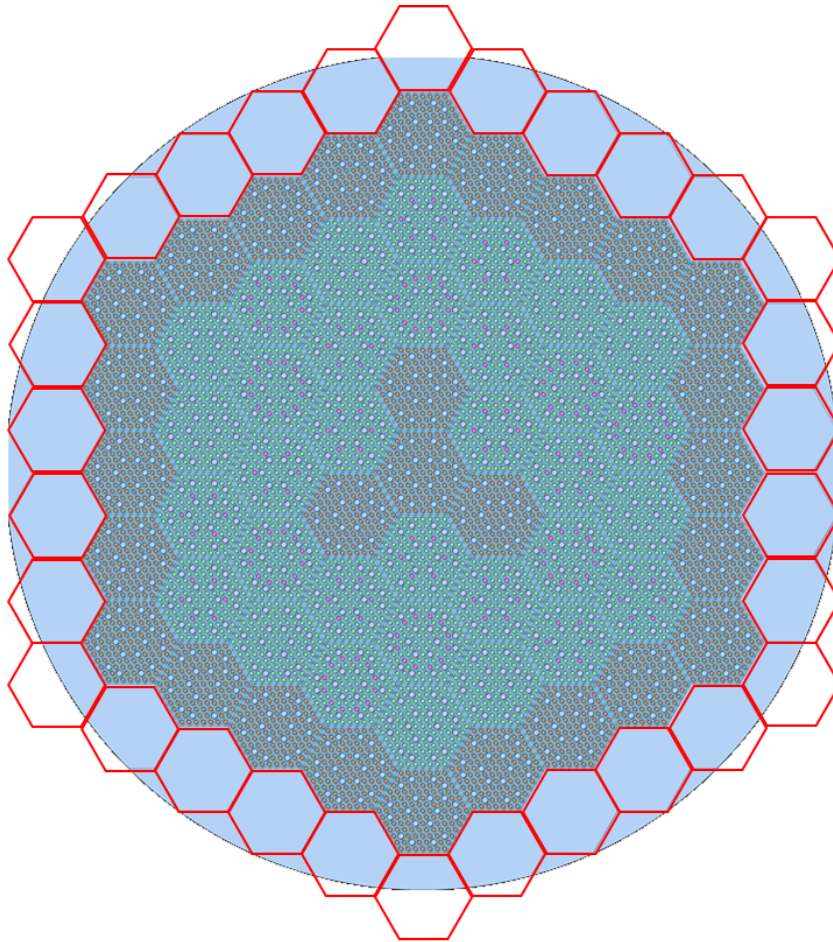


*Figure 6: SERPENT2 2D radial reflector model. Red hexagons surround each of the reflector elements for XS generation and DFs calculation.*

For this deliverable, the leakage correction used for fuel assemblies was a fundamental mode using CMM (Cumulative Migration Method) diffusion coefficient. Transport correction for hydrogen in reflector water was used as explained in Section 3.2. Discontinuity factors generated by SERPENT2 were used as well. The energy discretization consisted in a classic 2 group scheme. In a future, the analysis Appendix A could help to improve the solution.

The core neutronic was modeled radially with 1 node per FA or reflector element (it indirectly contains subnodes due to the TPEN method used which subdivides the hexagons in 6 triangles) and axially with a discretization of 36 elements: 28 for the active height, 4 for the bottom reflector and 4 for the upper reflector. In SCF only the active height was modeled with the same radial and axial discretization as the neutronic model. Each FA was modeled as a single channel with a representative rod for thermal behavior as can be observed in Figure 7. The correlations used are shown in Table 3.

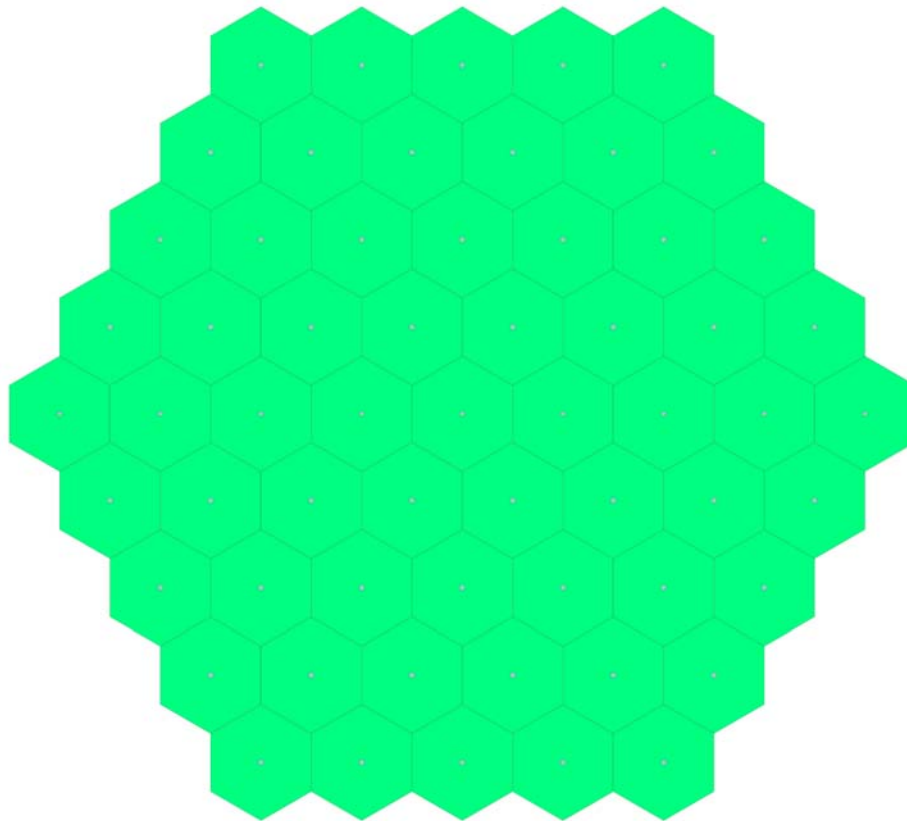


Figure 7: SCF 3D model. Each FA is considered as one channel with a representative rod for TH calculations

Table 3: SUBCHANFLOW correlations used in the model.

Correlation	Option selected
Turbulent friction	Blasius
Heat transfer	Dittus Boelter
CHF	Westinghouse-3

The core calculations were done with the aforementioned PARCS-SCF ICoCo coupling. The main advantage of the coupling with ICoCo is that it does not interfere with the syntax of the codes, i.e. inputs have to be made for PARCS and SCF as usual. A MED mesh (a type of mesh available in SALOME [9]) is generated using a MED pre-processor, implemented by M. Garcia [10], for the codes to store the variables fields, and, via ICoCo routines, both codes communicate using *get* and *set* functions for fields and time step definition. It is also in charge of the steady-state or transient coupling strategy. The transient calculations were performed with an explicit time scheme between neutronics and TH with a time step of 0.01 s without relaxation factors applied during the fields' exchange.

### Acknowledgements

The cross sections generations ran for this KIT work for all branches and reflectors requires multiple runs of computationally expensive Monte Carlo simulations.

This work was performed on the HoreKa supercomputer funded by the Ministry of Science, Research and the Arts Baden-Württemberg and by the Federal Ministry of Education and Research.

In addition, part of the post processing has been performed with the aid of *serpent-tools* [11].

### 2.3. Models (CNEA)

A model for the CAREM-like reactor core was developed for PUMA v6.0.11 [12] coupled with SUBCHANFLOW v3.1. PUMA is the CNEA neutronic deterministic core-code, which solves the neutron transport equation with neutron diffusion approximation by the finite difference method, in 3-D geometries.

The XS were generated with HUEMUL v4.3.2 [13] deterministic cell-code and the results were presented in deliverable D3.2. In order to have a proper core neutronic model in PUMA, cell models which consider the presence of spacer grids and control rods distribution were also generated with HUEMUL, as well as for the axial and radial reflectors, in addition to those generated for deliverable D3.2. Cell parameters were condensed to 5 groups, and calculated with the JEFF-3.1 nuclear data library. In addition, branch calculations were made with variations of fuel temperature, coolant temperature and coolant density, in order to properly represent the variation of these parameters during the transient, as is shown in Table 2. All these XS considered the presence of Xenon in equilibrium condition. For the radial water reflector, a radial 2-D model was developed, considering a homogeneous core mix surrounded by water, and extracting the XS only from this zone. For the axial water reflectors, a slab 1-D model was developed, using the same homogeneous core mix, surrounded axially by water at different densities and temperatures, in order to consider the change in water properties before and after crossing the core.

The CAREM-like neutronic core model developed in PUMA is presented in Figure 8. Triangular geometry was used, represented with fine lines in the figure. Every fuel channel was composed of 6 triangles, represented with thick lines. The core was surrounded by a water radial reflector, which was also surrounded by void. The core has an axial discretization of 5 cm with a total of 28 axial zones, the water axial reflectors have a length of 20 cm each with 4 axial zones of 5 cm each. With this discretization, spacer grids are located in axial zones 1, 11 and 21 (from bottom to top, counting only the active zone). The positions of control rods are bank #1 in 14, bank #2 in 24, and bank #9 in 19.

The model developed in SUBCHANFLOW consisted of 61 hexagonal channels, one for each fuel assembly, and without reflectors. The axial and radial discretization was the same used in PUMA. Generic values were considered for materials parameters and conductivities. As both models have the same discretization, no interpolation is required to map parameters between codes. Border condition profiles are calculated by SUBCHANFLOW. Correlations used in the model are depicted in Table 4.

The coupling of PUMA and SUBCHANFLOW, referred to as PUMA-SCF, is performed through their respective PYTHON interfaces, implemented at CNEA by M. Dalinger and M. Garcia [14] respectively. For the initial state, the converged state is reached through an iterative scheme. The convergence criteria between two successive iterations for power, fuel temperature, coolant temperature and density, is set to 1% for each parameter, and to 1e-4 for the effective multiplication factor. A relaxation factor of  $w=0.7$  is considered for thermo-hydraulic parameters.

For transient calculations, an explicit scheme is used. PUMA calculates and advances in time first, sends power distribution to the previous step in SUBCHANFLOW, the thermo-hydraulic code advances the same time step and sends the thermo-hydraulic distributions to PUMA, and so on. No relaxation factor is considered during transient calculations. A time step of 0.01 sec was used for the transient simulation.

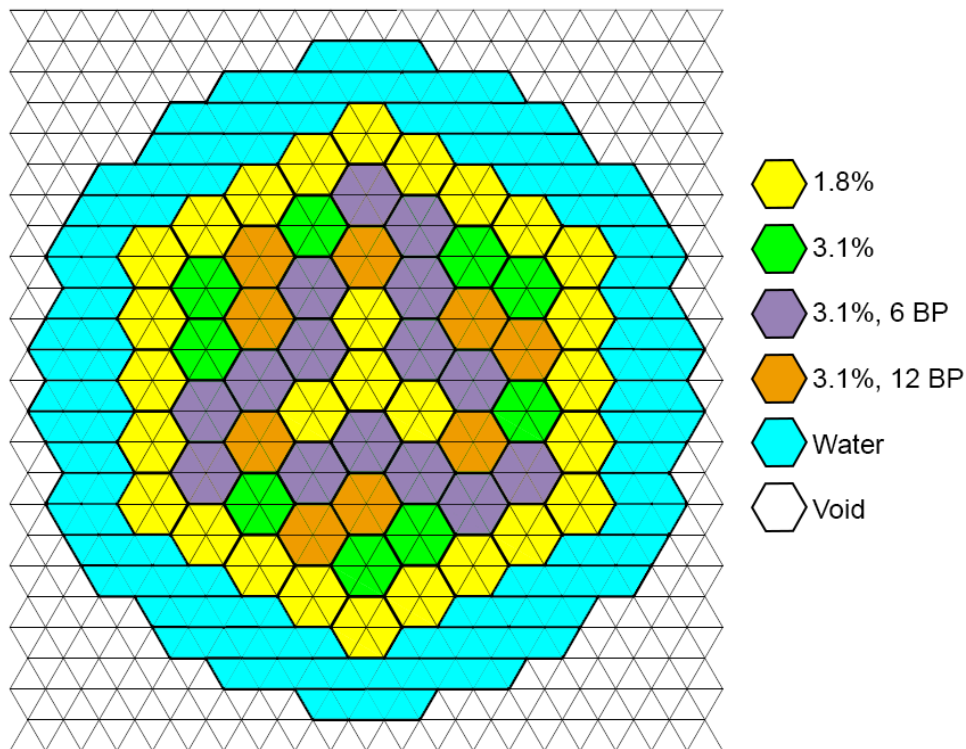


Figure 8: CAREM-like core model developed in PUMA.

Table 4: SUBCHANFLOW correlations used in the model.

Correlation	Option selected
Subcooled void	Bowring
Boiling void	Armand modified
Two phase friction	Armand
Turbulent friction	Blasius
Heat transfer	Dittus Boelter
CHF	Westinghouse-3
Shape CHF	Uniform

## 2.4. Results

Results from both CAREM-like models (CNEA and KIT) have been obtained and compared. As a first step stationary results for All Rods Out (ARO) and All Rods In (ARI) configurations, and rod worth, were obtained without thermal hydraulic coupling for Hot Full Power (HFP), Cold Zero Power (CZP) and Hot Zero Power (HZP). Table 5 summarizes these results. A maximum discrepancy of 14.6% is observed overall and corresponds to a ARI in CZP, while the maximum discrepancy for unroded states is 7.7%.

Table 5: Comparison of reactivity at the state before the transient, without thermal hydraulic coupling.

Results coupling	without TH-	Reactivity [pcm]			
		PARCS-ICoCo	PUMA	Difference	Relative Difference
HFP	ARO	5513	5117	396	7.7%
	ARI	-20241	-20685	444	2.1%
	Rod Worth	25754	25802	-48	-0.18%
CZP	ARO	14148	13883	265	1.9%
	ARI	-4130	-4836	706	14.6%
	Rod Worth	18278	18719	-441	-2.4%
HZP	ARO	10513	10137	376	3.7%
	ARI	-12620	-13304	684	5.1%
	Rod Worth	23133	23442	-309	-1.3%

Results for calculations with thermal hydraulic coupling at HFP are summarized in Table 6. A maximum discrepancy of 11.8% is obtained overall and corresponds to the ARO configuration. For the “critical state”, i.e., the excess reactivity with the rods fixed at the specified position, a 61.8% discrepancy is found, which amounts to 57% of the delayed neutrons fraction. For the Power Peaking Factor and the DNBR, shown in Table 7, discrepancies of -5.9% and 7.6% were found, respectively.

Table 6: Comparison of reactivity at the state before the transient, with thermal hydraulic coupling.

Results with TH-coupling		Reactivity [pcm]			
		PARCS-SCF	PUMA-SCF	Difference	Relative Difference
HFP	ARO	4566	4084	482	11.8%
	ARI	-20322	-21405	1083	5.06%
	Rod Worth	24888	25489	-601	-2.4%
	Critic	-233	-611	378	61.8%

Table 7: Values at the state before the transient.

	PARCS-SCF	PUMA-SCF	Difference	Relative Difference
Power Peaking Factor	2.391	2.543	-0.152	-5.9%
DNBR	1.972	1.832	0.140	7.6%

The results for the transient state were calculated with thermal hydraulic coupling and with the mentioned fixed rod positions. The total core power is shown in Figure 9 and a very good agreement can be seen, with a maximum relative discrepancy of 0.39% which is negligible and a closer look will be taken by comparing power distributions.

The fuel core-averaged and space-maximum (peak value) temperatures are shown in Figure 10 and Figure 11, respectively. The agreement is also very good and the time evolution has a very similar behavior, with 3.2 and 10.3°C of maximum discrepancies representing 0.66% and 1.48%,



respectively. Some more discussion regarding these temperatures will be done analyzing the power distributions.

The cladding core-averaged and space-maximum (peak value) temperatures are shown in Figure 12 and Figure 13. Again, a very good agreement can be seen with maximum discrepancies of less than 1°C.

The coolant space-maximum (peak value) temperature can be seen in Figure 15 in which an almost perfect agreement can be observed. This is due to the fact that the coolant is saturated and the maximum temperature is only a function of pressure, independent of the power and its distribution. The coolant core-averaged temperature, however, does depend on the core power, its distribution and the void fraction generated, and is shown in Figure 14. The agreement between the results is very good and has a maximum discrepancy of 0.2°C which corresponds to 0.07%.

The coolant core-averaged and space-maximum (peak value) void fractions are shown in Figure 16 and Figure 17. The transient behavior of these quantities shows very good agreement in shape, but bigger discrepancies than for the previous quantities are observed, reaching 6.7% and 6.9%, respectively. These values are highly dependent on the power distribution and that could be one explanation for the discrepancies. However, a reason different than power distribution seems to be also present and seems to indicate that results could be easily approached to each other. This idea is based in the fact that some inconsistency can be seen between Figure 14 and Figure 16. The former indicates that KIT results for coolant average temperature are systematically below CNEA results. The latter indicates that KIT average void fraction is also systematically below CNEA results, but should be systematically above to account for energy balance. This discrepancy led us to find a yet unresolved discussion about the interpretation of void fraction axial discretization. We expect to solve this issue as soon as possible.

The DNBR evolution during the transient is shown in Figure 18. A very good agreement in the shape can be seen, however the same considerations as to the void fraction can be applied.

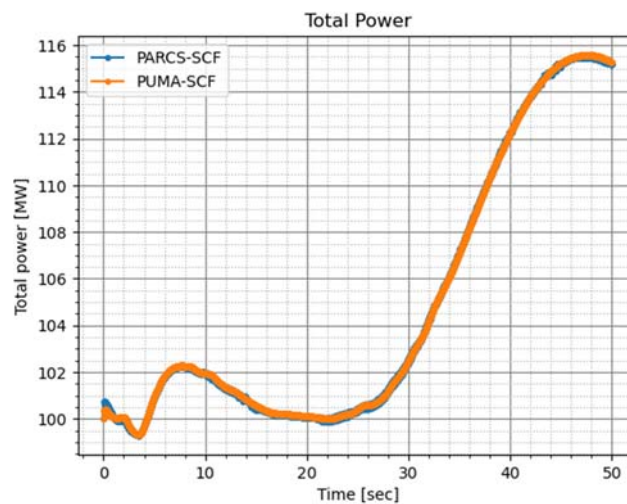


Figure 9: Total power during transient simulation.

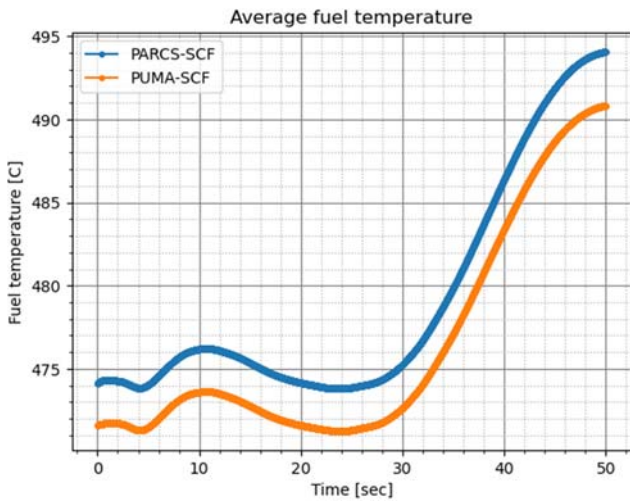


Figure 10: Average fuel temperature during transient simulation.

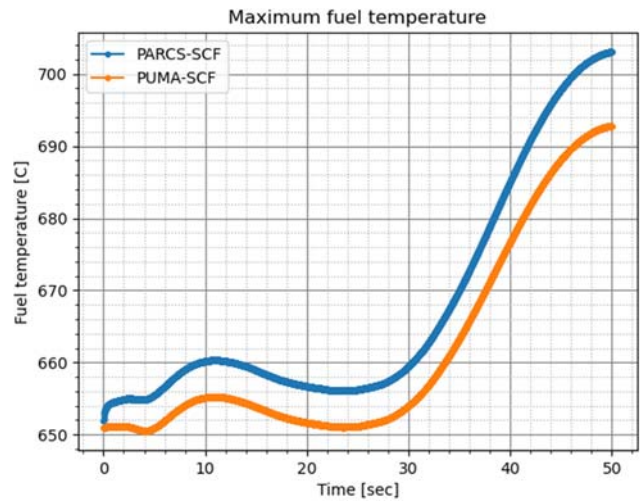


Figure 11: Maximum fuel temperature during transient simulation.

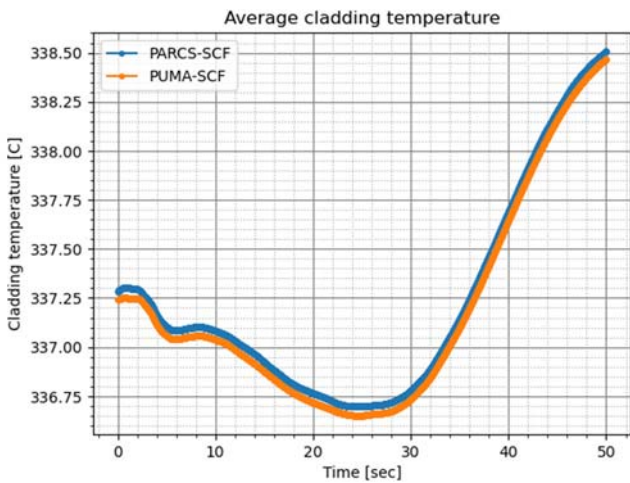


Figure 12: Average cladding temperature during transient simulation.

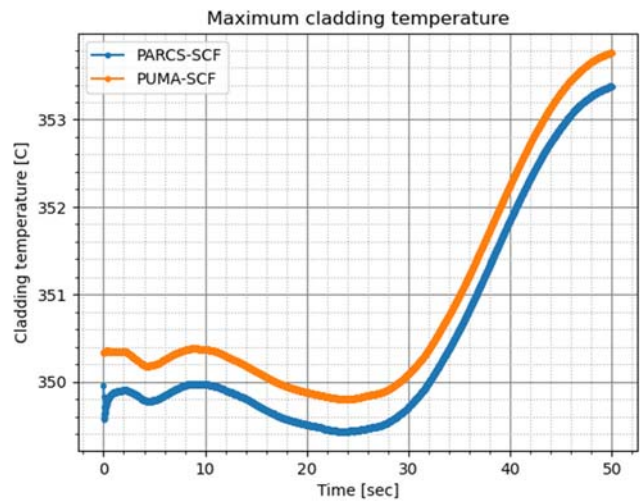


Figure 13: Maximum cladding temperature during transient simulation.

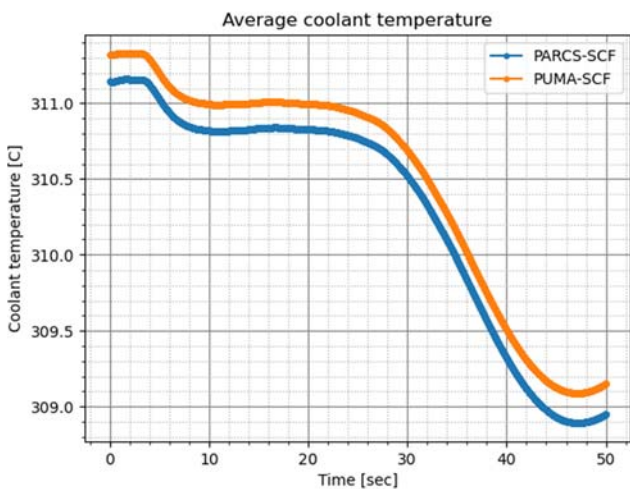


Figure 14: Average coolant temperature during transient simulation.

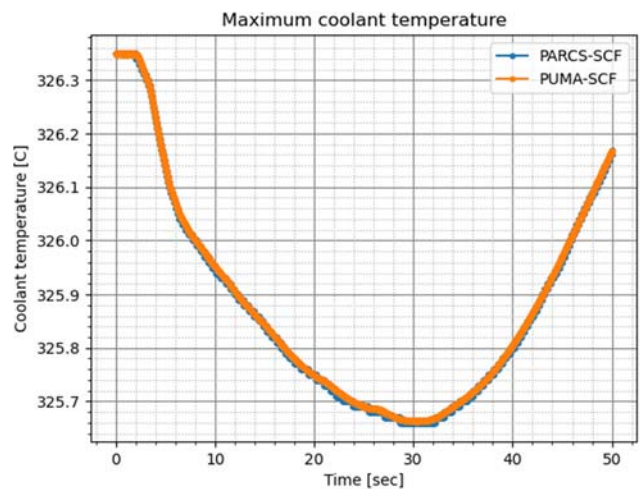


Figure 15: Maximum coolant temperature during transient simulation.

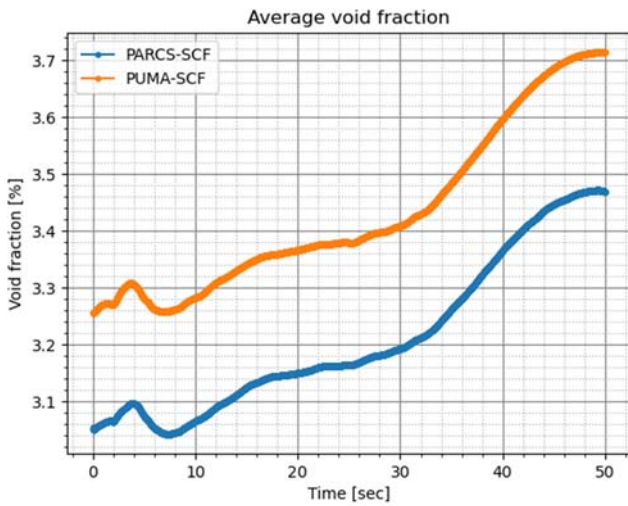


Figure 16: Average void fraction during transient simulation.

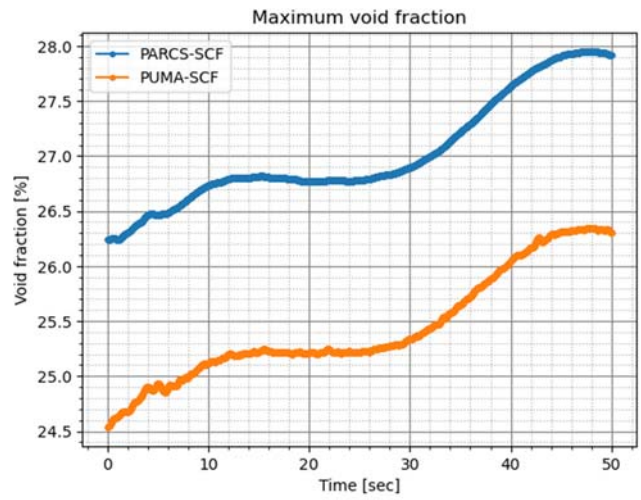


Figure 17: Maximum void fraction during transient simulation.

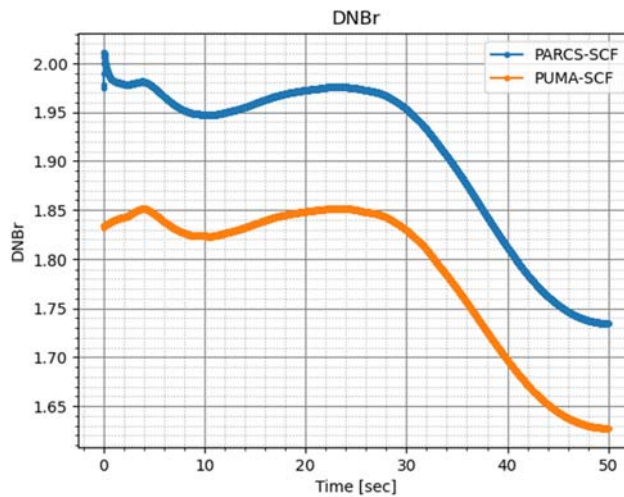


Figure 18: DNBr evolution during transient calculations

The comparison of the power profiles in a few selected fuel channels in the stationary state and the total power profile, previous the transient, is shown in Figure 19. These channels are organized from the center to a corner of the core, as shown in Figure 1. The channel #4 presents the higher local discrepancy between the two models. However even this channel shows a very good agreement in the profile. These small discrepancies together with the non-linearity of the fuel temperature are the reason for the discrepancies in fuel temperatures, considering that the same global power distributed differently gives a different average fuel temperature.

Accordingly, the profiles for fuel, cladding and coolant temperatures shown in Figure 20, Figure 21 and Figure 22, respectively, show a really good agreement.

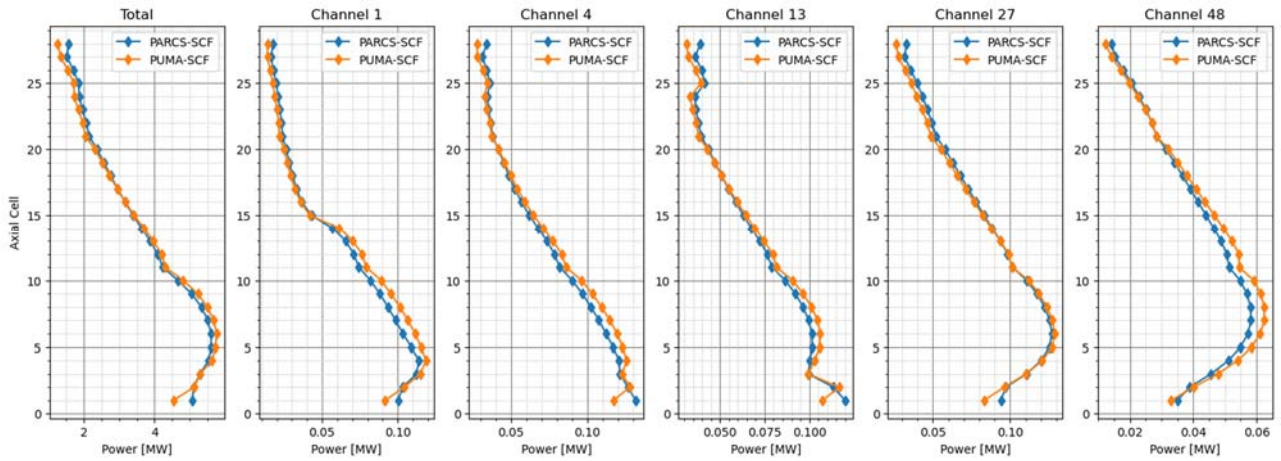


Figure 19: Power distributions calculated in PARCS-SCF and PUMA-SCF. State before the transient.

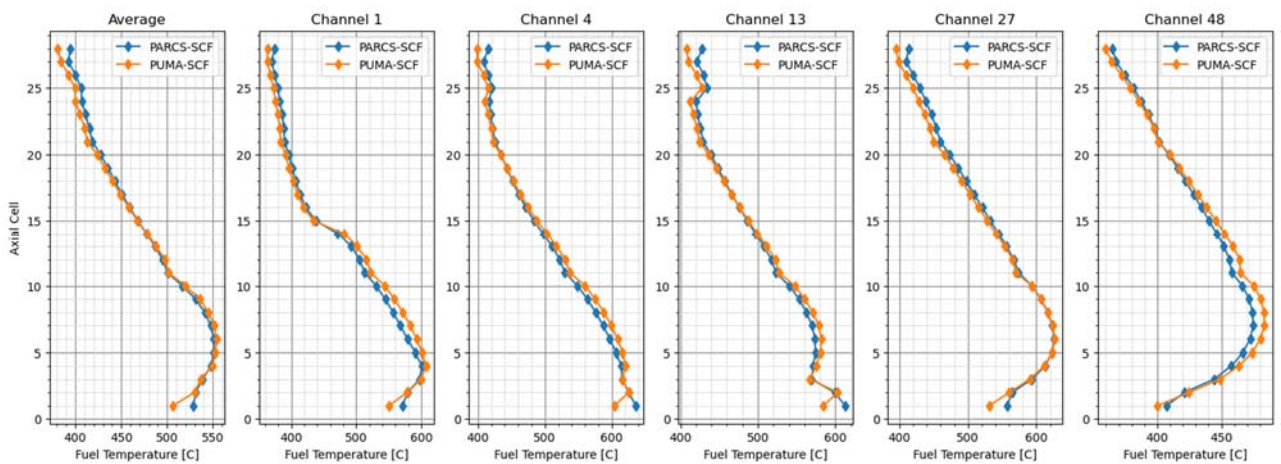


Figure 20: Fuel temperature distributions calculated in PARCS-SCF and PUMA-SCF. State before the transient.

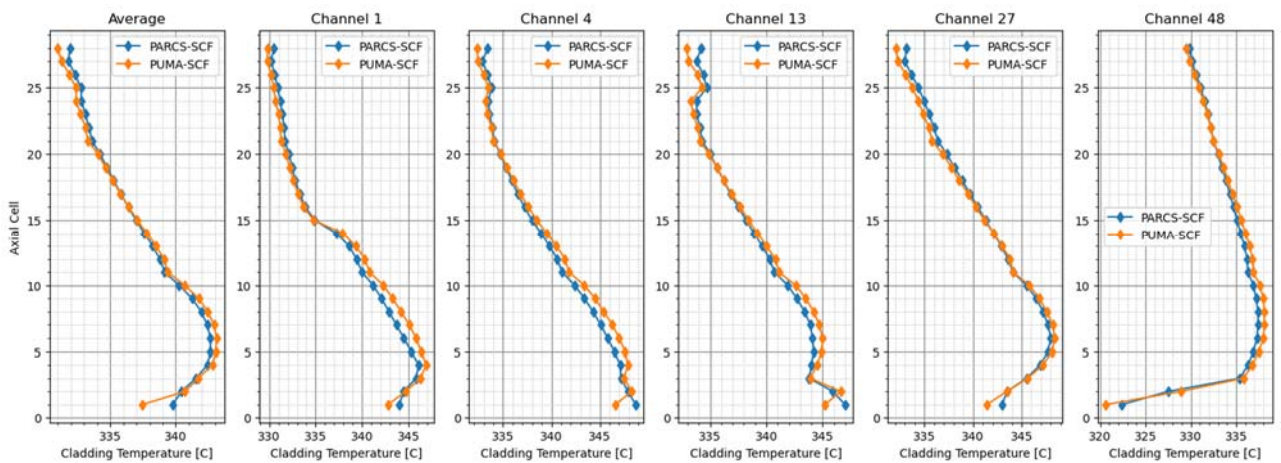


Figure 21: Cladding temperature distributions calculated in PARCS-SCF and PUMA-SCF. State before the transient.

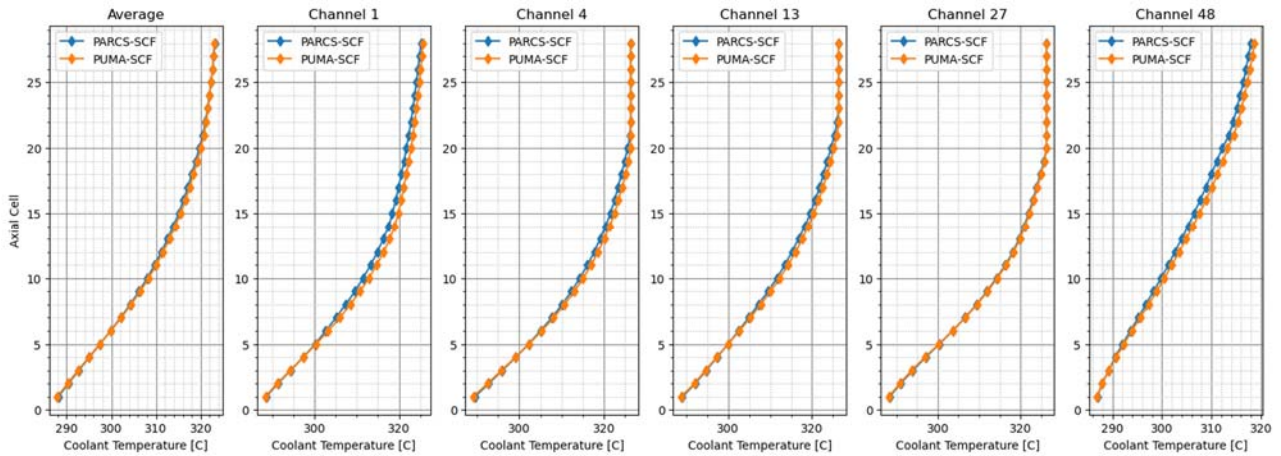


Figure 22: Coolant temperature distributions calculated in PARCS-SCF and PUMA-SCF. State before the transient.

The void fraction profiles are shown in Figure 23. In this figure the different interpretation in axial discretization is confirmed, and can be observed in a sudden jump at the end of the channel (position 28) that is present in all the channels. As said before, this issue will be studied as soon as possible and the reason for the discrepancies is expected to disappear giving closer results for the two models.

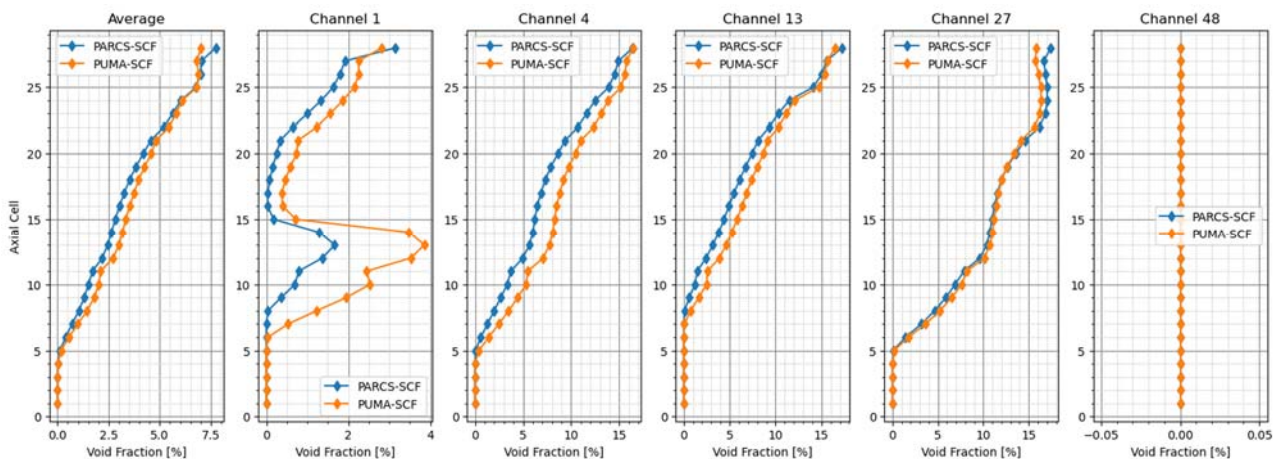


Figure 23: Void fraction distributions calculated in PARCS-SCF and PUMA-SCF. State before the transient.

### 3. SMART

In Task 3.2 of the MCSAFER proposal [15] calculation of transient scenarios for SMRs have to be provided using traditional nodal diffusion coupled to thermal hydraulics. This section corresponds to such studies for the SMART concept at KIT.

The SMART core concept developed at KIT (KSMR) [1,16,17] has 57 Fuel Assemblies (FAs) formed by 6 types of assemblies with different enrichments and burnable poison concentrations. In addition, it counts with 6 types of control rods. In an effort to control the flux shape in this boron free design, both, the FAs and the control rods, have axial profiles, i.e., their compositions are heterogeneous in the axial direction. This way, a radially and axially highly heterogeneous core is obtained, being a challenge to standard state-of-the-art nodal codes. The KSMR core description can be found in D3.1 [1].

#### 3.1. Description of the transient scenarios

The transient scenario consists in a Rod Ejection Accident (REA) [1,18]. As explained in D3.1, this could be caused by a mechanical failure of the CRDM (Control Rod Drive Mechanism). In safety analysis, the case studied is when the rod with the highest worth is ejected. In particular, this is studied at Hot Zero Power (HZIP) conditions where, in typical PWRs, the excess reactivity is controlled by control rods insertion.

The initial core configuration is shown in Figure 24. In this arrangement, all the boron carbide (B<sub>4</sub>C) control rods are fully extracted whereas the rest are fully inserted. The initial conditions are summarized in Table 8 (from D3.1 [1]). This configuration is not critical but, under these conditions, the most reactive control rod to be ejected (Figure 24) is worth approximately 1.48\$. Thus, enabling the possibility of studying a super-prompt critical transient with an asymmetrical power distribution.

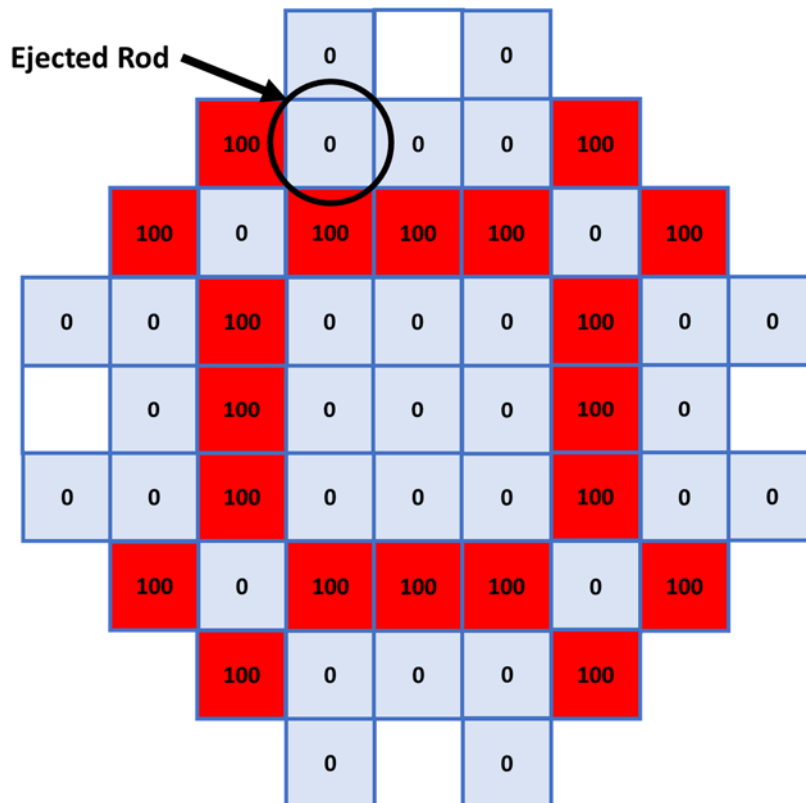


Figure 24 REA initial CRs configuration and ejected CR position at HZIP condition.

(Note: “100” means CR is fully extracted and “0” means CR is fully inserted. “White-boxes” mean there is no CR at that position) Based on D3.1 [1].

Table 8 Transient condition for Rod Ejection Accident at Hot Zero Power

Parameters	Value
Initial core power (% of nominal power)	1.0E-4
Highest CR worth (pcm) [\$]	1014 [1.48] <sup>3</sup>
Ejection duration (s)	0.05
End of transient simulation (s)	3.0
Fuel irradiation status	BOL

To summarize, the core configuration from Figure 24 is initially at HZP conditions with an initial power of  $10^{-4}$  % of the nominal power with an inlet mass flow rate of 2006.4 kg/s at 296°C and an exit pressure of 15 MPa [1,16]. From this point, the control rod is ejected at a constant velocity in 0.05 s [1,16].

### 3.2. Models (KIT)

The methodology employed for modelling the SMART KSMR concept has been described in D3.2 [2]. Due to some modifications, a brief description is given here of the modelling along with the calculation chain used. The scheme used can be observed in Figure 25 where SERPENT v2.1.29 and v2.1.32 [3] was the lattice code used for XS generation, the output files were adapted by GenPMAXS v6.2<sup>4</sup> and v6.3 [4,19] to the PMAXS format later used by PARCS v3.3.1 [5] for core nodal neutronics. Moreover, PARCS was coupled at KIT by M. Garcia with SUBCHANFLOW v3.7.1 [6] KIT’s code for subchannel thermal-hydraulics. This coupling was done using the CEA’s ICoCo C++ API [7]. We will refer to this coupling as PARCS-SCF<sup>5</sup>.

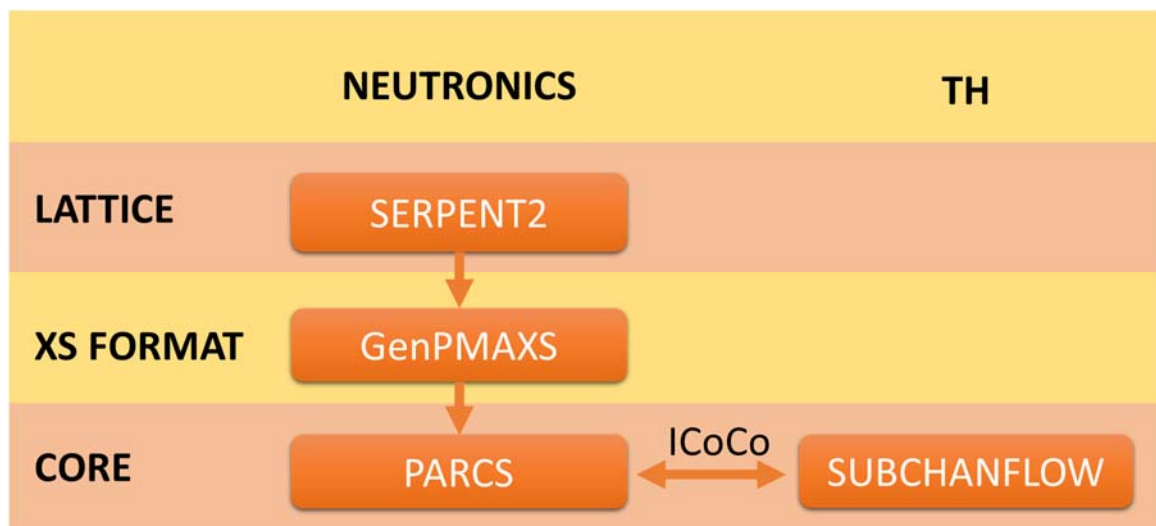


Figure 25 SERPENT2-PARCS-SCF core calculation chain

As explained before, the first step of the model consists in the transport calculation at the lattice level. The code chosen for this task was the continuous-in-energy SERPENT2 using the ENDFB7 nuclear data library. Each FA geometry was explicitly modeled in a 2D array (infinite lattice) with reflective boundary conditions. The condensed and homogenized few groups cross sections were generated with SERPENT2 capabilities with the branches as specified in D3.2 [2]. As pointed out by VTT in D3.2, the Discontinuity Factors (DFs) provided by SERPENT2 can be used when there are net-zero boundary conditions. Corner Discontinuity Factors (CDFs) and Power Form Functions

<sup>3</sup> Calculated with PARCS-ICoCo at Steady-State HZP with REA CR configurations with and without ejected CR

<sup>4</sup> Some small modifications or external scripting have been done for correct reading of DFs and CDFs. So, it will be referred to as GenPMAXS-KIT.

<sup>5</sup> PARCS v3.3.1 neutronics stand-alone calculations were also performed with the ICoCo interface for extracting fields variables. Even though its behavior is not modified it will be referred to as PARCS-ICoCo.

(PFFs) for later Pin Power Reconstruction (PPR) were also automatically generated by the code at this step.

As shown by other partners in D3.2 [2], especially VTT, the number of condensed groups, leakage models, discontinuity factors, reflectors models, transport correction for reflector water, among others, can affect the results. A similar study is provided in Appendix B for neutronics stand-alone comparison against SERPENT v2.1.32 full core calculations.

The axial reflector cross sections were calculated by modeling a 3D Fuel Assembly with radially reflective and axially vacuum boundary conditions. Both, top and bottom reflectors, were set to the core inlet temperature (HZP conditions).

The radial reflector cross sections were generated in a 2D full core model as shown in Figure 26. Each neighboring reflector was condensed and homogenized independently. This way, the cross sections can be calculated with a more accurate spectrum including local perturbations and the correct materials compositions (right amount of baffle is included). The discontinuity factors for the radial reflector elements was calculated using GenPMAXS [19] capability with ADFMULT card. The neutron currents/fluxes of the element as well as its North, West, East and South neighbors obtained from SERPENT2 were provided to GenPMAXS. The latter produced the DFs based on the homogenous solution based in NEM [8] (Nodal Expansion Method). The same that was later used in the core nodal code. The DF between reflectors nodes was set to unity. Due to the absence of its capability in GenPMAXS, the CDFs were obtained directly from SERPENT2, which uses an AFEN [8] based homogeneous solution. Even though, this is not consistent with the nodal code, it was shown to improve the solution as it was shown in Appendix B.

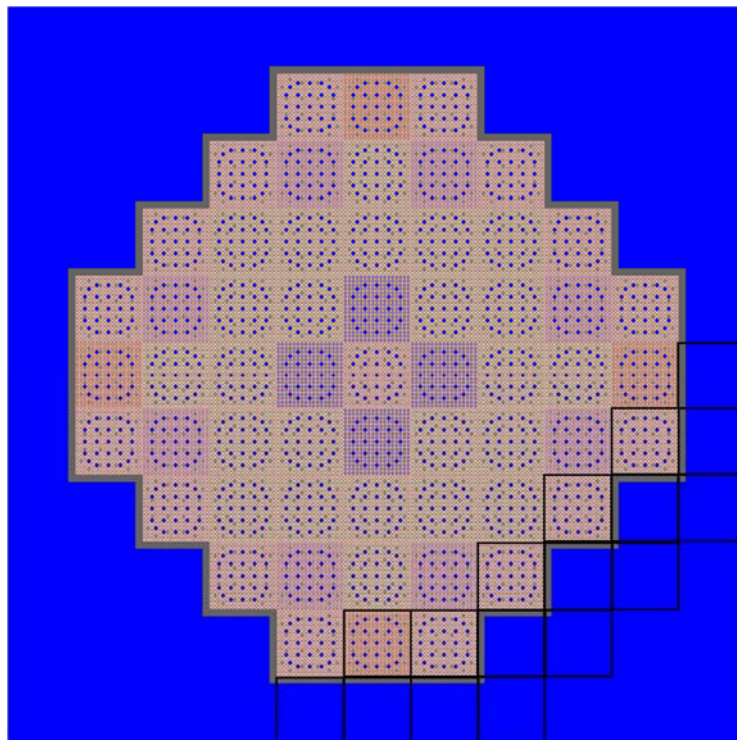


*Figure 26 2D SERPENT reflector model. Black boxes surround each of the reflector elements and its neighbors for DFs calculation with GenPMAXS.*

For the axial and radial reflector models the diffusion coefficients have transport correction for hydrogen in water as explained by VTT in D3.2. An infinite homogeneous hydrogen media was used to calculate the energy-dependent transport correction factor in a Monte Carlo external source independent calculation. It was obtained as the ratio of the CMM transport cross section to the infinite total cross section in a 70-groups energy grid [20,21]. Then, this factor was introduced in the reflector



models through the *set trc* card existing in SERPENT2 to correct hydrogen’s non-isotropic scattering behavior.

For this deliverable, the cross sections use the infinite leakage model at 2 energy groups<sup>6</sup> with DFs, CDFs and transport correction using 4 subnodes, since SERPENT v2.1.29 output files were readily available for FAs [16]. New radial and axial reflector cross sections were generated with the aforementioned methodology with SERPENT v2.1.32, as well as, for FAs for the analysis provided in Appendix B. In further tasks, when comparing to high-fidelity multi-physics, it may be necessary to add complexity to the model with other leakage models or higher number of energy groups. In a future, the analysis from Appendix B could help to improve the solution.

The core neutronic model consists radially in 1 node per FA or reflector element (it may contain subnodes) and has an axial discretization of 27 elements: 20 for the active height, 3 for the bottom reflector and 4 for the upper reflector. For SCF only the active height was modeled with the same radial and axial discretization as the neutronic model. Each FA is modeled as a single channel with a representative rod as it can be observed in Figure 27. SCF calculations were done with a 3D model (channel connectivity both axial and radial). 1D calculation is also possible considering each FA as a canned element (no radial coupling/ channel connectivity). However, computational cost was only slightly higher for the 3D case and results variation was small. The correlations used are shown in Table 9.

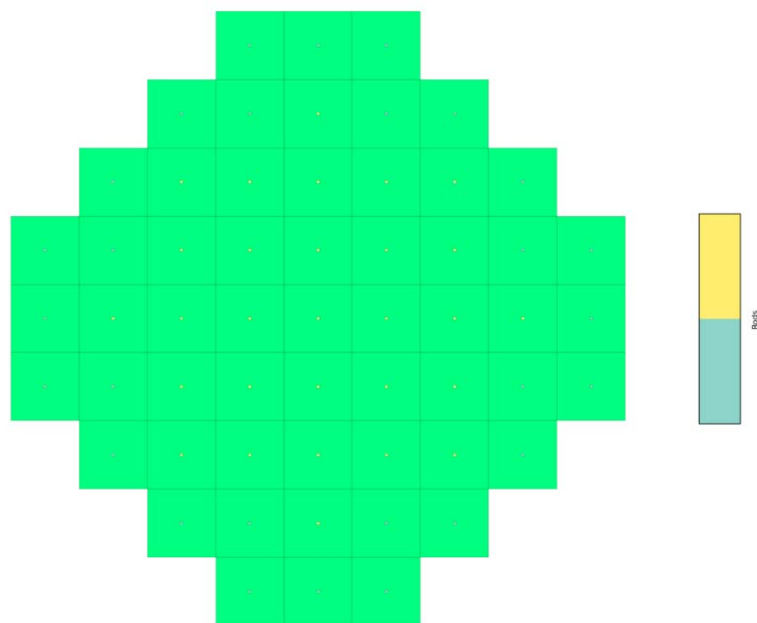


Figure 27 SCF model. Each FA is considered as one channel with a representative rod for TH calculations

Table 9 SUBCHANFLOW correlations used in the model.

<sup>6</sup> Studies were performed with 2 energy groups because PARCS v3.3.1 only provides PPR for 2-groups calculations [5].

Correlation	Option selected
Turbulent friction	Blasius
Heat transfer	Dittus Boelter
CHF	Westinghouse-3

The core calculations were done with PARCS-SCF. The main advantage of the coupling with ICoCo is that it does not interfere with the syntax of the codes, i.e. inputs have to be made for PARCS and SCF as usual. A MED mesh (a type of mesh available in SALOME [9]) is generated using a MED preprocessor, implemented by M. Garcia [10], for the codes to store the variables fields, and, via ICoCo routines, both codes communicate using *get* and *set* functions for fields and time step definition. It is also in charge of the steady-state or transient coupling strategy.

The transient calculation was performed with an explicit time scheme between neutronics and TH with a time step of 0.0005 s without relaxation factors applied during the fields exchange. Given that the system is not initially critical, PARCS-SCF normalized the fission source at the beginning of the transient calculations.

### Acknowledgements

The new cross sections generations ran for this KIT work and reflectors requires multiple runs of computationally expensive Monte Carlo simulations.

This work was performed on the HoreKa supercomputer funded by the Ministry of Science, Research and the Arts Baden-Württemberg and by the Federal Ministry of Education and Research.

In addition, part of the post processing has been performed with the aid of *serpent-tools* [11].

### 3.3. Results

The neutronics model was analyzed at different states: HFP, HZP and CZP with the fuel and moderator temperatures and densities summarized in Table 10. This was done at ARO and ARI conditions. Reactivity ( $\rho$ ) results are summarized in

Table 11 and reactivity ( $\Delta\rho$ ), Root Mean Square (RMS) and Maximum (MAX) discrepancies against SERPENT2 full core results are summarized in Table 12. An overall good agreement is observed with less than 100 pcm and 1-3% RMS difference in power profiles for ARO configurations. On the other hand, under ARI conditions this value goes up to ca. 500 pcm and ca. 12% for RMS difference. This is expected since the presence of strong absorbers challenges the diffusion limits. Moreover, in ARI configuration 53 out of the 57 FAs are roded with axially heterogeneous CRs. This can be improved using a leakage correction for XS and/or more energy groups as it was reported in Appendix B.

Table 10 CZP, HZP and HFP TH states

	Fuel Temperature [K]	Coolant Temperature [K]	Coolant Density [kg/m <sup>3</sup> ]
<b>CZP</b>	300	300	0.99656
<b>HZP</b>	569.15	569.15	0.73371
<b>HFP</b>	900	590	0.68700

Table 11 Reactivity calculations for all states (CZP, HZP, HFP) with stand-alone neutronics

		Multiplication Factor (k-eff)			Reactivity ( $\rho$ )		Difference
		PARCS-ICoCo	SERPENT	SERPENT	PARCS-ICoCo	SERPENT	SERPENT-PARCS-ICoCo
		Value [a.u.]	Value [a.u.]	Error [a.u.]	Value [pcm]	Value [pcm]	Value [pcm]
HFP	ARO	1.03225	1.0312	1.00E-05	3124	3026	-98
	ARI	0.81290	0.8146	2.00E-05	-23016	-22759	257
	ROD WORTH	--	--	--	26140	25785	-355
HZP	ARO	1.0544	1.05373	3.00E-05	5159	5099	-60
	ARI	0.83708	0.83914	7.00E-05	-19462	-19170	292
	ROD WORTH	--	--	--	24621	24269	-352
CZP	ARO	1.14093	1.14126	3.00E-05	12352	12378	26
	ARI	0.94637	0.95015	6.00E-05	-5667	-5247	420
	ROD WORTH	--	--	--	18019	17625	-394

Table 12 PARCS-ICoCo -SERPENT2 discrepancies for all states (CZP, HZP, HFP) with stand-alone neutronics using infinite leakage model, 4 subnodes, DFs, CDFs and TRC. EG stands for energy groups and SN for subnodes.

		EG	SN	Leakage Model	$\Delta\rho$	Axial Power		FA Power		PIN Power	
					[pcm]	RMS [%]	MAX [%]	RMS [%]	MAX [%]	RMS [%]	MAX [%]
HFP	ARO	2	4	INF	-98	1.28	4.38	1.80	3.26	2.92	15.00
	ARI	2	4	INF	257	5.60	12.74	6.90	15.84	8.68	30.34
HZP	ARO	2	4	INF	-60	1.39	3.95	1.54	2.96	2.69	14.65
	ARI	2	4	INF	292	5.95	14.29	7.16	16.53	9.09	32.3
CZP	ARO	2	4	INF	26	2.93	9.01	1.41	2.98	2.34	16.86
	ARI	2	4	INF	420	8.61	22.99	8.30	15.20	11.19	39.91

The initial conditions of the transient were explained in Section 3.1. The rods configuration was shown in Figure 24. The system is initially at HZP at 10<sup>-4</sup>% of the nominal power, then, the whole system is at the inlet temperature coinciding with the HZP neutronics stand-alone calculations. The reactivity, RMS and MAX comparison against SERPENT2 full core model are summarized in Table 13. For this condition, results discrepancies are in between ARO and ARI conditions as expected. In addition, Figure 28-Figure 33 show the axial power, axial difference with SERPENT2 model, power distribution, power difference against SERPENT2 model, pin power distribution and pin power

distribution difference with SERPENT2 model respectively. Once again, these discrepancies can be improved using a leakage correction for XS and/or more energy groups as it was reported in Appendix B, especially for ARI conditions when almost all FAs have CRs inserted.

Table 13 PARCS-ICoCo -SERPENT2 discrepancies for HZP REA using infinite leakage model, 4 subnodes, DFs, CDFs and TRC. EG stands for energy groups and SN for subnodes.

EG	SN	Leakage Model	$\Delta\rho$ [pcm]	Axial Power		FA Power		PIN Power	
				RMS [%]	MAX [%]	RMS [%]	MAX [%]	RMS [%]	MAX [%]
2	4	INF	36	3.59	10.01	3.83	7.44	5.05	22.84

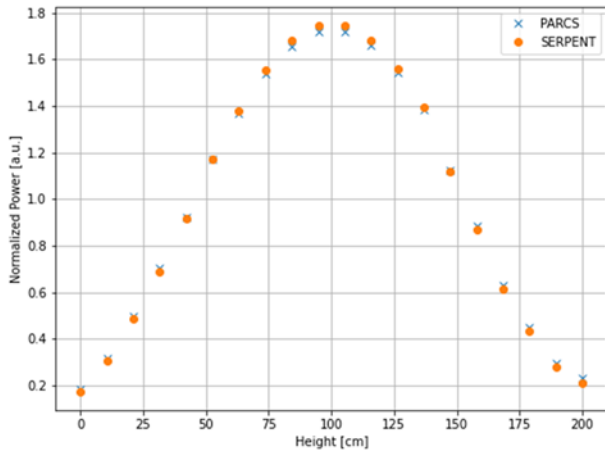


Figure 28 PARCS-ICoCo -SERPENT2 Normalized axial power comparison for REA initial condition at HZP

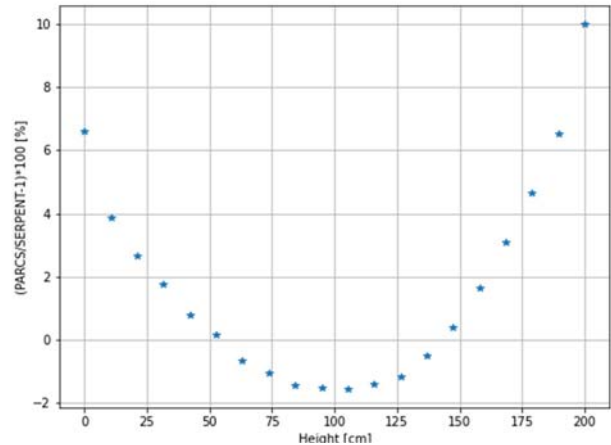


Figure 29 PARCS-ICoCo -SERPENT2 Normalized axial power comparison for REA initial condition at HZP relative difference

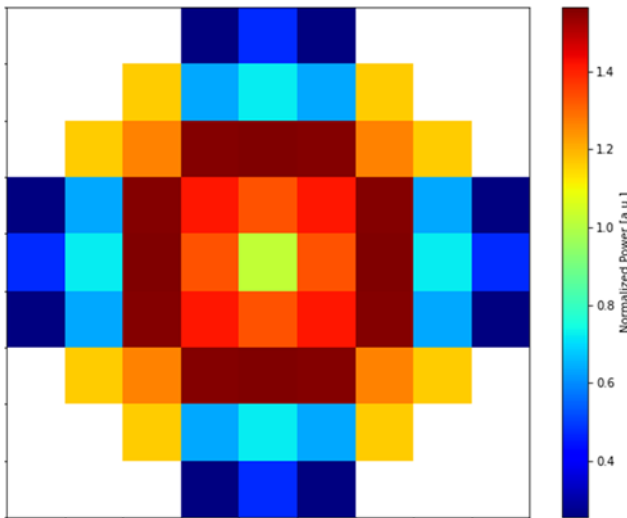


Figure 30 PARCS-ICoCo axially integrated FA normalized radial power for REA initial condition at HZP

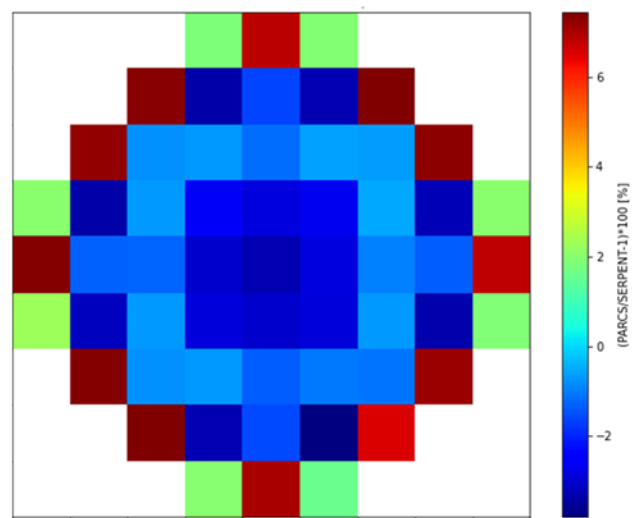


Figure 31 PARCS-ICoCo -SERPENT2 axially integrated FA normalized radial power relative difference for REA initial condition at HZP

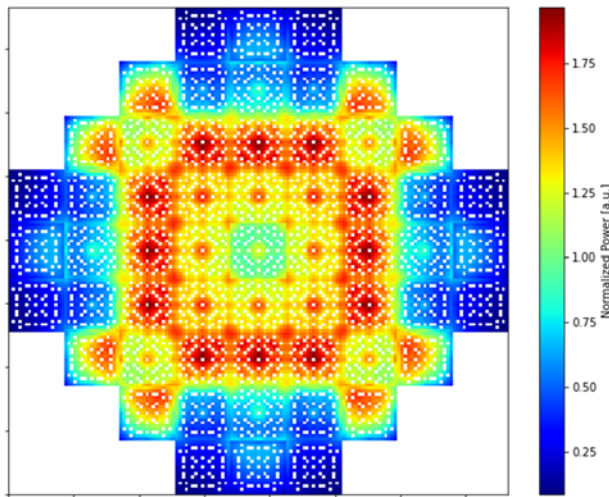


Figure 32 PARCS-ICoCo axially integrated pin normalized radial power for REA initial condition at HZP

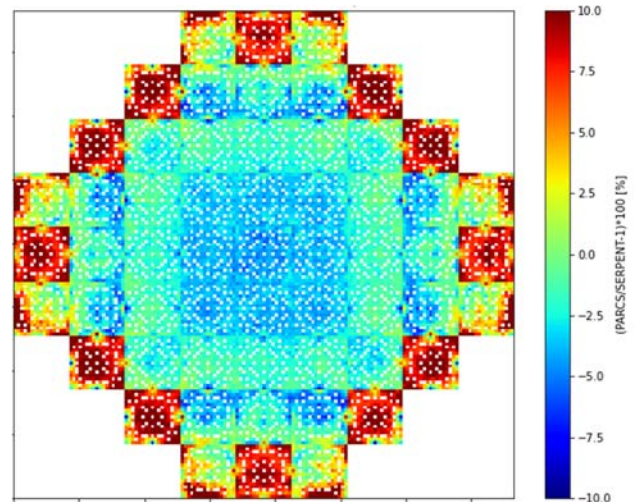


Figure 33 PARCS-ICoCo -SERPENT2 axially integrated pin normalized radial power relative difference for REA initial condition at HZP. Values are truncated in the interval [-10; 10] %. Lower or higher values can be expected.

Beginning from the aforementioned initial condition the rod marked in Figure 24 was ejected taking 0.05 s to pass from fully inserted to fully extracted conditions. Given that the rod worth is over 1\$ the system quickly becomes super prompt critical and, therefore, the fission chain can be sustained only by prompt neutrons with generation times of a few micro seconds ( $\mu$ s). This way, an extremely rapid exponential power increase is observed in Figure 34. The increase in the fuel temperature first and the density decrease of the moderator later will counteract this reactivity with some delay due to the energy deposition mechanisms until it reaches a value under 1\$. At this point, the fission chain is no longer sustained only by prompt neutrons but it will also need the delayed neutrons production. This will cause the power to decrease until the generation of delayed neutrons is enough to sustained the fission chain again. The power peak of 48.35 times the nominal power is achieved at 0.1645 s when the reactivity crosses under 1\$ as observed in Figure 35. Fuel temperature will continue to rise as well as the coolant density will continue to decrease with the rate of the power from some instant before and, thus, the effect in the reactivity will be higher than the instantaneous power. As shown in Figure 35 reactivity becomes negative and then starts to increase once the coolant and fuel decreases in temperature as observed in Figure 36 and Figure 37 for maximum coolant and fuel centerline temperature respectively. Figure 38 and Figure 39 show the maximum cladding outer and inner temperature during the evolution of the transient. Figure 40 and Figure 41 are the normalized FA and Pin axially integrated power at peak time.

The system will continue to evolve until the reactivity reaches zero and a new steady state will be achieved but it is out of the scope of the duration of the transient analyzed here (3 s). The final power is 0.23 times the nominal power with a minimum DNBR of 4.5304 a.u. The minimum DNBR during the transient was of 1.6154 a.u.

In conclusion, the PARCS-SCF model for the SMART KSMR concept was obtained. So far, this transient simulation represents a blind test to be complemented, in a future, by further high-fidelity studies in Tasks 3.3 and 3.4. Thus, some modification of the model may be needed at the moment of comparison with the aid of the studies performed in Appendix B.

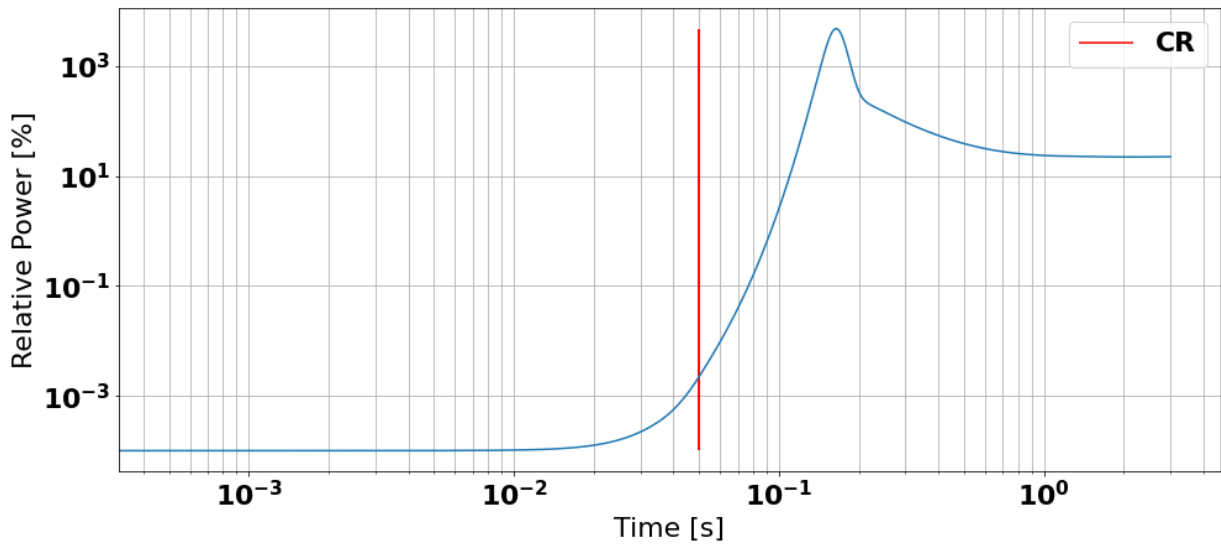


Figure 34 REA relative power evolution in time. The red line marks when the CR is fully extracted.

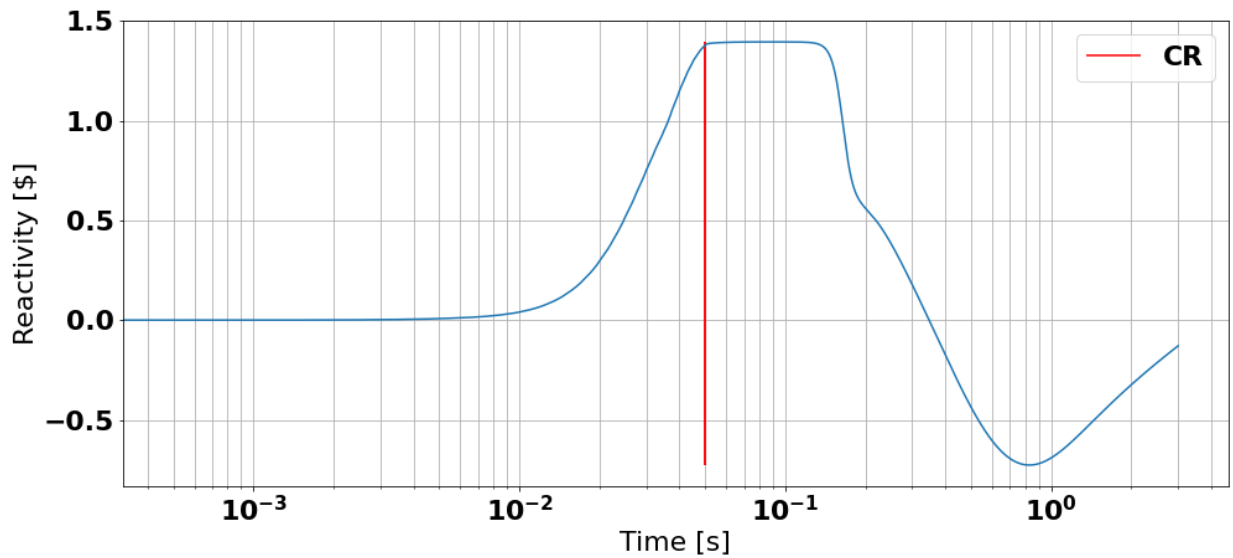


Figure 35 REA reactivity evolution in time. The red line marks when the CR is fully extracted.

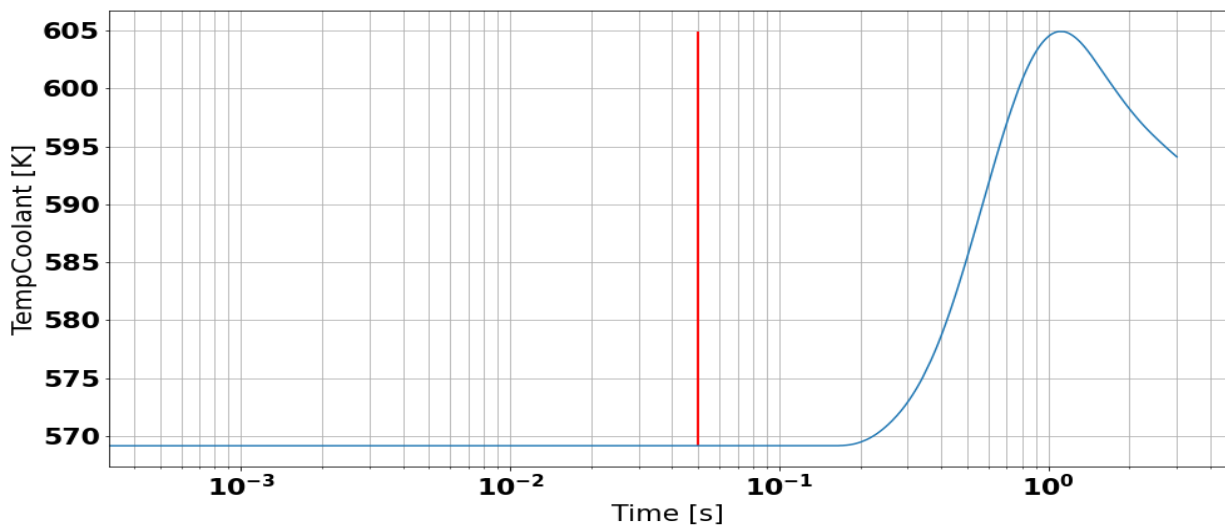


Figure 36 REA maximum coolant temperature evolution in time. The red line marks when the CR is fully extracted.

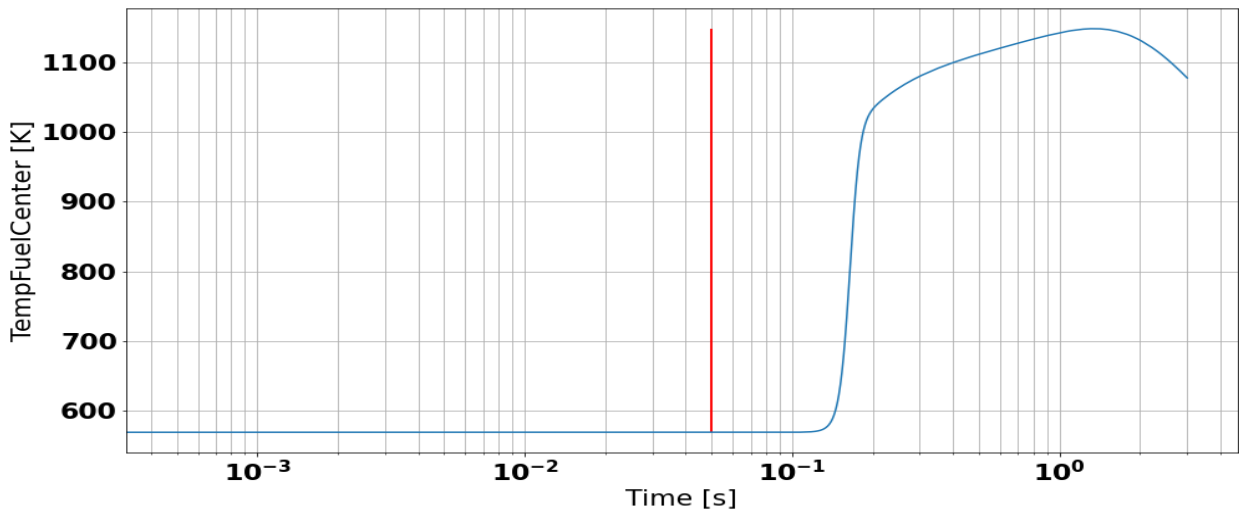


Figure 37 REA maximum fuel centerline temperature evolution in time. The red line marks when the CR is fully extracted.

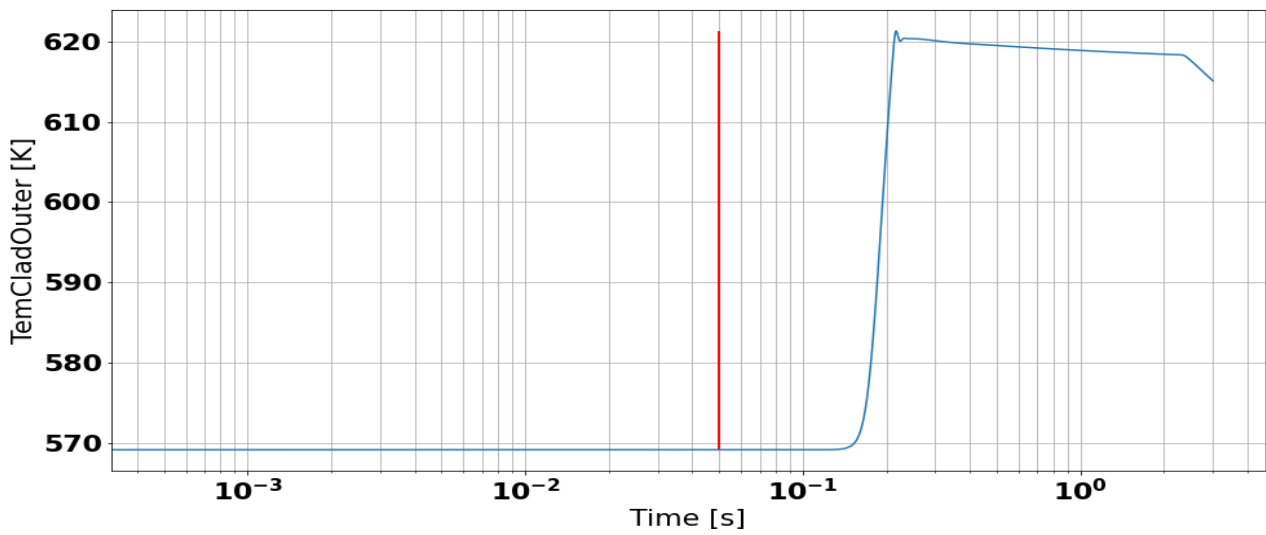


Figure 38 REA maximum cladding outer temperature evolution in time. The red line marks when the CR is fully extracted.

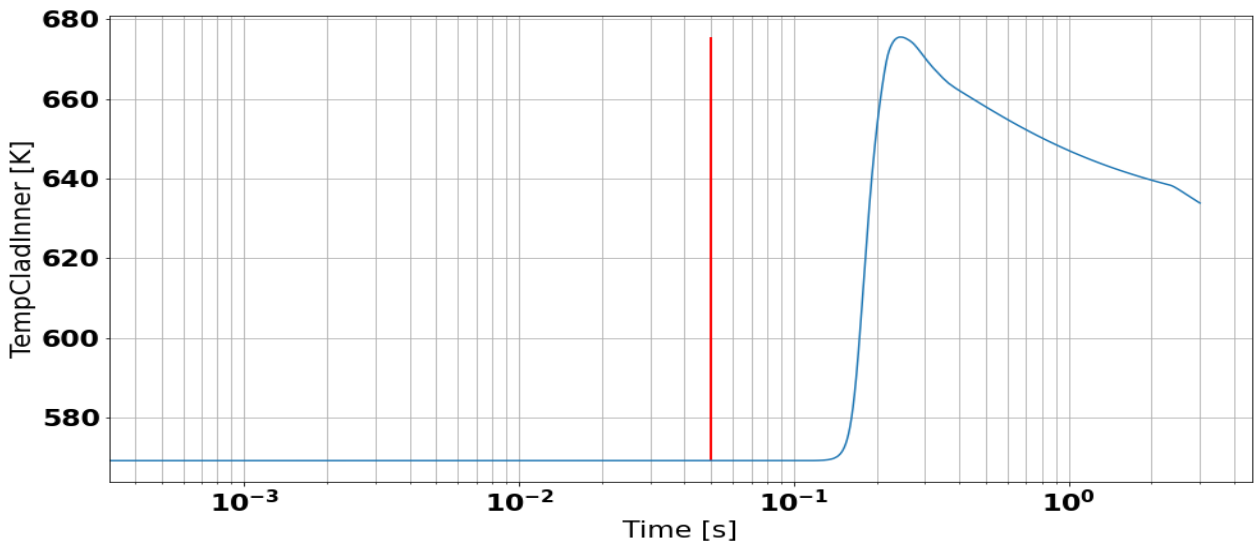


Figure 39 REA maximum inner cladding temperature evolution in time. The red line marks when the CR is fully extracted.

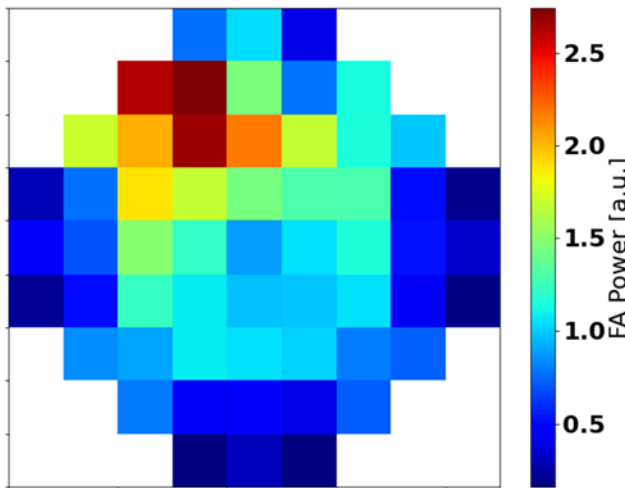


Figure 40 PARCS-SCF axially integrated FA normalized radial power for REA at peak time.

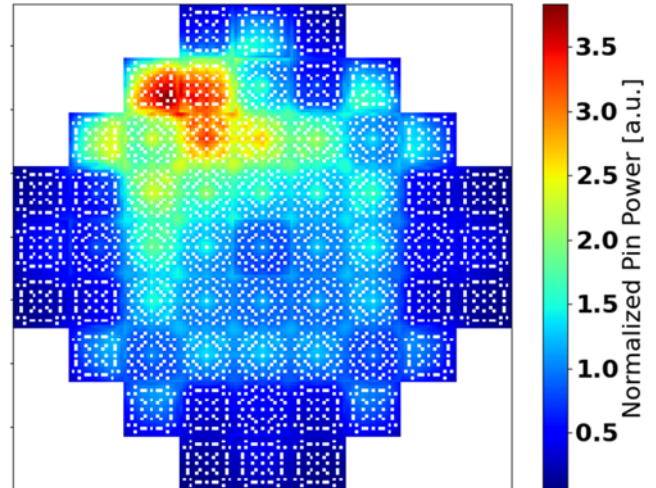


Figure 41 PARCS-SCF axially integrated pin normalized radial power for REA at peak time.



## 4. F-SMR

Transient calculation on the F-SMR core has been performed by CEA using an industrial type calculation scheme based on 3D full core calculation at assembly level. The calculation codes used for such calculation are APOLLO3® for neutronics and FLICA5 for Thermal-hydraulics. Both codes are coupled together using the C3PO coupler through an image of their ICoCo interface called *PhysicsDriver*.

The transient calculated in this document corresponds to a cold water insertion at the bottom of the core leading to an important increase in reactivity due to highly negative moderator coefficients in a non-borated core.

### 4.1. Description of the transient scenarios

The description of the F-SMR core is available in [D3.1](#) ([1]). The transient is performed at beginning of cycle, all assemblies being fresh ones.

#### 4.1.1. Initial conditions

The initial status of the reactor is a full power (300 MWth) critical core at beginning of cycle. Table 14 summarizes the status of the core before the transient.

Table 14 : Thermal hydraulic conditions of the core before transient

Parameter	Nominal operation value
Core power	300 MWth
System pressure (core outlet)	15 MPa
Core flow rate	2145.8 kg/m <sup>2</sup> /s
Core inlet temperature	553 K

Criticality is obtained by an adjustment of the control rod insertion. Figure 42 presents the position of the controls rods in the core. Critical state in these conditions requires a full insertion of control rods of groups 1, 2 and 3 and the insertion of group 4 for up to 334 steps.

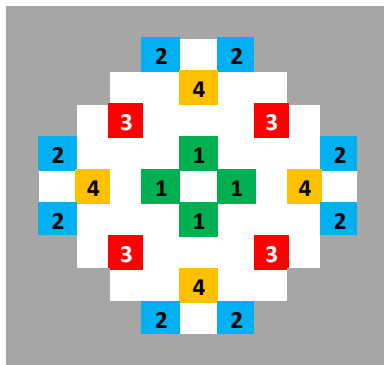


Figure 42 : position of control rod groups

Figure 43 presents the power distribution in the core.

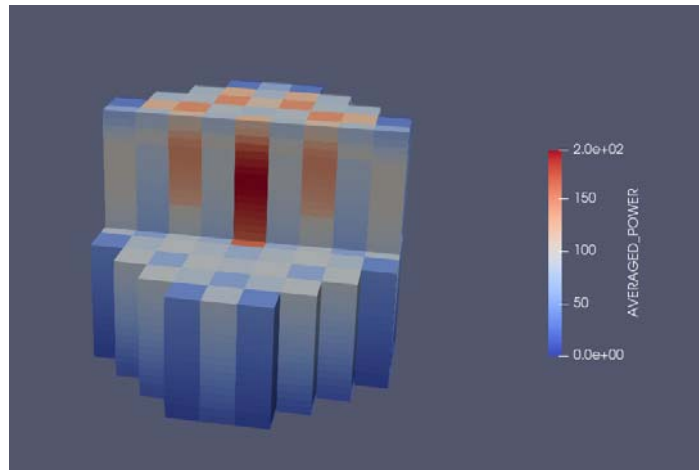


Figure 43 : Power distribution in the core at BOC

#### 4.1.2. Sequence of events

The sequence of events is as follow.

- At  $t < 0$ : The core is at BOC in critical state.
- At  $t = 0$ : Inlet water temperature drops in 0.1 s from 280°C to 150°C
- SCRAM is activated when the reactor power reaches 105%  $P_{nom}$  with a delay of 0.01 s.
- Control rods used for core reactivity control are fully inserted at  $t = 0.55$  s.
- Safety control rods are fully inserted at  $t = 1.15$  s. Core is stabilized and subcritical before the complete insertion of control safety control rods.

*This transient is only made to evaluate the impact of a cold water insertion without any consideration on the reason such drop in temperature happens.*

A reference calculation has been made with an inlet water temperature of 150°C. In order to push the capacity of the calculation scheme, a second point has been performed with an inlet temperature of 100°C. Figure 44 presents the power evolution for both transients.

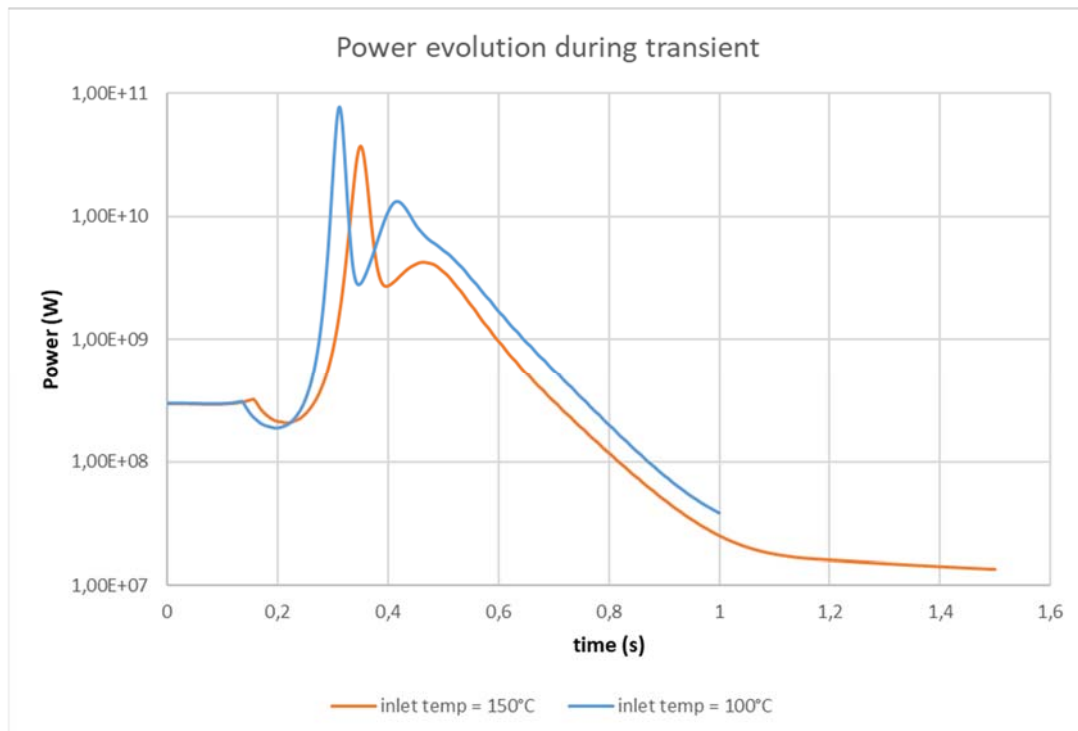


Figure 44 : Impact of inlet temperature on power evolution during transient

## 4.2. Models (CEA)

CEA models uses a two codes couplings through the C3PO coupler:

- Neutronics is performed by APOLLO3® [25] in a standard 2 steps calculation;
- Core thermalhydraulics is performed by FLICA5 [26];
- Communication between the two codes are orchestrated by a C3PO python script.

### 4.2.1. Neutronics model

The lattice scheme used to produce the homogenized cross sections for the neutronics core calculation has been described in D3.2 [2]. Table 15 presents the list of parameters at which cross sections have been produced.

*Table 15: List of parameters used for the cross section libraries.*

Fuel temperature [°C]	Moderator temperature [°C]	Moderator density [g/cm <sup>3</sup> ]	Burnup [MWd/t]
10	10	1.00670	0
20	20	1.00504	1007
30	30	1.00215	2013
280	125	0.94239	4026
650	200	0.86904	8051
800	280	0.76464	12075
1200	311	0.70246	16098
2700	324	0.66808	20121
	344	0.60225	30143
	356	0.48857	40193
			49768
			59811
			69852
			79891
			89930

During the core calculation, a standard linear interpolation is performed between those parameters for every cell of the calculation.

Cross sections used to model to core reflector are obtained through an equivalence process consisting in adjusting an equivalence coefficient in order to preserve the core/reflector albedo.

Between lattice and core calculation, an SPH equivalence is performed in order to preserve reaction rates in the assembly during core calculation.

The core solver used in this case is a diffusion solver based on finite elements called MINOS. Each assembly into the core is divided into 4 (2x2) radial mesh and the core height is divided into 40.

The neutronic calculation performs a power calculation on the quarter of assembly mesh. This power distribution is then used by the thermalhydraulics code to perform temperatures and density calculation.

#### **4.2.2. Core thermal hydraulics model**

FLICA5 code is CEA's newest 4 equations code for core thermal hydraulics and two-phase flow analysis [25]. The code is based on a three-dimensional porous modelisation. Using power source terms, boundary conditions and some closure models, FLICA5 performs both the thermal hydraulics calculation in the coolant and the thermal calculation in the fuel. The thermal equation is solved with an implicit Finite Element solver, whereas the two-phase flows equations are solved with a semi-implicit solver based on a MAC Finite Volume discretization.

In this industrial type calculation, each assembly is modelled by a single channel for hydraulics and each channel includes a single fuel rod (averaged rod considered representative for the whole assembly) for fuel thermal calculation. At the moment, no grid has been introduced in the thermal hydraulics calculations, their position being still under investigation. The axial direction is uniformly discretized with 48 cells, whereas the radial direction is discretized with one cell per channel

As  $^{235}\text{U}$  enrichment variation and number of gadolinium rods stay low from one assembly to another and as fuel rods are averaged in the assemblies, it is considered for thermal hydraulics calculation that fuel pellets can be modelled as pure  $\text{UO}_2$  material with temperature laws for specific mass, conductivity and heat capacity. Also the gap conductance is given as uniform value set to  $10000 \text{ W}/(\text{m}^2 \cdot \text{K})$ .

As the neutronics only provides power on a homogenized cell, FLICA5 performs a distribution of the power between fuel and water. It is considered in our case that 97.4% of the power is deposited in the fuel pellets (the fuel cladding receives no power from the neutronics) and 2.6% is directly deposited in the water. For transient calculation, we model the cold inlet water temperature drop by an instantaneous liquid enthalpy drop imposed on the inlet boundary condition. However, for stability reasons, we may consider a steep time ramp of enthalpy instead of strict instantaneous drop.

### 4.2.3. Coupling and transient calculation

The C3PO code coupler consists of python script allowing to couple the codes through their ICoCo interface. Figure 45 presents the organization of the coupling between APOLLO3® and FLICA5.

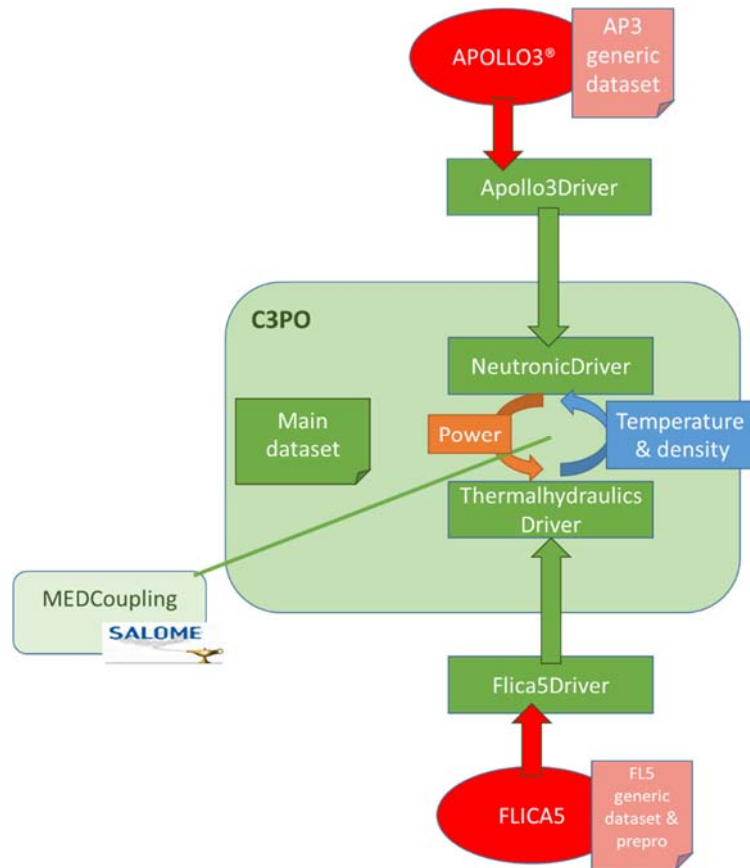


Figure 45 : C3PO coupling between APOLLO3® and FLICA5

All the coupling, both for permanent and transient calculation is driven in the C3PO python script. For transient calculation, the time loop is also managed with a fixed-point explicit coupling using a time step of 1 ms maximum.

### 4.3. Results

This sections provides the results of the simulation of a F-SMR core with APOLLO3® and FLICA5 on a cold water insertion transient. Quantities of interest are:

- Evolution of the core global power
- Evolution of the core reactivity
- Maximum fuel temperature in the core
- Void fraction
- Evolution of the Fq power factor

Figure 46 presents the power evolution during transient with the position of the control rods. Operational rod insertion is in cumulated steps, safety control rods is in absolute steps, all rods being inserted at once.

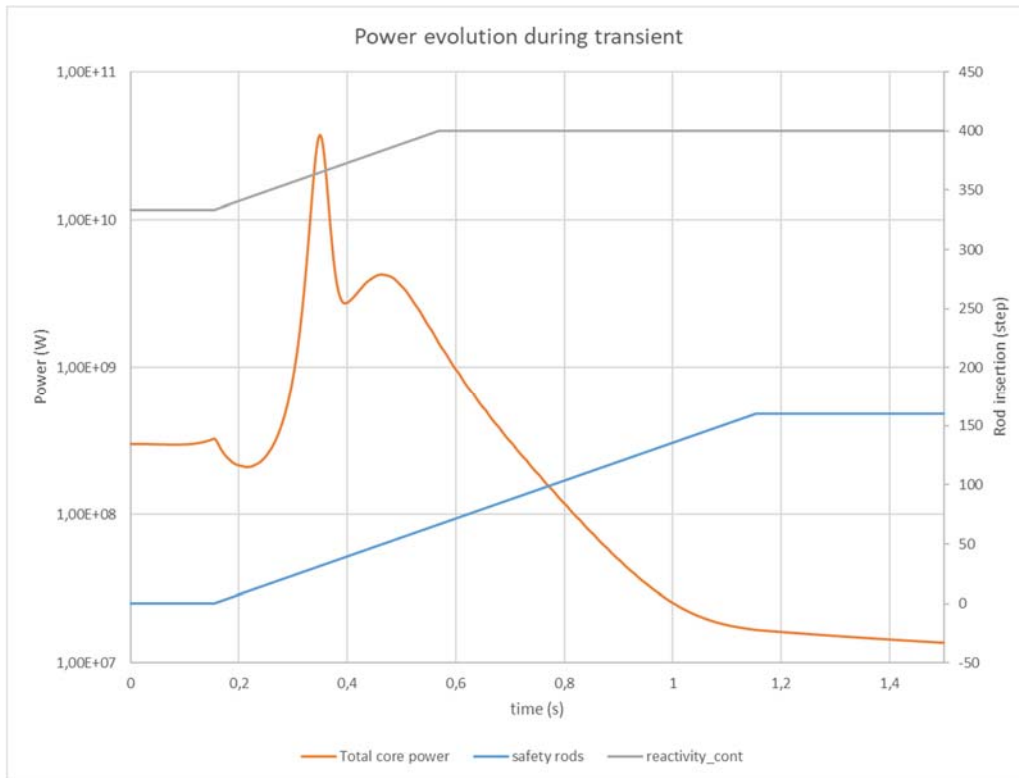


Figure 46 : Power evolution during transient

Power starts to decrease with the rod insertion which is not quick enough to counter the reactivity insertion of cold water. The power distribution in the core is represented in Figure 47 at different moments of the transient:

- a) Initial core power distribution
- b) First power peak leading to SCRAM at  $t = 0.155$  s
- c) Power decrease at  $t = 0.216$  s
- d) Second power peak at  $t = 0.35$  s reaching a total power of  $3.75 \times 10^{10}$  W
- e) Second decrease at  $t = 0.396$  s
- f) Third power peak at  $t = 0.463$  s
- g) End of transient at  $t = 1.4$  s

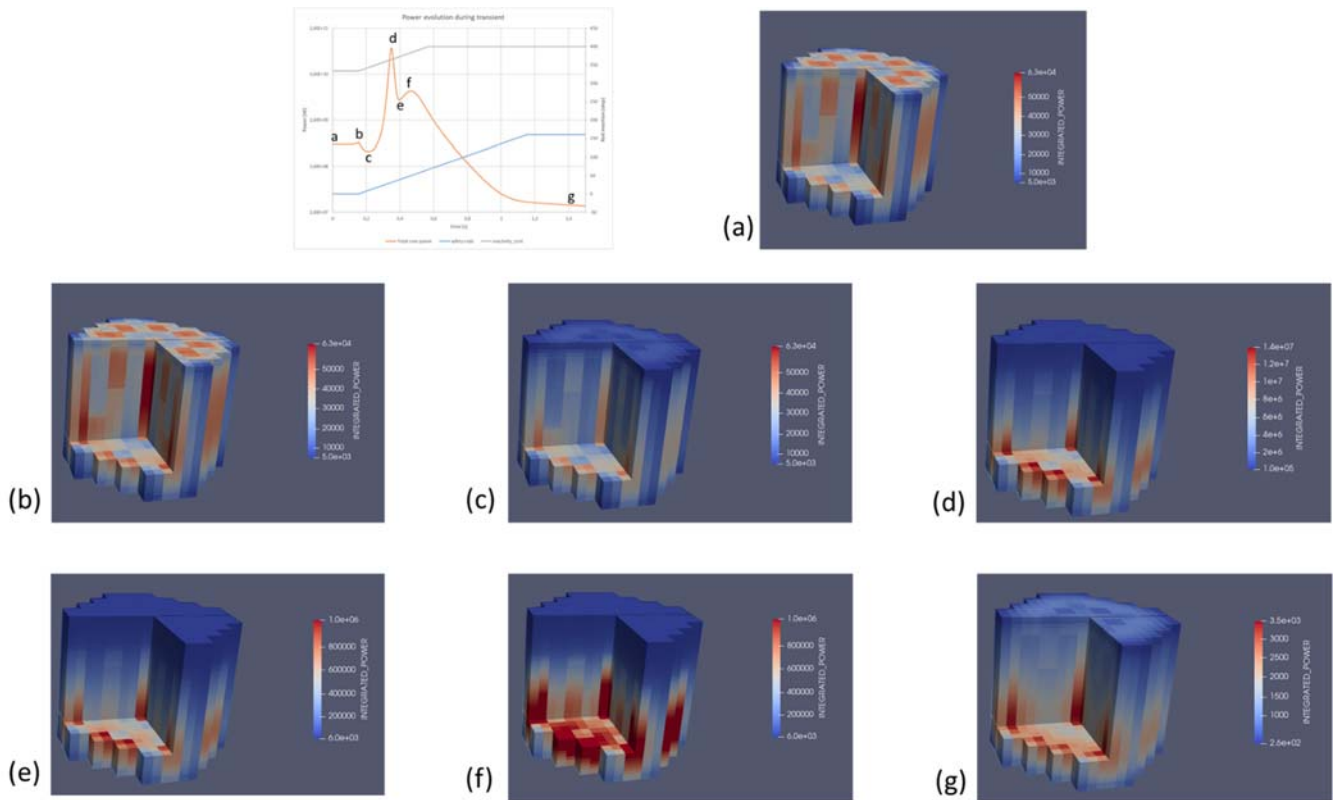


Figure 47 : 3D power field during transient

This 3D field evolution can be summarized through the Fq and Axial offset values as presented in Figure 48.

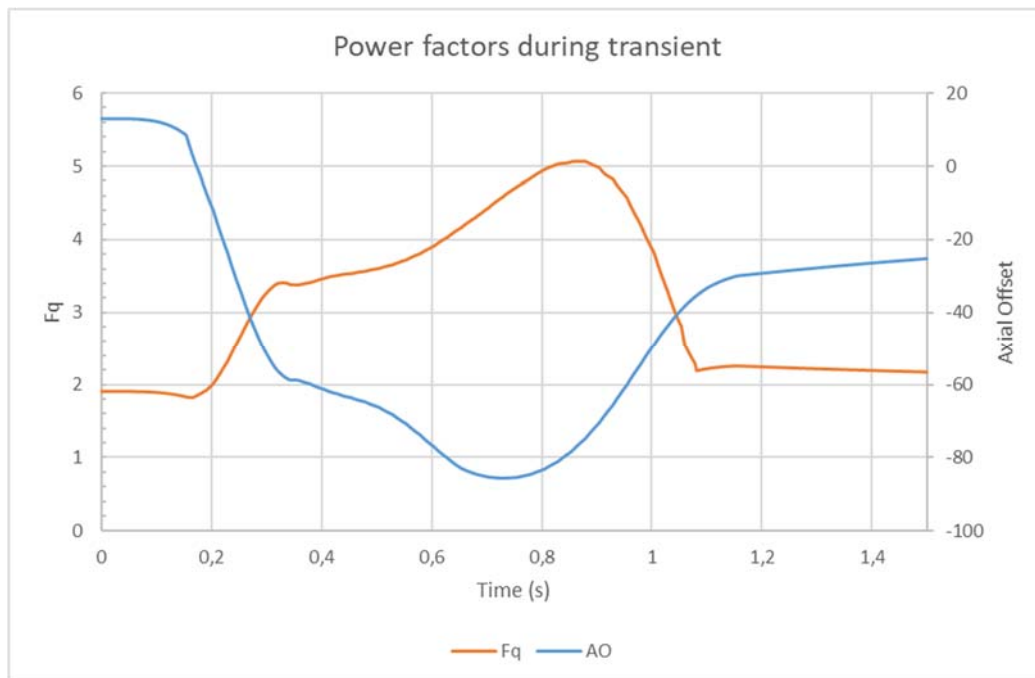


Figure 48 : Power factor evolution during transient

In the same way, Figure 49 presents the reactivity evolution in the core. A comparison of core power and reactivity is proposed in Figure 50.

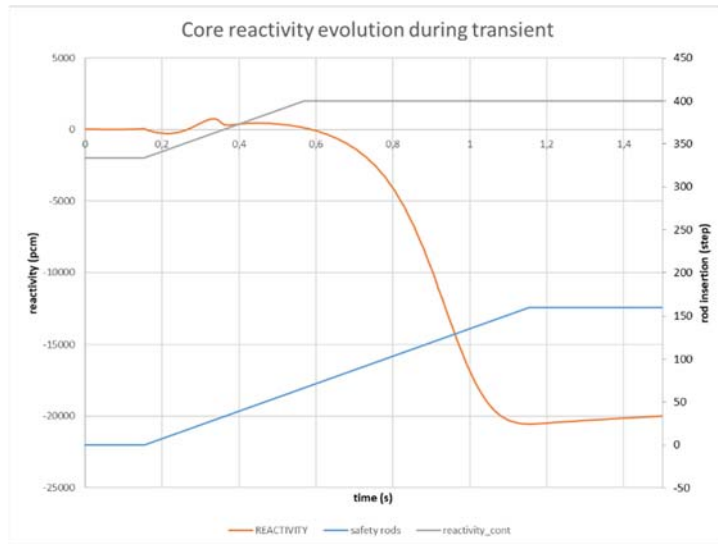


Figure 49 : Reactivity evolution during transient

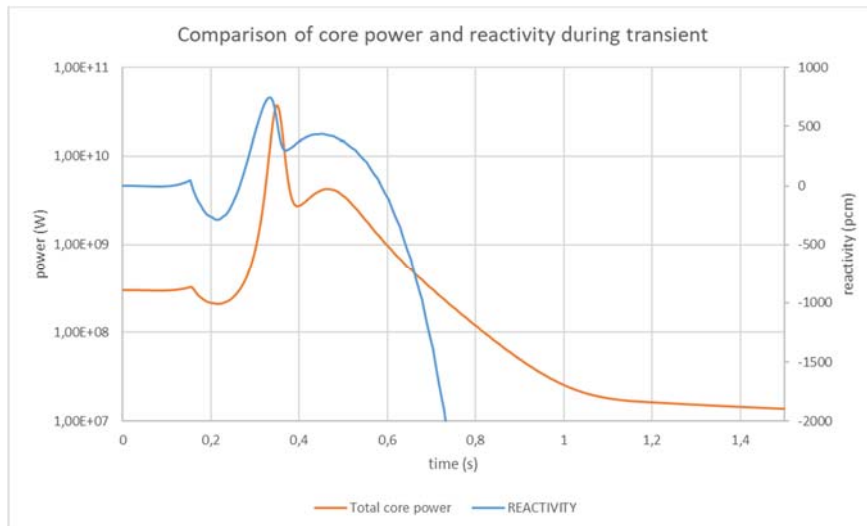


Figure 50 : Comparison of FSMR core power and reactivity during cold water insertion transient

The large power increase during this transient leads to an important fuel temperature increase. Figure 51 presents the evolution of the maximum fuel temperature. For neutronic calculation, an effective fuel temperature is calculated through the Rowland formula, this effective fuel temperature is also plotted on the figure.



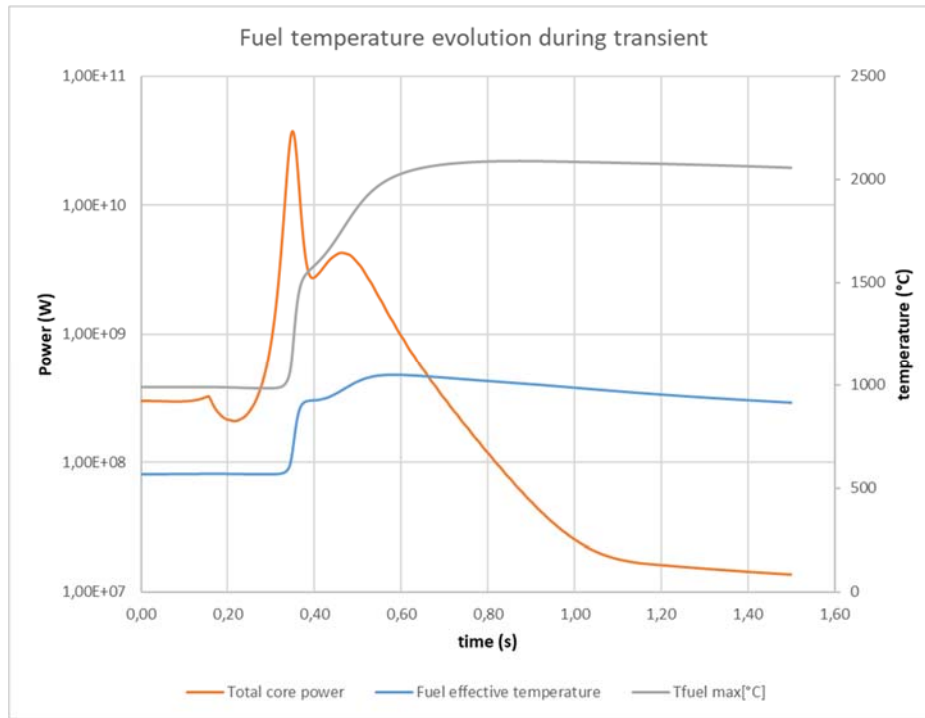


Figure 51 : Maximum fuel temperature evolution during transient

The evolution of the effective fuel temperature field is presented in Figure 52 at different instants of the transient :

- a) Initial core condition  $t= 0$  s
- b) Second power peak at  $t=0.35$  s
- c) Second decrease at  $t= 0.396$  s
- d) End of transient at  $t=1.4$  s

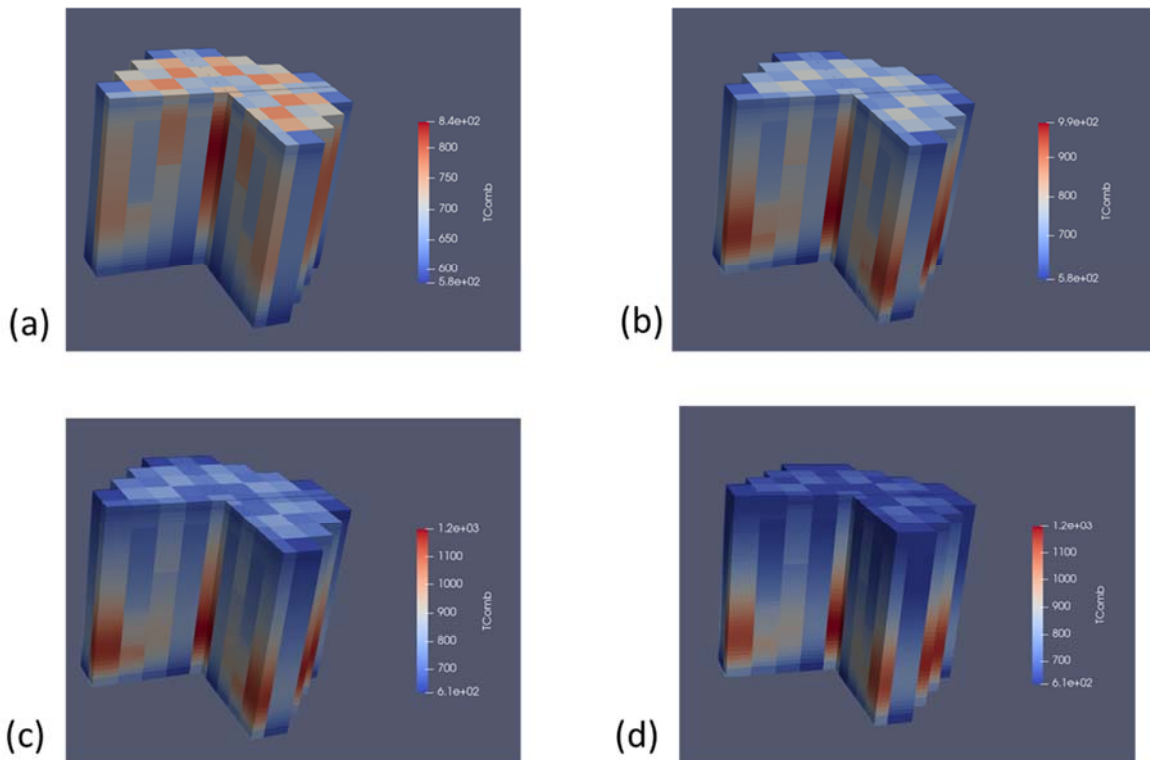


Figure 52 : Effective fuel temperature evolution at different instants of the transient

Figure 53 presents the evolution of void fraction in the core during the transient.

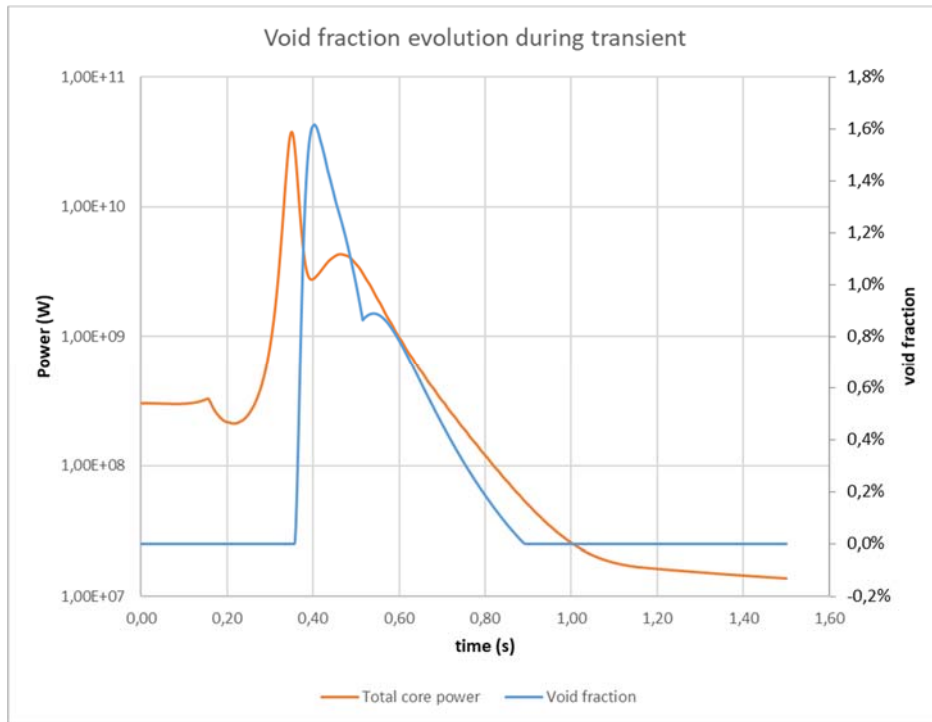


Figure 53 : Evolution of void fraction during transient

Figure 54 presents the 3D fields of void fraction at different instants of the transient:

- a) At the beginning of boiling  $t = 0.37$  s
- b) At the peak of boiling  $t = 0.40$  s
- c) At the first decrease :  $t = 0.51$  s
- d) At the second peak of boiling  $t = 0.54$  s
- e) Before steam fully evacuated  $t = 0.85$  s

It shows in particular that the voiding appears primarily in the central assembly and in the peripheral assemblies whose control rods are not used for reactivity control during operation.

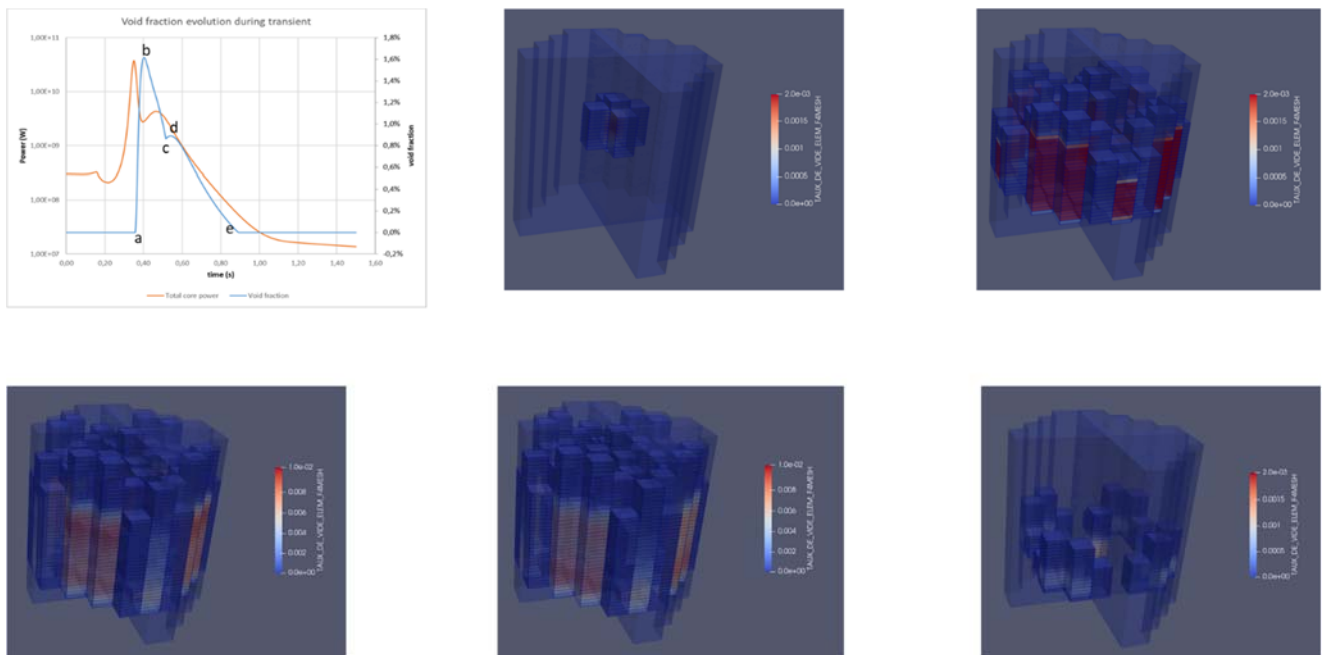


Figure 54 : Field of void fraction during the transient

## 5. NuScale

Transient calculation of NuScale were performed by HZDR, VTT, TBL, and PEL using 4 different 3D full core simulators namely, DYN3D, ANTS, PANTHER, and SIMULATE5/S3K.

Description of the transient scenario, models used by the partners, and results of the transient calculations are presented in the following sub-sections.

### 5.1. Description of the transient scenario

The transient type chosen for the NuScale concept is the accidental ejection of control rod assembly (CRA) from the core. As shown in Figure 55, the NuScale control system comprises two regulating CRA banks (RE1 and RE2) and two shutdown banks (SH3 and SH4). The selected scenario considers ejection of a single regulating CRA from approx. Power Dependent Insertion Limit (PDEL) at 75% power level. The scenario is “realistic” and is analyzed in the FSAR.

#### 5.1.1. NuScale core specifications

Detailed NuScale core specifications are provide in [D3.1](#) ([1]) and supplemented by an Excel file on SharePoint ([link](#)).

#### 5.1.2. Initial conditions for the transient

The initial conditions for the REA are summarized in Table 16. Some additional clarifications to the data shown in Table 16 are provided below:

- In all cases, all-fresh fuel with zero Xe should be used.
- Steady-state critical boron concentration should be evaluated by the participants.
- CRA positions are further clarified in Figure 56.

Table 16: Summary of the initial conditions for different REA scenarios

Power		Flow rate	T inlet	Operating pressure	Boron	CRA position			
%	MWt	kg/s	°C	bar		RE1	RE2	SH3	SH4
75%	120	521.6	262	127.5	Critical	100	56	100	100

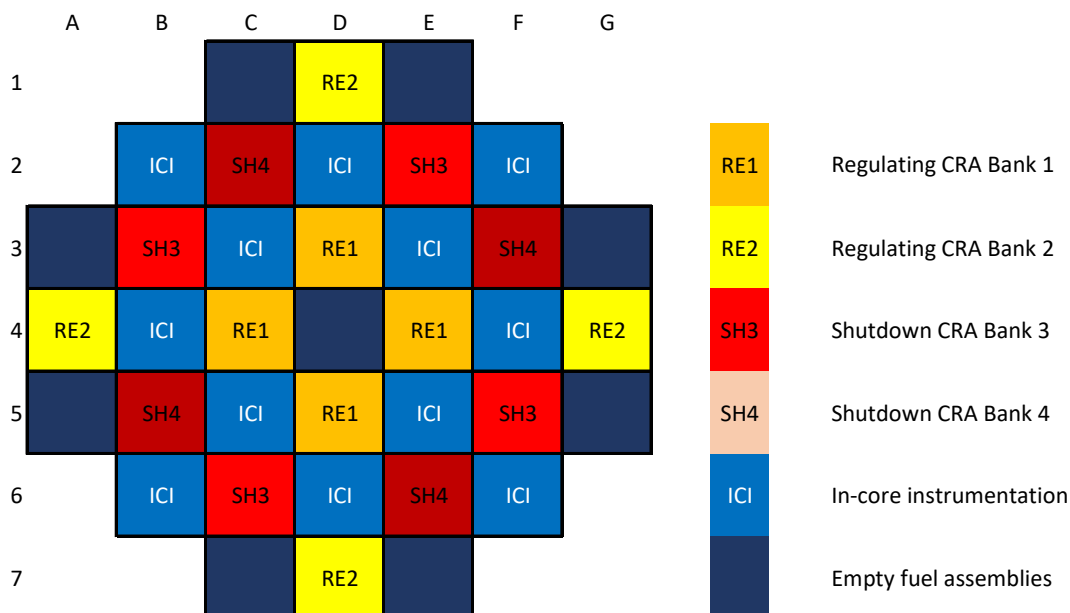


Figure 55. NuScale core map and location of the CRA banks.

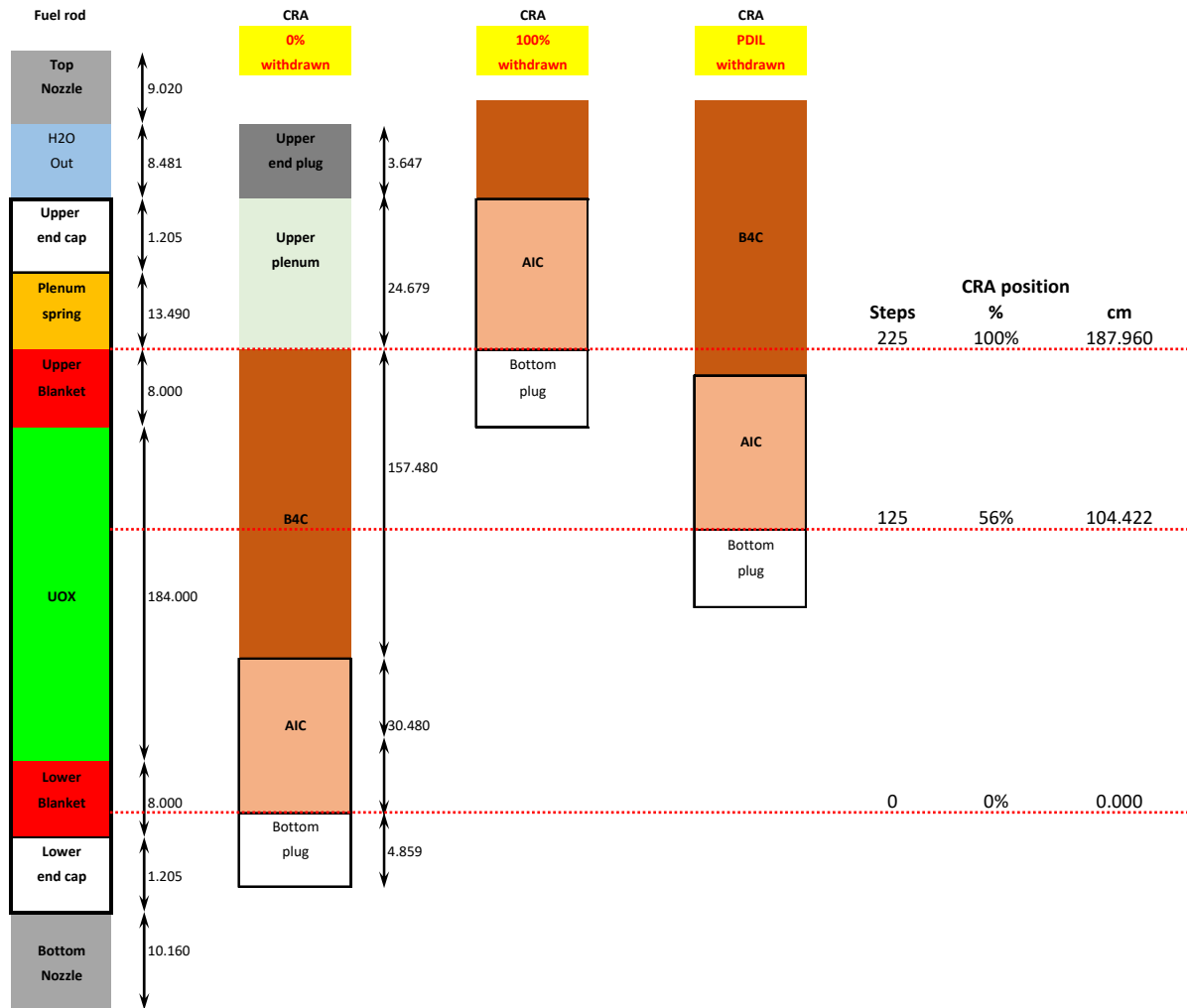


Figure 56. Clarification on CRA positioning.

### 5.1.3. Fuel rod thermal-physical properties

Two alternative approaches can be used:

- Application of own best-estimate dynamic fuel rod models
- Application of fixed thermal-physical properties as recommended in Table 17.

Table 17: Fixed thermal-physical properties of the fuel rod

Property	Units	Value
Fuel density	g/cm <sup>3</sup>	10.5216
Fuel thermal conductivity	W/(m · K)	3.5
Fuel specific heat	J/(kg · K)	290
Clad density	g/cm <sup>3</sup>	6.5500
Clad thermal conductivity	W/(m · K)	13.0
Clad specific heat	J/(kg · K)	300
Gap conductance	W/(m <sup>2</sup> · K)	10000

### 5.1.4. Effective Doppler temperature for XS data

It is recommended to estimate the effective Doppler temperature ( $T_f$ ) from the fuel surface temperature ( $T_{f,s}$ ) and the fuel centerline temperature ( $T_{f,c}$ ) using the following expression:

$$T_f = \alpha \cdot T_{f,s} + (1 - \alpha) \cdot T_{f,c} \quad \text{Eq. 1}$$

with  $\alpha=0.7$ .

### 5.1.5. Sequence of Events

- $t \leq 0$ : the system is first made critical at the core state and power level specified for the transient scenario by adjusting CBC.
- $0.0 \leq t \leq 0.1$  sec: CRA assembly is ejected from the core at a constant speed within 0.1 sec.
- $0.1 \leq t \leq 2.0$  sec: Transient without any additional changes applied to the system.
- $2.0 \leq t \leq 3.0$  sec: SCRAM at a constant speed within 1.0 sec. All CRAs except a) ejected rod; b) stuck rod (see Table 18)
- $3.0 \leq t \leq 4.0$  sec: Transient without any additional changes applied to the system.

Table 18: Initial position of CRA banks, ejected and stuck CRAs

Initial position				Ejected CRA	Stuck CRA
% withdrawal					
RE1	RE2	SH3	SH4		
100	56	100	100	A4 (RE2)	B5 (SH4)

## 5.2. HZDR Models - Serpent/DYN3D

### 5.2.1. Cross section library

The library of the four-group homogenized fuel properties (XS) for DYN3D is generated with Monte Carlo code Serpent 2.1.32 applying ENDF/B-VII.1 nuclear data. The XS methodology is described in the deliverable D3.2 [2]. The range of feedback parameters is shown in Table 19.

Table 19: Range of feedback parameters of RIA XS-library used by DYN3D

Feedback parameter	Number of points	Min. value	Max. value
Moderator density, g/cc	6	0.3	0.9
Fuel temperature, K	3	500	1800
Boron concentration, ppm	3	0	2000

Linear interpolation is applied between table points for moderator density and boron concentration. Square root linear interpolation is used for fuel temperature.

### 5.2.2. Nodal code modelling

The RIA was modeled with the DYN3D nodal diffusion code comprising the build-in thermo-hydraulic solver.

Main modeling assumptions:

- radial discretization 4 nodes per fuel assembly;
- fixed time step 0.001 sec.;
- each radial node represented as TH channel (4 channel per assembly);
- no cross-flows are modeled between channels;
- hottest pin is represented by a “hot channel” with corresponding power peak factor;
- TH fuel properties are fixed to the benchmark specification values;
- DNBR calculated using the BIASI correlation.

### 5.3. VTT Model - Serpent/ANTS

#### 5.3.1. Cross section library

The library of the four-group homogenized fuel properties (XS) for Ants is based on the same data as the DYN3D library. The XS are parametrized according to the following polynomial model:

$$\Sigma(T_f, \rho_c, \rho_B) = \Sigma(T_f^0, \rho_c^0, \rho_B^0) + c_1 \Delta \sqrt{T_f} + c_2 (\Delta \sqrt{T_f})^2 + c_3 \Delta \rho_c + c_4 (\Delta \rho_c)^2 + c_5 (\Delta \rho_c)^3 + c_6 \Delta \rho_B + c_7 (\Delta \rho_B)^2 + c_8 (\Delta \rho_B)^3 + c_9 \Delta \rho_c \rho_B$$

where:

- $\Sigma(T_f^0, \rho_c^0, \rho_B^0)$  is the value of the group constant at the nominal point  $(T_f^0, \rho_c^0, \rho_B^0)$
- $T_f$  is the fuel temperature (K)
- $\rho_c$  is the coolant density (g/cm<sup>3</sup>)
- $\rho_B$  is the coolant boron density (ppm\*g/cm<sup>3</sup>)
- $\Delta$  represents the absolute deviation of a feedback variable from the nominal point i.e.  $\Delta \sqrt{T_f} = \sqrt{T_f} - \sqrt{T_f^0}$ , etc.
- $c_i$  are the polynomial coefficients fitted based on the values of each group constant at the group constant generation branch points.

The nominal point for the polynomial fit was (900 K, 0.8 g/cm<sup>3</sup>, 800 ppm\*g/cm<sup>3</sup>).

#### 5.3.2. Nodal code modelling

The RIA was modeled with the Ants nodal diffusion solver coupled to the SUBCHANFLOW thermo-hydraulic solver.

Main modeling assumptions:

- radial discretization:
  - 2x2 = 4 nodes per fuel assembly in neutronics;
  - pin- and subchannel resolved thermal-hydraulics model (channel centered coolant mesh);
- fixed time step 0.001 sec.;
- pin-power reconstruction used in Ants to evaluate the power in each individual fuel rod;
- the power from each Ants pin was mapped to corresponding pin in the SUBCHANFLOW model;
- TH fuel properties are fixed to the benchmark specification values;
- a Doppler temperature was calculated separately for each SUBCHANFLOW fuel rod based on their surface ( $T^{\text{surf}}$ ) and centerline ( $T^{\text{center}}$ ) temperatures.
- $T_f^{\text{Doppler}} = 0.7 \times T^{\text{surf}} + 0.3 \times T^{\text{center}}$
- the thermal hydraulic state for coolant (from subchannels) and fuel (from rods) was mapped from SUBCHANFLOW to Ants calculation nodes (1/4 assembly) using volume based averaging;
- cross-flows between subchannels was allowed;
- as all fuel rods are individually modelled by SUBCHANFLOW, the maximum fuel temperature is the maximum centerline fuel temperature over all rods in the core.
- similarly, minimum DNBR is obtained as the minimum of all DNBR values evaluated by SUBCHANFLOW;
- DNBR is calculated using the BIASI correlation.

## 5.4. TBL Models - WIMS10/PANTHER

### 5.4.1. Fuel & reflector model

The nuclear constants for fuel and reflector constituents are generated by means of the lattice code WIMS10 ru2 and the ENDF/B VII.1 library of microscopic data (XMAS scheme of 172 energy groups). The neutron transport problem is solved by means of a method of characteristics in 2D considering 22 neutron groups, and results in 2-group, homogenized constants in infinite medium.

### 5.4.2. Fuel constituents

The model follows the specification of geometry and composition as closely as possible, with some minor deviations introduced for practical reasons or imposed by code limitations:

- the cladding material of fuel and absorber rods is mixed with the He-filled gap
- zones with and without grid are modelled separately, resulting in three sets of nuclear constants per assembly type
- grid masses are best-estimate and the grid material is homogenized with the coolant
- the tip of absorber rods (plenum + cap) is not modelled;
- exact isotope compositions are only possible for He, B, Ag, Gd and U
- WIMS10 default compositions apply to C, O, Si, Cr, Mn, Fe, Ni, Zr, Cd, In and Sn

The dependency on boron, coolant density and temperature is tabulated for a grid of 0, 550, 1200 and 1800 ppm by 600, 675, 753, 796 and 860 kg/m<sup>3</sup> by 531, 557 and 592 K (at a fuel temperature of 900 K). The dependency on fuel temperature is represented by a set of coefficients derived from the above combinations and extra perturbations at 500 and 1300 K (at a boron concentration of 550 ppm and a coolant density and temperature of 675 kg/m<sup>3</sup> and 557 K).

### 5.4.3. Reflector constituents

The reflector constants are derived from a rectangular supercell calculation with roughly two parts fuel and one part reflector. The method requires some approximations:

- axial geometry cannot be truthfully represented in 2D and needs to be transposed to a planar equivalent;
- the zone above the fissile column is sliced up in 4 homogenized zones, representing the different material composition of the axial sections with springs, top caps, water and top nozzle (accounting for the water filled guide tubes where appropriate). For simplicity, the He in the spring plenum was omitted and for the spring mass, a best-estimate value was used;
- likewise, the zone below the fissile column is sliced up in 3 homogenized zones, representing the bottom caps, water and bottom nozzle;
- in the radial model, the varying thickness of the zone between the outer boundaries of the core and its barrel cannot be truthfully represented. Instead, two types of radial reflector were created: a thick one, to be placed in F:1 and symmetric positions, and a thin one, to be placed in all other reflector positions.

The dependency on boron and coolant density is tabulated for a grid 0, 550, 1200 and 1800 ppm by 725, 796 and 851 kg/m<sup>3</sup> for the bottom and radial reflectors. The density axis for the top reflector has points at 643, 753 and 851 kg/m<sup>3</sup>.

### 5.4.4. Core model

Core simulations are performed with PANTHER 5.6.6, a 2-group neutron diffusion code that applies a nodal method on a coarse 3D mesh. The fine-grained power distribution is accessible through pin power reconstruction. PANTHER has a built-in module, derived from VIPRE-01, for the calculation of thermal and thermal-hydraulic feedback, based on the concept of an equivalent pin in a closed channel at constant pressure.

The reactor height is subdivided in 48 axial layers of varying thickness: 4 layers of 8 cm for the axial reflectors and 44 core layers between 3.5 and 4.6 cm. The irregular axial discretization is a direct

consequence of the explicit grid model. Radially, there are 4 nodes per assembly. The TH module operates on a sub-mesh of nine concentric annuli per node in the main mesh: six in the fuel pellet and one for each of the gap, cladding and coolant.

#### **5.4.5. Transient model**

The transient was simulated with a timestep of 2 ms.

### **5.5. PEL Models - CASMO5/SIMULATE5/S3K**

#### **5.5.1. Cross section generation**

Cross sections are generated with CASMO5 version 2.08 [22]. The code uses a pre-compiled 586-group LWR library based on ENDF/B-VII.1 and uses the methods of characteristics to solve the 2-dimensional neutron transport equation. Cross sections assume a full geometry layout without internal symmetry conditions and are condensed into a 4-group format for reactor simulations. Fuel assembly geometry is an infinite lattice of identical fuel assemblies. The branch calculations consider boron concentrations between 0.1 and 2400 ppm, fuel temperatures between 293K and 1500K, moderator temperatures between 293K and 602K and configurations without control rod, inserted control rod tip and inserted control rod body. Moreover, branches with and without fission products and Xenon and Samarium are included.

#### **5.5.2. Steady state calculations**

Steady state reactor conditions before the transient are determined with SIMULATE5 version 1.19 [23]. Fuel assemblies are treated with four radial sub-nodes per assembly and 25 axial nodes. The three-dimensional multigroup diffusion equations are solved by the analytic nodal method. During the solution process fuel assemblies are axially divided into sub-nodes such that they are always materially uniform. Hence during inserted control rods sub-node boundaries change from assembly to assembly.

#### **5.5.3. Transient calculations**

Transient calculations are done with S3K version 2.08 [24] based on a steady-state SIMULATE5 restart file. S3K uses a six-group model for delayed neutron precursors and is based on a transient version of the 3-dimensional QPANDA nodal solution method. The core is nodalized with one thermal-hydraulic channel per fuel assembly without cross flow. The hydraulic model uses a 5-equation, fully implicit representation. Fuel-pin temperatures and heat fluxes are computed using a 1-dimensional radial finite-difference heat conduction equation with burnup- and temperature-dependent properties. Pin-by-pin power reconstruction can be requested in a post-processing step. Thermal-hydraulic feedback to nodal cross sections is computed using the above described CASMO5 cross section library. Time step size is set to a maximum of 0.01 seconds.

Sub-channel analysis is done in a one-way coupling mode after the S3K transient calculations are finished. Pin-by-pin power histories are transferred to a COBRA-TF version 2 [25] model which determines sub-channel parameters for each fuel assembly. The model locates each assembly in the center of a 3x3 fuel assembly matrix and solves the two-fluid, three-field representation of a potentially two-phase flow condition. Departure of nucleate boiling ratio is based on the Doroschuk lookup table.



## 5.6. Models (UJV)

### 5.6.1. Cross section generation

In this phase of the project we have focused on shifting the HELIOS/DYN3D workflow from `data case` calculations (where explicit, unparametrized cross-section data were given for each node, including control rods movement etc.) to a full-stack solution with complete parametrized libraries in a modern format for the DYN3D code.

The first step in this effort was to develop a module for building the DYN3D libraries in the modern NEMTAB (IWQS=22) format. This was achieved by adapting the former DynLib tool (used for generating the libraries in the legacy IWQS=2/3 formats) and creating a new version, DynLib2. The new version is built on top of our QUADRIGA3 framework, which allows to build lattice code (such as HELIOS) models. DynLib2 includes additional data needed for DYN3D libraries and handles the respective overhead that comes with the multidimensional interpolation approach, since the number of branch calculations needed exceeds the allowed calculation run size in HELIOS and the calculation space needs to be partitioned. Additional features as multi-segment control rod clusters need to be supported as well.

The HELIOS geometry and material models were described in the D3.2 deliverable report and were left unchanged.

### 5.6.2. Steady state calculations

As the DYN3D input files are rather complex (the input is mostly numeric instead of keyword-based) we have decided to build a frontend tool, called RDyn. It allows to build the DYN3D input files either using a simple DSL in the Ruby programming language or by converting an input deck for the ANDREA core physics code.

In order to be able to use HZDR cross-section libraries for validation and comparison, we also had to implement multigroup interface to DynLib2+RDyn, as DYN3D has a slightly different input file format for two-group and multigroup calculations.

The RDyn tool allows not only single state (and burnup) calculations, but also rod worth calculation (using the fixed-feedback option in DYN3D) and transient calculations with movement of control banks.

Example of the beginning of an input file generated with RDyn:

```
$ General (1):  
$ ICON = -1 -- steady state calculation, no restart file generated  
$ IWQS = 22 -- XS library  
$ using library IWQS22.nemtab with MD5 b481ce115acd697646c4b9af05f6da3b  
$ IREWIN = 0 -- store all steps  
$ TOTIM = 1440 -- Computer time for stopping the transient calculation in minutes  
$ DTREST = 3600 -- Time steps (problem time), after which the data needed for  
$ restart are transferred to the file exam_rs2.dat (to be given in s).  
-1 22 0 1440 3600  
$ General(2): ISTART -- data set on the restart file is used  
1  
$ General(3): STR -- solver  
CARTESIAN  
$ General(3a): STR_MAP -- give maps top to bottom  
STANDARD MAP INPUT  
$ METH, FINE, SPH... (tbd)  
$ General(5): IBKTYP -- CR / vver1000 - multiple segments of variable size  
5  
$ General(4a/b): power distribution -- no given -> nil
```

```
$ (6) SCON
CONTROL OF CALCULATION
$ ITIM = 1 - Output of 3-dimensional distribution on the binary file, exam_red.dat - flux output
$ IOINP = 3 - Output of all input data and maybe something more
$ IH1 = 0 - If the user has insight into details of code, some arrays will be printed to search
$       errors of the input data. Information about shifted VVER-440 control assemblies
$       will also be printed
$ IH2 = 2 - Listing of actual cross section of each node
$ IH3 = 0 - No output of addresses at the end of the iterations.
$ IH4 - dummy
$ IH5 = 1 - Output of fluxes and net currents at the node faces after steady- state calculation.
1 3 0 2 0 0 1
$ (8) SPHYD
FIXED FEEDBACK PARAMETERS
$ (9) I_PHYD - Standard steady-state calculation with output of feedback parameters
1
$ (10) SDI
DIMENSIONS OF ARRAYS
$ Dimensions (11):
$ ISYM = 360 - Whole core
$ NJMAX = 9 - Number of horizontal rows in the sector
$ NIMAX = 9 - Max. number of columns in sector
$ NCAS = 69 - Number of assemblies in the sector
$ NZ = 24 - Number of layers in z-direction
$ NOBOU = 36 - Number of outer faces of the assemblies in the radial sector
$ NOSYM = 0 - Number of faces of the assemblies at the symmetry boundaries of the sector
$ NOMAS = 55 - Number of different cross section types (material types)
$ NOBT = 2 - Number of different boundary conditions at the outer boundaries
360 9 9 69 24 36 0 55 2
```

We have successfully run the static calculations from the previous phase and the static and transient calculations from the REA benchmark task. The results were `sensible' and demonstrated that the developed tools are qualitatively in working order.

However, the results even for static calculations were unacceptably different from our reference (Monte Carlo / Serpent) calculations. We continue our effort to find the source of discrepancies and to provide an acceptable solution for both the static and transient calculations and will publish a separate report afterwards.

### **5.6.3. Transient calculations**

As mentioned in previous paragraph, up to now we were not able to find reason for the difference between our results and the reference results for the static (initial) state calculations. In such case any results of transient calculations are unfortunately not credible.

Currently, UJV continues to work on the problem and intends to solve the issue in the near future.

## 5.7. Results

This section summarizes the results of the NuScale RIA analysis performed with the DYN3D, Ants, Panther, and SIMULATE nodal diffusion codes.

First, a set of steady-state parameters are evaluated and compared to insure the consistency of the core models used by the participants. After that, a comparison of the transient results is carried out.

The integral steady-state core parameters such as nominal CBC, reactivity worth of the ejected RE2 CRA, and total SCRAM worth are compared in Figure 57. A comparison of radial power distributions at nominal state, after ejection of the regulation rod RE2, and after SCRAM is shown in Figure 58.

In general, all steady state integral parameters are in reasonable agreement. However, compared to other codes, SIMULATE shows somewhat higher CBC and ejected CRW and noticeably lower SCRAM worth.

Compared to DYN3D and Ants, the “nominal” radial power distribution estimated by Panther, and SIMULATE shows a slight tilt towards the core center. The maximum difference between two groups of codes is about 3.3%. A similar tendency can be observed for the radial power distribution after the ejection of the RE2 CRA. All codes show consistent agreement in prediction of radial power distribution of the SCRAMed core.

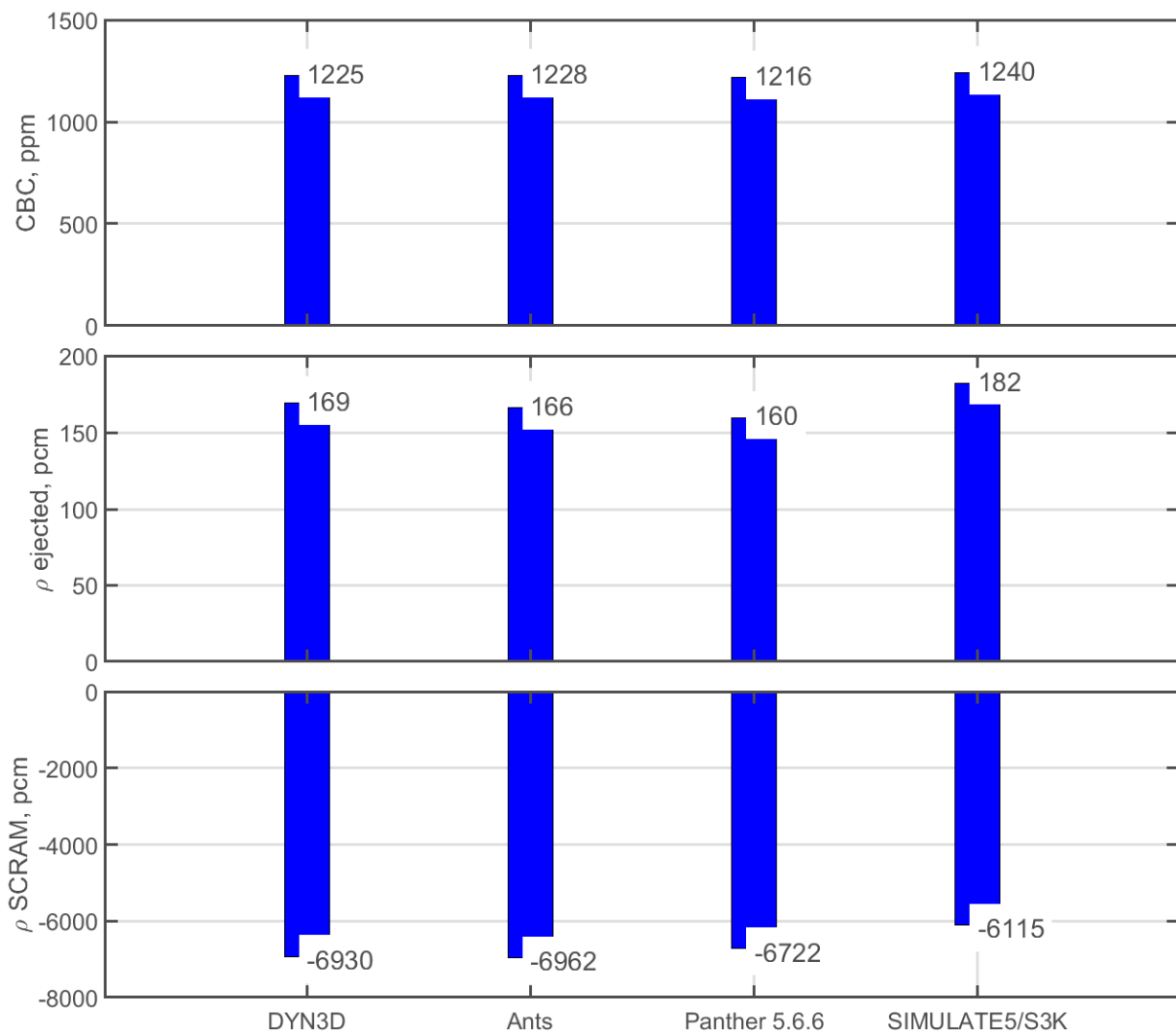


Figure 57. Integral core parameters from steady-state calculations

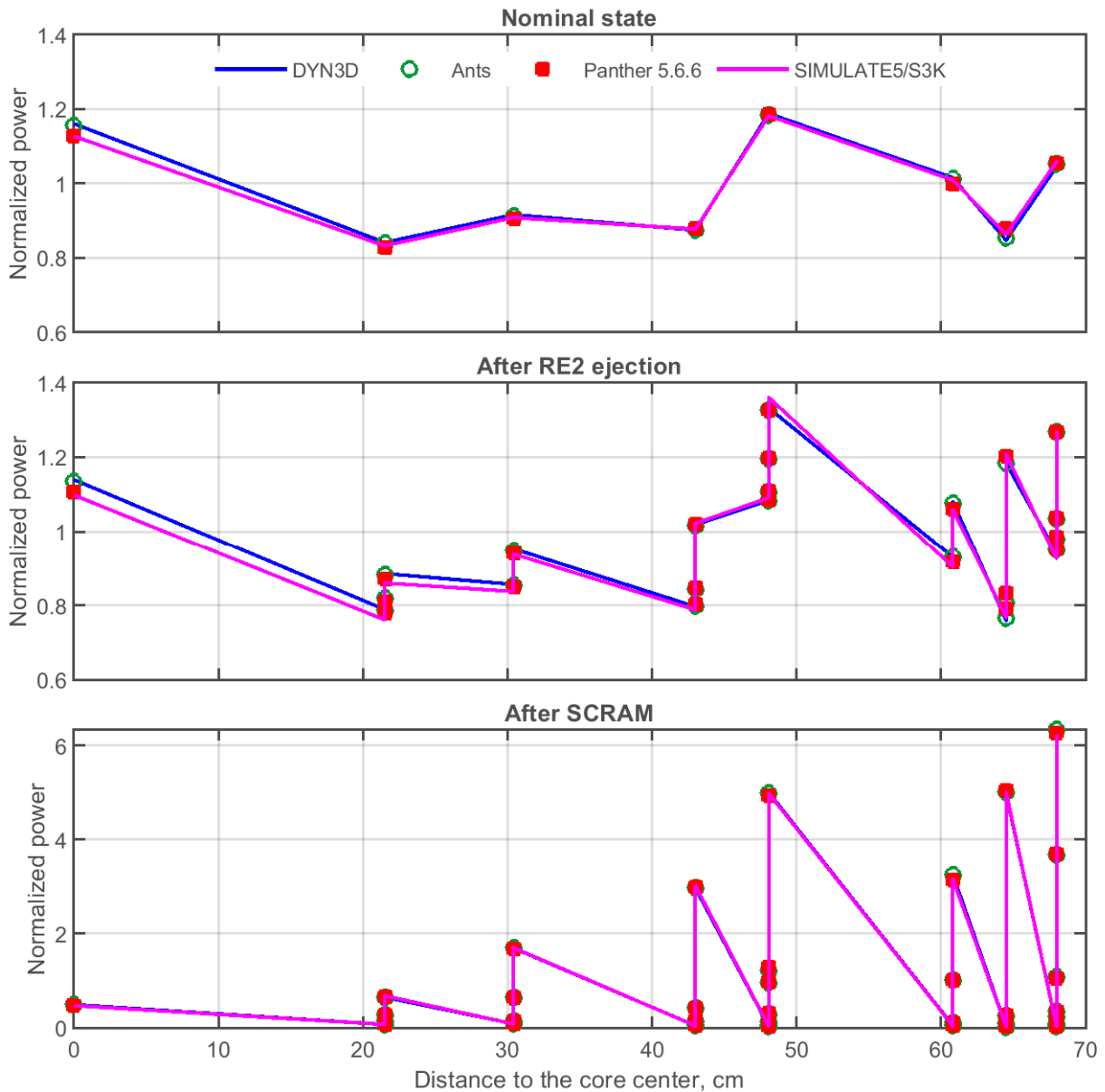


Figure 58. Radial power distribution from steady-state calculations.

The transient results are compared in Figure 59 and Figure 60. The simulated REA scenario is relatively mild and leads to a power rise from 75% to about 100% of nominal power. The maximum transient power

All codes predicted similar maximum power of 102.0%, 101.9%, 100.0%, and 102.4% for DYN3D, Ants, Panther, and SIMULATE respectively (upper panel of Figure 59). SIMULATE slightly overestimated the ejected reactivity which is in line with the steady state results. The ejected reactivity estimated via steady state and dynamic calculations are in very good agreement i.e. 169 vs. 170 pcm for DYN3D, 160 vs. 165 pcm for Panther, and 182 vs. 186 pcm for SIMULATE (middle panels of Figure 59). It should be noted that currently the Ants code is not capable of calculating dynamic reactivity. Lower panel of Figure 59 compares 3D core power peaking factor ( $F_q$ ). From 0 to 2 sec within the transient (before SCRAM), the difference in  $F_q$  between the codes does not exceed 0.1%. After SCRAM, the differences between the codes noticeably increased, especially for SIMULATE. Nevertheless, the importance of  $F_q$  is also reduced due to the fast drop in the core power after SCRAM.

The maximum centerline fuel temperature is compared in Figure 60. The peak fuel temperature was observed around 2.1 sec after the initiation of the transient. The peak values are spread between 812 and 861 °C. The temporal behavior of centerline fuel temperature, calculated by SIMULATE, differs noticeably from other codes.

Maximum cladding outer temperatures, showed in Figure 60 (2<sup>nd</sup> panel from top), agree within 2 °C up to about 3.3 sec. After that, the differences increase due to sharp drop in the total core power.

Despite very good agreement in  $F_q$ , there is a very large difference in estimated DNBR values. The main reason is different critical heat flux correlations used by the participants.

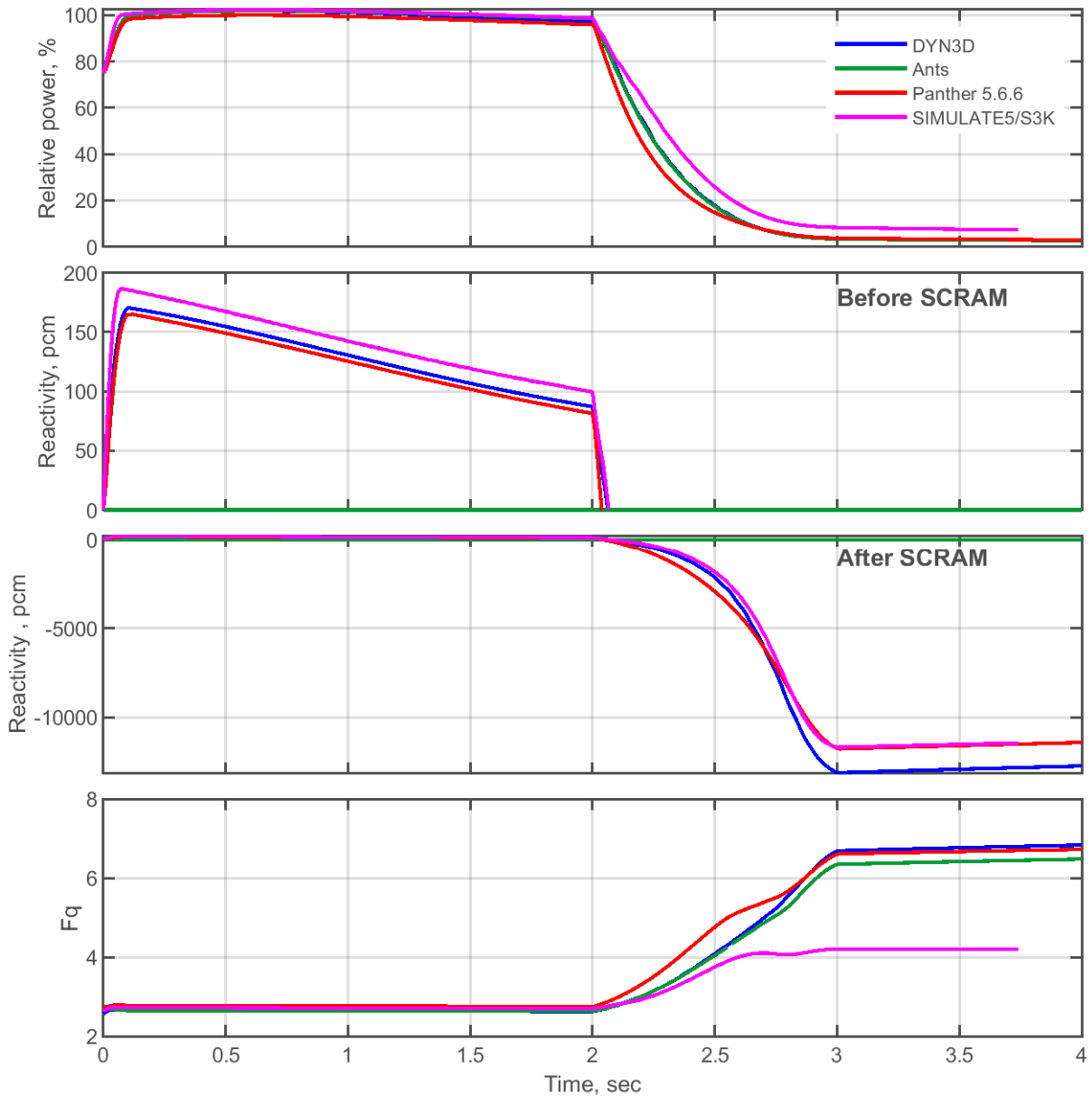


Figure 59. Transient power, reactivity, and core power peak.

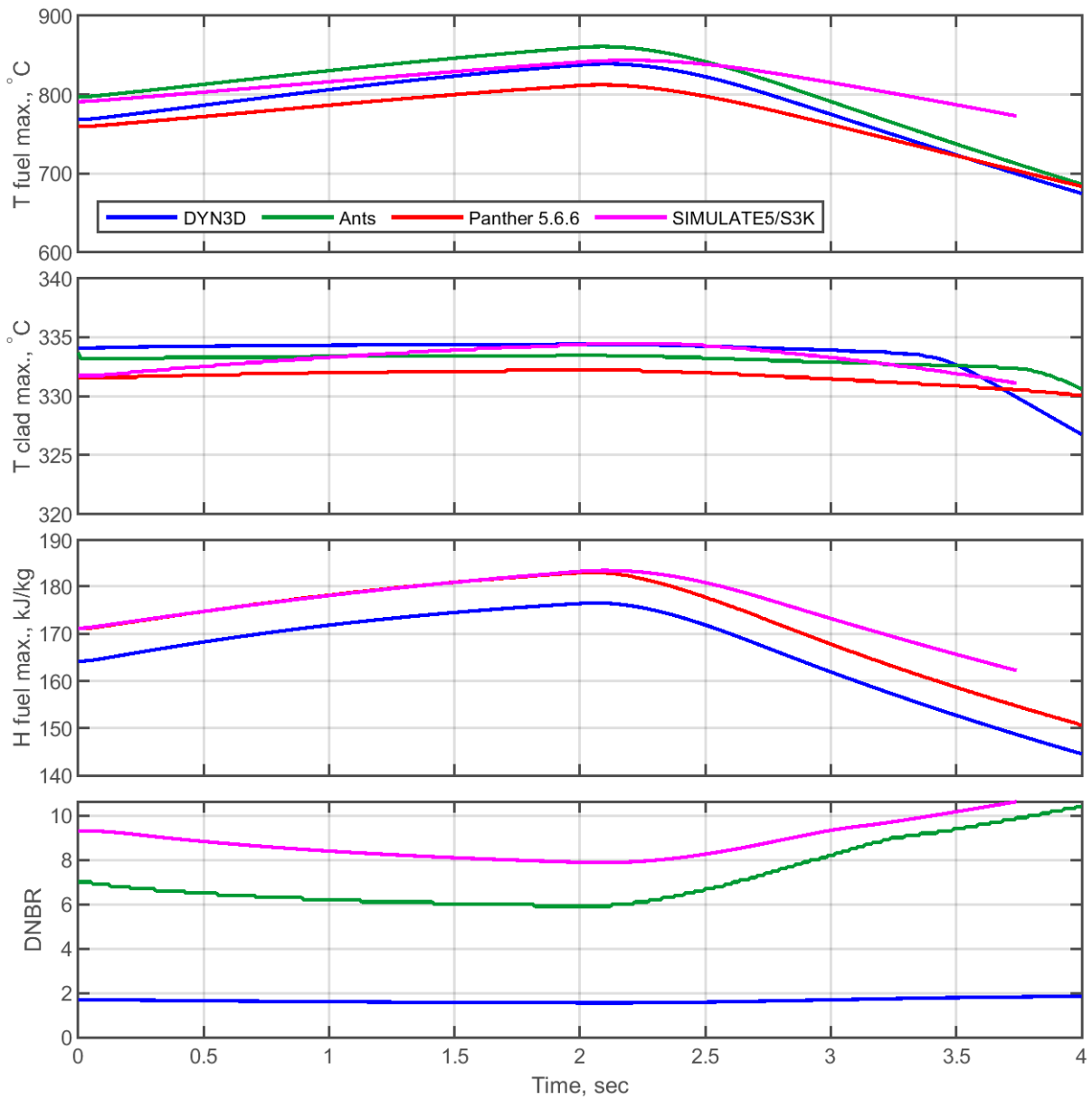


Figure 60. Transient fuel and clad temperatures, fuel enthalpy, and DNBR

## 6. Reference

- [1] VALTAVIRTA, V., FARD, A., FRIDMAN, E., LESTANI, H., and MERCATALI, L., McSAFER D3.1: Specifications for the reactivity transients scenarios in the four SMR cores, (2021).
- [2] FRIDMAN, E. *et al.*, McSAFER D3.2: Group constant generation for the state-of-the-art codes, (2021).
- [3] LEPPÄNEN, J., PUSA, M., VIITANEN, T., VALTAVIRTA, V., and KALTIAISENAHO, T., The Serpent Monte Carlo code: Status, development and applications in 2013, *Ann. Nucl. Energy* **82** (2015) 142.
- [4] WARD, A. . X. Y. . D. T., GenPMAXS – V6.2. Code for Generating the PARCS Cross Section Interface File PMAXS, Michigan, (2016).
- [5] DOWNAR, T. *et al.*, PARCS. NRC - v3.3.1 Release. Volume I: Input Manual,.
- [6] IMKE, U., User manual for SUBCHANFLOW 3.7.1, (2021).
- [7] The ICoCo API, . <https://docs.salome-platform.org/7/dev/MEDCoupling/icoco.html>
- [8] DOWNAR, T., XU, Y., and SEKER, V., PARCS v3.0 U.S. NRC Core Neutronics Simulator. Theory Manual, (2012).
- [9] CEA/DEN EFD R&D, OPEN CASCADE. (Version: 5.1.6). Salome Platform Documentation. MEDMEM library, . <https://docs.salome-platform.org/5/med/user/medmem.html>
- [10] GARCÍA, M., IMKE, U., FERRARO, D., SANCHEZ-ESPINOZA, V., and MERCATALI, L., Advanced modelling capabilities for pin-level subchannel analysis of PWR and VVER reactors, 2019.
- [11] JOHNSON, A. E., KOTLYAR, D., TERLIZZI, S., and RIDLEY, G., serpentTools: A Python Package for Expediting Analysis with Serpent, *Nucl. Sci. Eng.* **194** (2020).
- [12] GRANT, C., PUMA System Manual version 6, CNEA, MCO-06-REC-2 Rev.: 0., (2010).
- [13] GRANT, C., HUEMUL System Manual version 4, CNEA, MCO-06-REC-1 Rev.: 0, (2013).
- [14] GARCIA, M., Documentation of Python modules for PUMA and SUBCHANFLOW, CNEA, MA-EN\_GIN-FR-001 Rev.: 0., (2017).
- [15] High-Performance Advanced Methods and Experimental Investigations for the Safety Evaluation of Generic Small Modular Reactors– McSAFER. Horizon 2020. , Proposal number 945063, (2020).
- [16] ALZABEN, Y. I. ., Neutronics and Thermal-hydraulics Safety Related Investigations of an Innovative Boron-free Core Integrated Within a Generic Small Modular Reactor , Doctoral dissertation, Karlsruhe Institut für Technologie , 2019.
- [17] ALZABEN, Y., SANCHEZ-ESPINOZA, V. H., and STIEGLITZ, R., Core neutronics and safety characteristics of a boron-free core for Small Modular Reactors, *Ann. Nucl. Energy* **132** (2019).
- [18] ALZABEN, Y., SANCHEZ-ESPINOZA, V. H., and STIEGLITZ, R., Analysis of a control rod ejection accident in a boron-free small modular reactor with coupled neutronics/thermal-hydraulics code, *Ann. Nucl. Energy* **134** (2019).
- [19] WARD, A. . X. Y. . D. T., GenPMAXS – V6.3 Release. Code for Generating the PARCS Cross Section Interface File PMAXS, (2020).
- [20] VALTAVIRTA, V., Discussion forum for serpent users. Diffusion Coefficients at Different Reactor Regions - Discussion forum for Serpent users, . <https://ttuki.vtt.fi/serpent/viewtopic.php?f=15&t=3322&p=10380&hilit=transport%2Bcorrectio n#p10380> (accessed Feb. 14, 2022).

- [21] LEPPÄNEN, J. and RINTALA, A., Energy-dependent transport correction factor. Energy-dependent transport correction factor - Serpent Wiki, 2022. [http://serpent.vtt.fi/mediawiki/index.php/Energy-dependent\\_transport\\_correction\\_factor](http://serpent.vtt.fi/mediawiki/index.php/Energy-dependent_transport_correction_factor) (accessed Feb. 14, 2022).
- [22] RHODES, J., SMITH, K., and LEE, D., CASMO-5 development and applications, in *PHYSOR-2006 - American Nuclear Society's Topical Meeting on Reactor Physics*, 2006, **2006**.
- [23] BAHADIR, T. and LINDAHL, S. Ö., Studsvik's next generation nodal code SIMULATE-5, in *American Nuclear Society - 4th Topical Meeting on Advances in Nuclear Fuel Management 2009, ANFM IV*, 2009, **2**.
- [24] G. GRANDI, SIMULATE-3K, Models and Methodology, (2009).
- [25] AVRAMOVA, M. N. and SALKO, R. K., CTF Theory Manual, Oak Ridge, TN (United States), (2016).
- [25] D. Schneider, et al. (2016). APOLLO3® : CEA/DEN DETERMINISTIC MULTI-PURPOSE CODE FOR REACTOR PHYSICS ANALYSIS.
- [26] Mathieu Niezgoda. Description des modèles de fermetures et des corrélations de FLICA5. Technical report, Note technique DEN/DANS/DM2S/STMF/LMEC/2019-65392/A/DR, 2019.



## Appendix A: Verification of PARCS-ICoCo vs. Serpent (CAREM)

A neutronic stand-alone parametric study was done to assess the level of accuracy obtained from PARCS-ICoCo nodal calculation in comparison with a Monte Carlo calculation of the full core. The parameters studied were applied to full core calculation with temperatures and densities corresponding to Hot Full Power (HFP) nominal condition (Table 2) with its corresponding reflector properties. CRs were positioned at a configuration corresponding to criticality as shown in D3.2.

The following parameters were studied:

- Energy groups: 2, 4 and 8.
- Leakage model: infinite (INF) and fundamental mode (FM) calculated with CMM diffusion coefficient. In addition, the infinite leakage model with CMM diffusion coefficient calculation was used (INF+CMM).
- Transport Correction (TRC) for hydrogen in water at axial and radial reflectors.
- Use of DFs for FAs and radial reflector.
- All Rods Out (ARO) and All Rods In (ARI) configurations.

Table 20 shows the reactivity difference, and the Root Mean Square (RMS) and Maximum (Max) error of the axial power integrated in each plane and axially integrated FA power of PARCS-ICoCo solution compared to a SERPENT2 calculation taken as the reference solution. These tables include calculations with several leakage models for 2, 4, and 8 energy groups. In all cases, DFs and TRC were activated during calculations. It can be observed, in most cases, that there is an improvement of the parameters (mainly axially) with higher discretization of the energy. In the version of PARCS use for this study, pin power reconstruction (PPR) was not available for hexagonal geometry.

Table 20: PARCS-ICoCo -SERPENT2 discrepancies for critical HFP configuration using DFs and TRC. Several leakage models are shown. EG stands for energy groups.

EG	Leakage Model	Delta Rho [pcm]	Axial Power		FA Power	
			RMS [%]	MAX [%]	RMS [%]	MAX [%]
2	CMM	57	1.68	5.1	2.68	7.08
2	INF	-291	2.49	6.36	2.3	6.17
2	INF+CMM	-668	2.7	6.35	2.49	7.13
4	CMM	56	1.33	3.06	2.92	7.6
4	INF	66	0.93	2.11	2.65	6.91
4	INF+CMM	-227	0.75	1.75	2.65	7.22
8	CMM	84	1.17	3.06	2.74	7.09
8	INF	193	0.97	2.46	2.65	6.59
8	INF+CMM	-82	0.79	2.09	2.58	6.88

Table 21 shows the effect of the discontinuity factors for FAs and reflector. These cases were simulated under the same conditions as the reference case but with DFs deactivated. DFs introduce information on the continuity of the flux. The heterogeneous flux is continuous but this does not mean that the homogeneous flux will be. The effect is not as for cartesian geometry in the case of the SMART KSMR, where the solution improved. The discontinuity factors for this reactor was generated by SERPENT2, which, for the reflector DFs, uses an AFEN homogenous flux which is different from the TPEN approach used by PARCS. This could be a possible source of error.

Table 21: PARCS-ICoCo -SERPENT2 discrepancies for critical HFP configuration TRC (no DFs). Several leakage models are shown. EG stands for energy groups.

EG	Leakage Model	Delta Rho	Axial Power		FA Power	
		[pcm]	RMS [%]	MAX [%]	RMS [%]	MAX [%]
2	CMM	112	1.63	5.04	2.21	4.67
2	INF	-216	2.59	6.57	1.74	4.84
2	INF+CMM	-610	2.83	6.62	1.59	3.29
4	CMM	194	1.38	3.15	2.46	4.29
4	INF	282	0.99	2.01	2.46	4.79
4	INF+CMM	-80	0.85	1.8	2.1	4.06
8	CMM	271	1.2	3.05	2.42	4.28
8	INF	454	0.96	2.34	2.57	4.87
8	INF+CMM	110	0.82	2.05	2.2	4.17

Table 22 shows the effect of turning off the transport correction for hydrogen in water. There is a clear deterioration of the RMS in all cases.

Table 22: PARCS-ICoCo -SERPENT2 discrepancies for critical HFP configuration using DFs (no TRC). Several leakage models are shown. EG stands for energy groups.

EG	Leakage Model	Delta Rho	Axial Power		FA Power	
		[pcm]	RMS [%]	MAX [%]	RMS [%]	MAX [%]
2	CMM	360	1.54	4.43	3.55	8.94
2	INF	15	2.39	6.31	2.87	8.04
2	INF+CMM	-379	2.63	6.29	3.17	9.32
4	CMM	280	1.4	3.31	3.29	8.15
4	INF	330	1.03	2.44	3.02	7.63
4	INF+CMM	1	0.79	1.86	3.01	7.79
8	CMM	308	1.33	3.38	3.09	7.62
8	INF	457	1.17	2.87	2.98	7.67
8	INF+CMM	145	0.96	2.42	2.92	7.43

Table 23 shows the effect of turning off the transport correction for hydrogen in water and the DFs. There is a clear deterioration of the RMS and reactivity in all cases compared to the reference.

Table 23: PARCS-ICoCo - SERPENT2 discrepancies for critical HFP configuration (no DFs nor TRC). Several leakage models are shown. EG stands for energy groups.

EG	Leakage Model	Delta Rho	Axial Power		FA Power	
		[pcm]	RMS [%]	MAX [%]	RMS [%]	MAX [%]
2	CMM	456	1.58	4.65	3.21	5.43
2	INF	132	2.58	6.67	2.31	5.41
2	INF+CMM	-281	2.83	6.69	2.5	4.74
4	CMM	475	1.4	3.22	3.17	5.71
4	INF	611	1.01	2.25	3.13	6.43

<b>4</b>	INF+CMM	204	0.82	1.73	2.82	5.52
<b>8</b>	CMM	550	1.27	3.27	3.12	5.69
<b>8</b>	INF	781	1.05	2.64	3.24	6.49
<b>8</b>	INF+CMM	392	0.88	2.28	2.91	5.62

Finally, Table 24 and Table 25 show the results obtained for ARO and ARI configurations. The same trends as for the critical conditions were observed. The accuracy increases with the number of groups of energy used. As expected, ARO conditions yields better results than ARI conditions. This is because of the effect of strong absorbers being one of the limitations of the diffusion theory.

*Table 24: PARCS-ICoCo - SERPENT2 discrepancies for HFP ARO configuration using DFs and TRC. Several leakage models are shown. EG stands for energy groups.*

EG	Leakage Model	Delta Rho [pcm]	Axial Power		FA Power	
			RMS [%]	MAX [%]	RMS [%]	MAX [%]
<b>2</b>	CMM	128	1.19	4.23	1.99	5.52
<b>2</b>	INF	-99	2.35	5.87	2.31	4.3
<b>2</b>	INF+CMM	-415	3.01	6.82	2.39	6.41
<b>4</b>	CMM	88	1.09	2.36	2.09	6.36
<b>4</b>	INF	85	1.61	3.09	1.94	4.75
<b>4</b>	INF+CMM	-179	0.40	1.08	2.14	6.41
<b>8</b>	CMM	79	1.16	2.78	1.99	5.96
<b>8</b>	INF	180	1.83	3.33	1.9	4.08
<b>8</b>	INF+CMM	122	0.82	1.85	2.04	5.98

*Table 25: PARCS-ICoCo - SERPENT2 discrepancies for HFP ARI configuration using DFs and TRC. Several leakage models are shown. EG stands for energy groups.*

EG	Leakage Model	Delta Rho [pcm]	Axial Power		FA Power	
			RMS [%]	MAX [%]	RMS [%]	MAX [%]
<b>2</b>	CMM	-66	1.86	4.97	3.53	8.21
<b>2</b>	INF	-598	3.15	8.69	4.65	7.82
<b>2</b>	INF+CMM	-1030	3.62	8.79	4.52	7.56
<b>4</b>	CMM	260	0.27	0.57	5.07	13.63
<b>4</b>	INF	341	0.61	2.06	4.9	13.27
<b>4</b>	INF+CMM	68	0.75	1.51	4.4	10.52
<b>8</b>	CMM	349	0.4	1.23	4.79	12.84
<b>8</b>	INF	472	0.75	3.12	4.91	13.55
<b>8</b>	INF+CMM	222	0.6	1.88	4.38	10.95

The neutronics stand-alone PARCS-ICoCo model using FM CMM leakage model, DFs and TRC with 2 energy groups used for Section 2.4 is compared with the SERPENT2 full core model. Table 26 and Table 27 show the results. An overall good agreement is found.

Table 26: Reactivity calculations for all states (CZP, HZP, HFP) with stand-alone neutronics using CMM leakage model, DFs and TRC. EG stands for energy groups.

		Multiplication Factor (k-eff)			Reactivity ( $\rho$ )		Difference
		PARCS-ICoCo	SERPENT	SERPENT	PARCS-ICoCo	SERPENT	SERPENT-PARCS-ICoCo
		Value [a.u.]	Value [a.u.]	Error [a.u.]	Value [pcm]	Value [pcm]	Value [pcm]
HFP	ARO	1.05835	1.05978	1.00E-05	5513	5641	128
	ARI	0.83166	0.83121	1.00E-05	-20241	-20307	-66
	ROD WORTH	--	--	--	25754	25948	194
HZP	ARO	1.11748	1.12066	1.00E-05	10513	10767	254
	ARI	0.88794	0.88717	1.00E-05	-12620	-12717	-97
	ROD WORTH	--	--	--	23133	23484	351
CZP	ARO	1.16479	1.16795	1.00E-05	14148	14380	232
	ARI	0.96034	0.95884	1.00E-05	-4130	-4293	-163
	ROD WORTH	--	--	--	18278	18673	395

Table 27: Reactivity calculations for all states (CZP, HZP, HFP) with stand-alone neutronics using CMM leakage model, DFs and TRC. EG stands for energy groups.

		EG	Leakage Model	Delta Rho	Axial Power		FA Power	
				[pcm]	RMS [%]	MAX [%]	RMS [%]	MAX [%]
HFP	ARO	2	CMM	128	1.19	4.23	1.99	5.52
	ARI	2	CMM	-66	1.86	4.97	3.53	8.21
HZP	ARO	2	CMM	254	1.21	4.27	1.93	4.57
	ARI	2	CMM	-97	1.09	3.23	2.8	5.32
CZP	ARO	2	CMM	232	2.06	5.82	3.5	7.8
	ARI	2	CMM	-163	1.78	4.12	4.24	7.07

The critical HFP configuration comparison is shown in Table 28. The axial power value and relative difference for PARCS-ICoCo and SERPENT2 models can be observed in Figure 61 and Figure 62. Its main discrepancy is near the reflector as expected, however, by increasing the number of energy groups, the solution improves as shown in Figure 63 and Figure 64. Finally, Figure 65 and Figure 66 show the axially integrated radial power distribution and the difference with the SERPENT2 full core model. We can observe that most of the discrepancies are either in the borders next to the reflectors or near the center where the control rods are inserted.

Table 28: PARCS-ICoCo - SERPENT2 discrepancies for critical HFP configuration with stand-alone neutronics using CMM leakage model, DFs, CDFs and TRC. EG stands for energy groups.

EG	Leakage Model	Delta Rho	Axial Power		FA Power	
		[pcm]	RMS [%]	MAX [%]	RMS [%]	MAX [%]
2	CMM	57	1.68	5.1	2.68	7.08

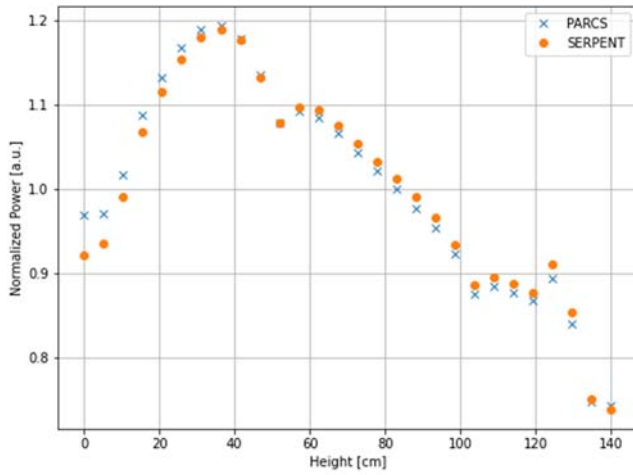


Figure 61: PARCS-ICoCo -SERPENT2 Normalized axial power comparison for critical HFP configuration using CMM leakage model, DFs, CDFs and TRC with 2 energy groups.

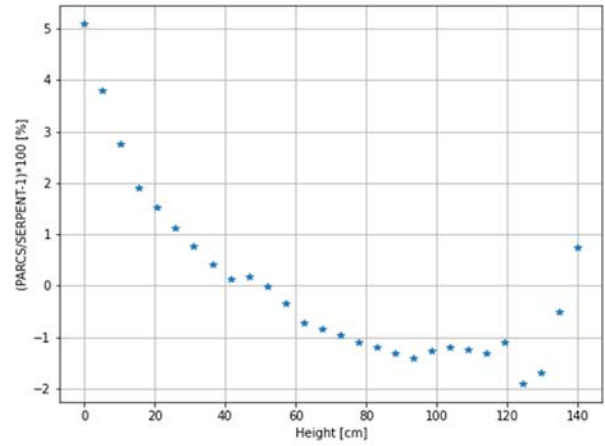


Figure 62: PARCS-ICoCo -SERPENT2 Normalized axial power comparison for critical HFP configuration using CMM leakage model, DFs, CDFs and TRC with 2 energy groups.

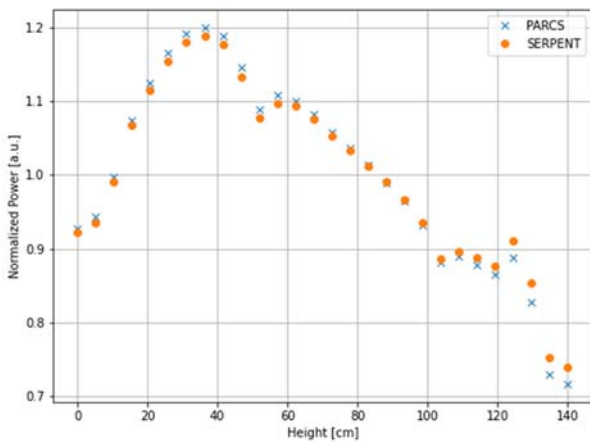


Figure 63: PARCS-ICoCo -SERPENT2 Normalized axial power comparison for critical HFP configuration using CMM leakage model, DFs, CDFs and TRC with 4 energy groups.

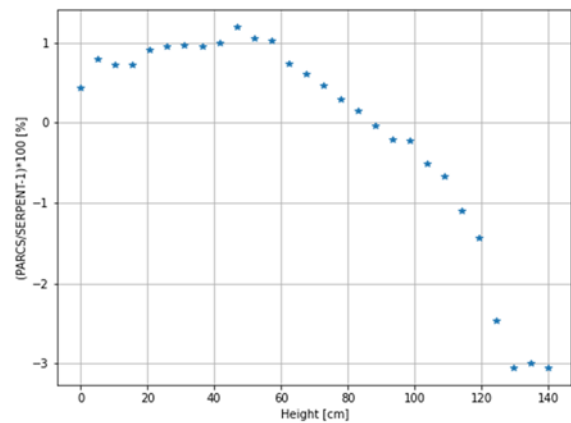


Figure 64: PARCS-ICoCo -SERPENT2 Normalized axial power comparison for critical HFP configuration using CMM leakage model, DFs, CDFs and TRC with 4 energy groups.

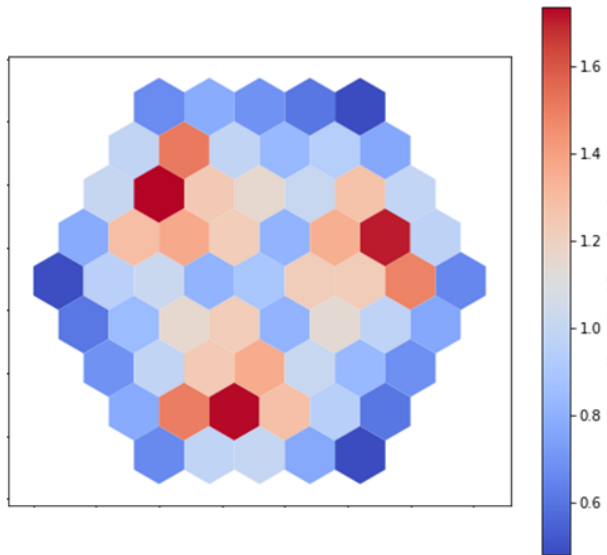


Figure 65: PARCS-ICoCo -SERPENT2 axially integrated FA normalized radial power using CMM leakage model, DFs, CDFs and TRC with 2 energy groups.

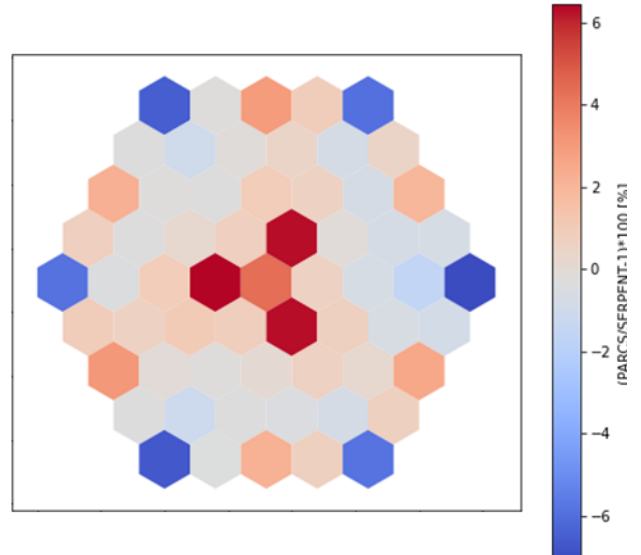


Figure 66: PARCS-ICoCo -SERPENT2 axially integrated FA normalized radial power relative difference using CMM leakage model, DFs and TRC with 2 groups.

## Appendix B: Verification of PARCS-ICoCo vs. Serpent (SMART)

As pointed out in Section 3, a first neutronic stand-alone parametric study was done to assess the level of accuracy obtained from the nodal calculation in comparison with a Monte Carlo calculation of the full core. The parameters studied were applied to full core calculation with temperatures and densities corresponding to Hot Full Power (HFP) average conditions (Table 29) and CRs at a configuration corresponding to criticality as shown in Figure 67. Reflector properties stayed the same as for HZP.

Table 29 Hot Full Power temperatures and densities

	Fuel Temperature [K]	Coolant Temperature [K]	Coolant Density [kg/m <sup>3</sup> ]
HFP	900	590	0.6870

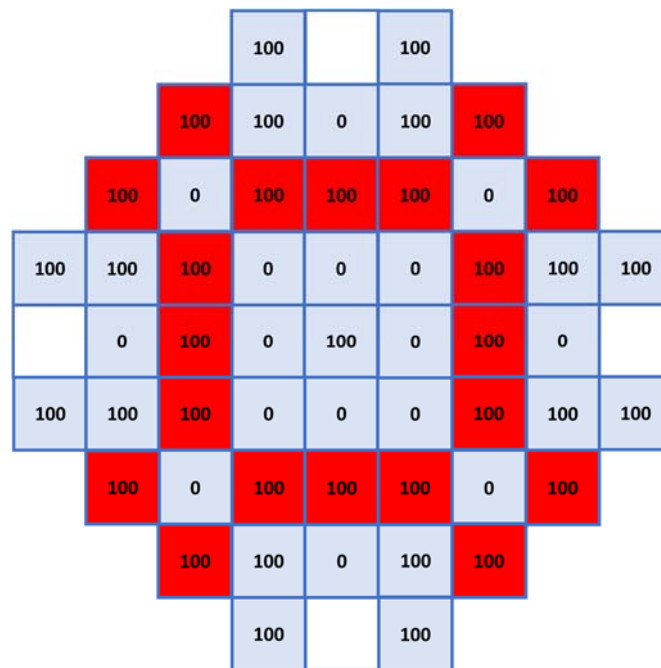


Figure 67 REA initial CRs configuration at HFP condition.

(Note: “100” means CR is fully extracted and “0” means CR is fully inserted; “White-boxes” mean there is no CR at that position) Based on D3.1 [1].

New FAs and reflectors XS were generated with SERPENT v2.1.32 for the following parameters to be studied:

- Subnodalization: 1 and 4 subnodes.
- Energy groups: 2, 4 and 8.
- Leakage model: infinite (INF), B1-mode and fundamental mode (FM) calculated with CMM diffusion coefficient. In addition, the infinite leakage model with CMM diffusion coefficient calculation was used (INF+CMM).
- Transport Correction (TRC) for hydrogen in water at axial and radial reflectors.
- Use of DFs for FAs and radial reflector
- Use of CDFs for FAs and radial reflector (only for PPR)
- All Rods Out (ARO) and All Rods In (ARI) configurations

Table 30 and Table 31 show the reactivity difference ( $\Delta\rho$ ), and the Root Mean Square (RMS) and Maximum (MAX) error of the axial power integrated in each plane, integrated FA power and integrated pin power of PARCS-ICoCo solution compared to a SERPENT2 calculation taken as the reference solution. These tables include calculations with several leakage models for 2, 4, and 8 energy groups and 1 and 4 subnodes inside each FA. In all cases, DFs, CDFs and TRC were

activated during calculations. It can be observed, in most cases, that there is an improvement of the parameters (mainly radially) with higher discretization of the energy. It should be noticed that an increase of subnodalization did not cause an improvement of the solution except for INF and INF+CMM cases at 2 energy groups. Pin power reconstruction also gets worse with subnodes but this could be due to a deterioration of the nodal solution and not an error in the PPR technique. In the version of PARCS use for this study, PPR was only available for 2 groups calculations.

Table 30 PARCS-ICoCo -SERPENT2 discrepancies for critical HFP configuration using DFs, CDFs and TRC. Several leakage models are shown for 1 subnode calculations. EG stands for energy groups and SN for subnodes.

EG	SN	Leakage Model	$\Delta\rho$	Axial Power		FA Power		PIN Power	
			[pcm]	RMS [%]	MAX [%]	RMS [%]	MAX [%]	RMS [%]	MAX [%]
2	1	INF	-386	1.35	4.42	3.55	4.98	4.54	16.31
2	1	INF+CMM	-606	2.27	5.62	4.25	7.4	5.24	15.27
2	1	CMM	89	2.29	3.36	1.49	2.69	2.39	12.00
2	1	B1	-164	0.86	1.46	0.84	1.41	2.53	11.41
4	1	INF	-14	2.36	3.68	1.40	3.87	N/A	N/A
4	1	INF+CMM	-186	1.22	2.84	1.19	2.82	N/A	N/A
4	1	CMM	89	2.61	5.57	1.64	3.55	N/A	N/A
4	1	B1	-157	1.39	4.19	0.85	1.70	N/A	N/A
8	1	INF	27	2.43	3.77	1.37	3.63	N/A	N/A
8	1	INF+CMM	-138	1.29	2.95	1.03	2.62	N/A	N/A
8	1	CMM	23	2.09	4.52	1.20	2.47	N/A	N/A

Table 31 PARCS-ICoCo -SERPENT2 discrepancies for critical HFP configuration using DFs, CDFs and TRC. Several leakage models are shown for 4 subnodes calculations. EG stands for energy groups and SN for subnodes.

EG	SN	Leakage Model	$\Delta\rho$	Axial Power		FA Power		PIN Power	
			[pcm]	RMS [%]	MAX [%]	RMS [%]	MAX [%]	RMS [%]	MAX [%]
2	4	INF	-187	1.21	3.62	2.60	4.31	3.68	16.31
2	4	INF+CMM	-393	1.74	4.71	3.15	5.34	4.24	15.25
2	4	CMM	275	2.72	4.11	2.37	5.09	2.64	15.79
2	4	B1	43	1.37	2.37	1.19	2.08	2.21	16.00
4	4	INF	167	2.77	4.36	1.62	4.74	N/A	N/A
4	4	INF+CMM	8	1.67	3.60	0.93	2.22	N/A	N/A
4	4	CMM	275	3.05	6.30	2.53	5.99	N/A	N/A
4	4	B1	50	1.87	5.07	1.28	2.85	N/A	N/A
8	4	INF	219	2.85	4.46	1.80	5.45	N/A	N/A
8	4	INF+CMM	68	1.77	3.72	1.11	2.61	N/A	N/A
8	4	CMM	223	2.56	5.28	2.10	5.07	N/A	N/A

Table 32 and Table 33 show the effect of the discontinuity factors for FAs and reflector. These cases were simulated under the same conditions as the reference case but with DFs deactivated. DFs introduce information on the continuity of the flux. The heterogeneous flux is continuous but this does not mean that the homogeneous flux will be. The effect is quite explicit for all cases.



Table 32 PARCS-ICoCo -SERPENT2 discrepancies for critical HFP configuration using CDFs and TRC (no DFs). Several leakage models are shown for 1 subnode calculations. EG stands for energy groups and SN for subnodes.

EG	SN	Leakage Model	$\Delta\rho$ [pcm]	Axial Power		FA Power		PIN Power	
				RMS [%]	MAX [%]	RMS [%]	MAX [%]	RMS [%]	MAX [%]
2	1	INF	-1809	1.84	3.87	16.32	25.04	25.65	126.69
2	1	INF+CMM	-2079	2.57	5.54	17.42	28.91	26.17	125.77
2	1	CMM	-1309	2.43	5.06	12.56	20.82	22.36	117.51
2	1	B1	-1521	1.41	3.28	13.29	22.97	22.48	116.08
4	1	INF	-1375	2.57	4.74	13.03	19.70	N/A	N/A
4	1	INF+CMM	-1607	1.52	3.37	13.98	23.47	N/A	N/A
4	1	CMM	-1304	2.52	4.78	12.26	20.07	N/A	N/A
4	1	B1	-1514	1.50	3.61	13.06	22.39	N/A	N/A
8	1	INF	-1325	2.71	4.87	12.80	19.19	N/A	N/A
8	1	INF+CMM	-1543	1.63	3.45	13.70	22.81	N/A	N/A
8	1	CMM	-1366	2.22	4.12	12.69	20.83	N/A	N/A

Table 33 PARCS-ICoCo -SERPENT2 discrepancies for critical HFP configuration using CDFs and TRC (no DFs). Several leakage models are shown for 4 subnodes calculations. EG stands for energy groups and SN for subnodes.

EG	SN	Leakage Model	$\Delta\rho$ [pcm]	Axial Power		FA Power		PIN Power	
				RMS [%]	MAX [%]	RMS [%]	MAX [%]	RMS [%]	MAX [%]
2	4	INF	-1844	1.88	3.79	16.73	25.72	26.84	148.42
2	4	INF+CMM	-2103	2.52	5.41	17.82	29.46	27.33	146.46
2	4	CMM	-1346	2.51	5.23	13.05	21.56	23.53	137.87
2	4	B1	-1544	1.53	3.54	13.76	23.58	23.67	135.96
4	4	INF	-1380	2.67	4.92	13.23	20.09	N/A	N/A
4	4	INF+CMM	-1602	1.64	3.62	14.18	23.75	N/A	N/A
4	4	CMM	-1303	2.65	4.90	12.50	20.40	N/A	N/A
4	4	B1	-1499	1.64	3.84	13.29	22.60	N/A	N/A
8	4	INF	-1335	2.81	5.06	13.02	19.68	N/A	N/A
8	4	INF+CMM	-1544	1.75	3.69	13.92	23.18	N/A	N/A
8	4	CMM	-1369	2.33	4.34	12.92	21.24	N/A	N/A

Table 34 and Table 35 show the effect of the CDFs by deactivating them. This only affects PPR calculations for cartesian geometries in PARCS<sup>7</sup> and not the nodal solution. Since the 2 groups PPR is the only option available, the CDFs effect is shown for these cases. A clear deterioration of the solution was observed.

<sup>7</sup> In hexagonal geometries it is used also in the nodal calculation.

Table 34 PARCS-ICoCo -SERPENT2 discrepancies for critical HFP configuration using DFs and TRC (no CDFs). Several leakage models are shown for 1 subnode calculations. EG stands for energy groups and SN for subnodes.

EG	SN	Leakage Model	$\Delta\rho$ [pcm]	Axial Power		FA Power		PIN Power	
				RMS [%]	MAX [%]	RMS [%]	MAX [%]	RMS [%]	MAX [%]
2	1	INF	-386	1.35	4.42	3.55	4.98	8.41	114.5
2	1	INF+CMM	-606	2.27	5.62	4.25	7.40	8.68	110.86
2	1	CMM	89	2.29	3.36	1.49	2.69	6.88	105.25
2	1	B1	-164	0.86	1.46	0.84	1.41	6.73	102.08

Table 35 PARCS-ICoCo -SERPENT2 discrepancies for critical HFP configuration using DFs and TRC (no CDFs). Several leakage models are shown for 4 subnodes calculations. EG stands for energy groups and SN for subnodes.

EG	SN	Leakage Model	$\Delta\rho$ [pcm]	Axial Power		FA Power		PIN Power	
				RMS [%]	MAX [%]	RMS [%]	MAX [%]	RMS [%]	MAX [%]
2	4	INF	-187	1.21	3.62	2.60	4.31	8.07	87.16
2	4	INF+CMM	-393	1.74	4.71	3.15	5.34	8.07	83.40
2	4	CMM	275	2.72	4.11	2.37	5.09	7.05	78.39
2	4	B1	43	1.37	2.37	1.19	2.08	6.75	75.86

Table 36 and Table 37 show the effect of turning off the transport correction for hydrogen in water. For all cases, except for infinite spectrum at 2 groups, not using TRC seems to deteriorate the solution.

Table 36 PARCS-ICoCo -SERPENT2 discrepancies for critical HFP configuration using DFs and CDFs (no TRC). Several leakage models are shown for 1 subnode calculations. EG stands for energy groups and SN for subnodes.

EG	SN	Leakage Model	$\Delta\rho$ [pcm]	Axial Power		FA Power		PIN Power	
				RMS [%]	MAX [%]	RMS [%]	MAX [%]	RMS [%]	MAX [%]
2	1	INF	-365	0.85	1.89	3.48	5.18	8.32	118.74
2	1	INF+CMM	-587	1.18	2.24	4.16	7.15	8.53	114.85
2	1	CMM	108	3.23	6.46	1.61	2.98	6.91	109.21
2	1	B1	-146	1.90	5.14	0.86	1.52	6.72	105.92
4	1	INF	25	3.23	6.53	1.47	4.02	N/A	N/A
4	1	INF+CMM	-153	2.12	5.53	1.14	2.97	N/A	N/A
4	1	CMM	120	3.45	8.12	1.82	4.00	N/A	N/A
4	1	B1	-128	2.23	6.71	0.9	1.84	N/A	N/A
8	1	INF	68	3.30	6.59	1.48	3.77	N/A	N/A
8	1	INF+CMM	-102	2.20	5.61	1.01	2.76	N/A	N/A
8	1	CMM	58	2.96	7.09	1.39	2.97	N/A	N/A

Table 37 PARCS-ICoCo -SERPENT2 discrepancies for critical HFP configuration using DFs and CDFs (no TRC). Several leakage models are shown for 4 subnodes calculations. EG stands for energy groups and SN for subnodes

EG	SN	Leakage Model	$\Delta\rho$ [pcm]	Axial Power		FA Power		PIN Power	
				RMS [%]	MAX [%]	RMS [%]	MAX [%]	RMS [%]	MAX [%]
2	4	INF	-166	1.17	2.28	2.54	4.51	8.08	91.89
2	4	INF+CMM	-373	0.69	1.61	3.06	5.08	8.05	87.95
2	4	CMM	293	3.67	7.19	2.5	5.38	7.15	82.80
2	4	B1	61	2.40	6.01	1.30	2.36	6.81	80.25
4	4	INF	209	3.63	7.16	1.81	5.32	N/A	N/A
4	4	INF+CMM	44	2.55	6.24	1.08	2.36	N/A	N/A
4	4	CMM	309	3.88	8.81	2.74	6.49	N/A	N/A
4	4	B1	83	2.70	7.55	1.47	3.32	N/A	N/A
8	4	INF	265	3.71	7.24	2.04	6.10	N/A	N/A
8	4	INF+CMM	108	2.65	6.33	1.32	3.18	N/A	N/A
8	4	CMM	262	3.40	7.8	2.34	5.63	N/A	N/A

Finally, Table 38 to Table 41 show the results obtains for ARO and ARI configurations. The same trends as for the critical conditions were observed. The accuracy increases with the number of groups of energy used and, except for the infinite leakage model at 2 groups, 4 subnodes did not improve the solutions. As expected, ARO conditions yields better results than ARI conditions. This is because of the effect of strong absorbers being one of the limitations of the diffusion theory.

Table 38 PARCS-ICoCo -SERPENT2 discrepancies for ARO HFP configuration using DFs, CDFs and TRC. Several leakage models are shown for 1 subnode calculations. EG stands for energy groups and SN for subnodes

EG	SN	Leakage Model	$\Delta\rho$ [pcm]	Axial Power		FA Power		PIN Power	
				RMS [%]	MAX [%]	RMS [%]	MAX [%]	RMS [%]	MAX [%]
2	1	INF	-236	1.41	4.86	2.64	4.26	3.61	14.69
2	1	INF+CMM	-417	2.25	5.11	3.11	5.63	4.10	14.13
2	1	CMM	45	1.57	2.66	1.55	2.91	2.13	10.10
2	1	B1	-159	0.65	1.59	0.89	1.92	2.19	10.23
4	1	INF	-29	1.41	2.35	0.88	1.98	N/A	N/A
4	1	INF+CMM	-181	0.75	2.19	0.78	1.54	N/A	N/A
4	1	CMM	56	1.74	4.45	1.19	2.44	N/A	N/A
4	1	B1	-145	1.28	3.99	0.71	1.49	N/A	N/A
8	1	INF	1	1.53	2.59	0.84	1.88	N/A	N/A
8	1	INF+CMM	-144	0.82	2.43	0.65	1.32	N/A	N/A
8	1	CMM	-10	1.38	3.72	0.79	1.73	N/A	N/A

Table 39 PARCS-ICoCo -SERPENT2 discrepancies for ARO HFP configuration using DFs, CDFs and TRC. Several leakage models are shown for 4 subnodes calculations. EG stands for energy groups and SN for subnodes

EG	SN	Leakage Model	$\Delta\rho$ [pcm]	Axial Power		FA Power		PIN Power	
				RMS [%]	MAX [%]	RMS [%]	MAX [%]	RMS [%]	MAX [%]
2	4	INF	-98	1.28	4.38	1.8	3.26	2.92	15.00
2	4	INF+CMM	-267	1.73	4.55	2.12	3.70	3.26	14.30
2	4	CMM	172	2.02	3.36	2.35	4.52	2.52	16.13
2	4	B1	-16	1.03	2.06	1.47	2.55	2.23	16.50
4	4	INF	95	1.84	2.76	1.02	2.73	N/A	N/A
4	4	INF+CMM	-48	1.02	2.65	0.56	0.96	N/A	N/A
4	4	CMM	184	2.13	4.88	1.98	3.98	N/A	N/A
4	4	B1	-1	1.46	4.52	1.06	2.05	N/A	N/A
8	4	INF	132	1.97	2.99	1.17	3.24	N/A	N/A
8	4	INF+CMM	-2	1.14	2.88	0.76	1.45	N/A	N/A
8	4	CMM	128	1.77	4.17	1.61	3.29	N/A	N/A

Table 40 PARCS-ICoCo -SERPENT2 discrepancies for ARI HFP configuration using DFs, CDFs and TRC. Several leakage models are shown for 1 subnode calculations. EG stands for energy groups and SN for subnodes

EG	SN	Leakage Model	$\Delta\rho$ [pcm]	Axial Power		FA Power		PIN Power	
				RMS [%]	MAX [%]	RMS [%]	MAX [%]	RMS [%]	MAX [%]
2	1	INF	188	6.33	14.41	8.35	20.56	10.21	35.14
2	1	INF+CMM	-285	3.10	6.86	5.97	15.95	7.26	26.83
2	1	CMM	-155	1.03	2.8	2.01	3.56	3.39	15.33
2	1	B1	-182	0.66	1.72	2.33	4.44	4.19	19.25
4	1	INF	542	3.38	7.31	4.41	7.77	N/A	N/A
4	1	INF+CMM	104	0.42	1.14	1.96	3.9	N/A	N/A
4	1	CMM	-79	0.69	1.4	1.85	3.74	N/A	N/A
4	1	B1	-86	1.66	3.14	2.67	3.6	N/A	N/A
8	1	INF	614	4.01	8.79	4.92	8.14	N/A	N/A
8	1	INF+CMM	190	0.68	1.26	1.95	3.43	N/A	N/A
8	1	CMM	84	1.05	1.77	1.93	3.48	N/A	N/A

Table 41 PARCS-ICoCo -SERPENT2 discrepancies for ARI HFP configuration using DFs, CDFs and TRC. Several leakage models are shown for 4 subnodes calculations. EG stands for energy groups and SN for subnodes

EG	SN	Leakage Model	$\Delta\rho$ [pcm]	Axial Power		FA Power		PIN Power	
				RMS [%]	MAX [%]	RMS [%]	MAX [%]	RMS [%]	MAX [%]
2	4	INF	257	5.60	12.74	6.9	15.84	8.68	30.34
2	4	INF+CMM	-217	2.33	5.62	4.42	11.11	5.67	22.22
2	4	CMM	-91	1.61	4.12	2.52	4.56	3.16	14.43
2	4	B1	-111	0.45	0.94	1.56	3.29	3.18	16.85
4	4	INF	608	2.84	6.06	3.51	6.20	N/A	N/A
4	4	INF+CMM	170	0.79	2.07	1.86	2.82	N/A	N/A
4	4	CMM	-16	0.57	1.56	2.22	4.56	N/A	N/A
4	4	B1	-16	1.11	2.01	2.12	4.35	N/A	N/A
8	4	INF	681	3.44	7.47	4.00	7.32	N/A	N/A
8	4	INF+CMM	257	0.35	0.83	1.62	2.73	N/A	N/A
8	4	CMM	149	0.59	1.37	1.95	4.03	N/A	N/A

In conclusion:

- DFs have an important effect on the solution obtained as well as CDFs for PPR
- Energy discretization also improves the solution.
- Subnodalization does not seem to improve the solution, except for the case with 2 groups infinite leakage model, though the differences are small
- TRC has improved the solution, especially the PPR in spite of the nodal power RMS difference being small in most cases
- Leakage models improve the solution, especially when coarser energy discretization are being used.

Additionally, two examples are provided as to the power distributions at ARO and ARI conditions. Figure 68 and Figure 69 show the axially integrated FAs and pin normalized power respectively for HFP ARO conditions obtained with the reference SERPENT2 full core model. In Figure 70 and Figure 71 PARCS-ICoCo using an infinite leakage model, DFs, CDFs, TRC and 4 subnodes is compared against the reference calculation. In Figure 72 and Figure 73 the same comparison is done but with a Fundamental Mode with CMM diffusion coefficient (FM CMM) leakage correction, DFs, CDFs, TRC and 1 subnode. Both models yield relatively good results being the major discrepancies situated near the reflector as expected. A similar comparison is performed in Figure 74 to Figure 79 for HFP ARI conditions. In this case, it can be observed a big improvement when passing from the infinite leakage model to the FM CMM correction. However, it should be noticed that in the 9 central FAs the power is ca. 4-10 times bigger than in the other assemblies, and, in this part, both models have better results.

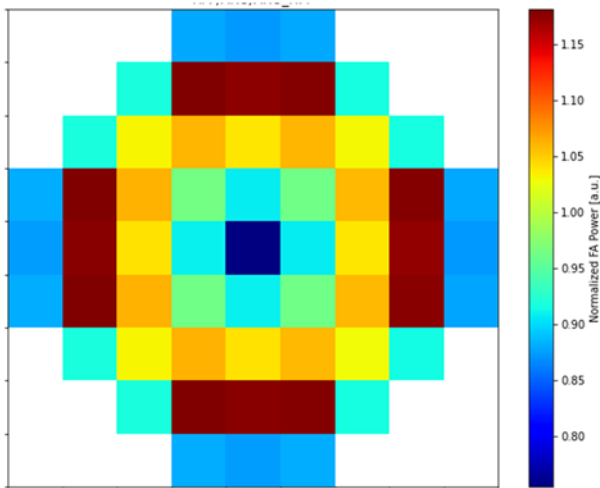


Figure 68 SERPENT2 axially integrated FA normalized radial power for HFP ARO.

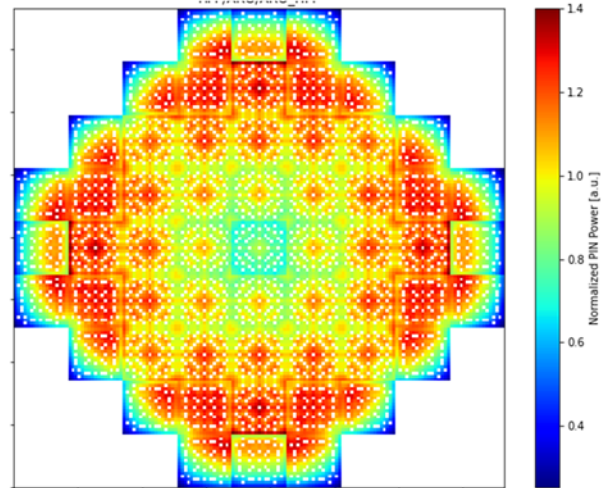


Figure 69 SERPENT2 axially integrated pin normalized radial power for HFP ARO.

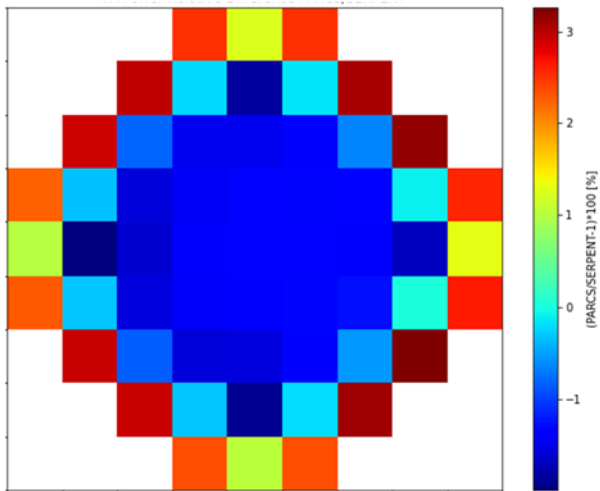


Figure 70 PARCS-ICoCo -SERPENT2 axially integrated FA normalized radial power relative difference for HFP ARO. Infinite leakage model with DFs, CDFs and TRC.

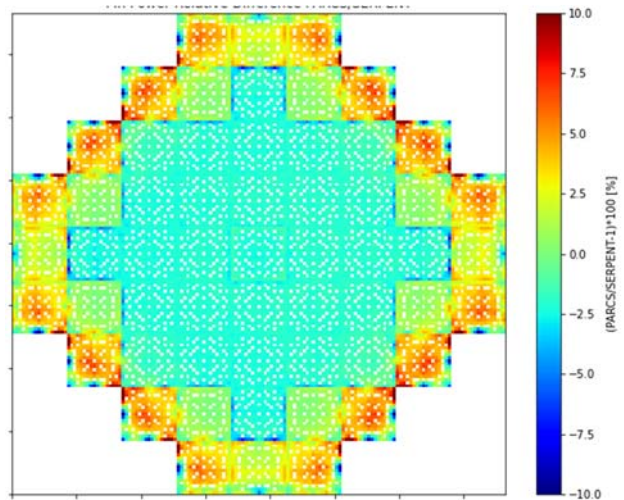


Figure 71 PARCS-ICoCo -SERPENT2 axially integrated pin normalized radial power relative difference for HFP ARO. Infinite leakage model with DFs, CDFs and TRC. Values are truncated in the interval [-10; 10] %

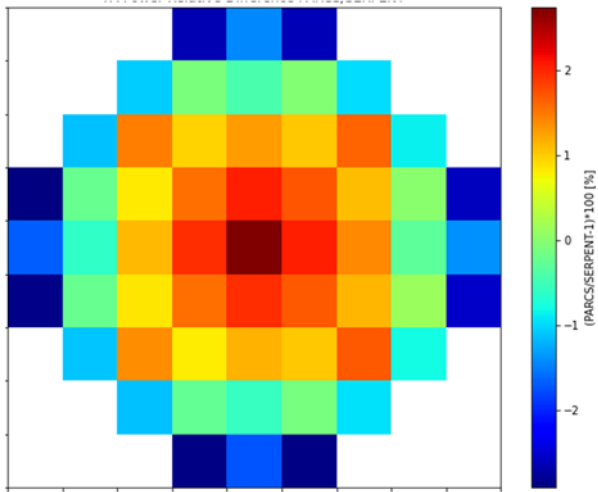


Figure 72 PARCS-ICoCo -SERPENT2 axially integrated FA normalized radial power relative difference for HFP ARO. FM CMM leakage model with DFs, CDFs and TRC.

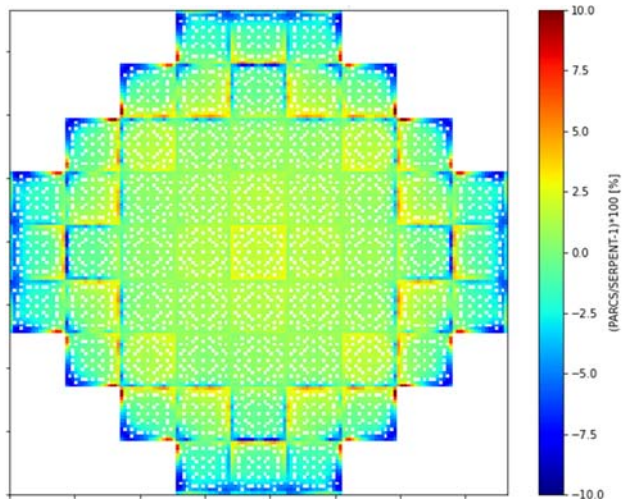


Figure 73 PARCS-ICoCo -SERPENT2 axially integrated pin normalized radial power relative difference for HFP ARO. FM CMM leakage model with DFs, CDFs and TRC. Values are truncated in the interval [-10; 10] %

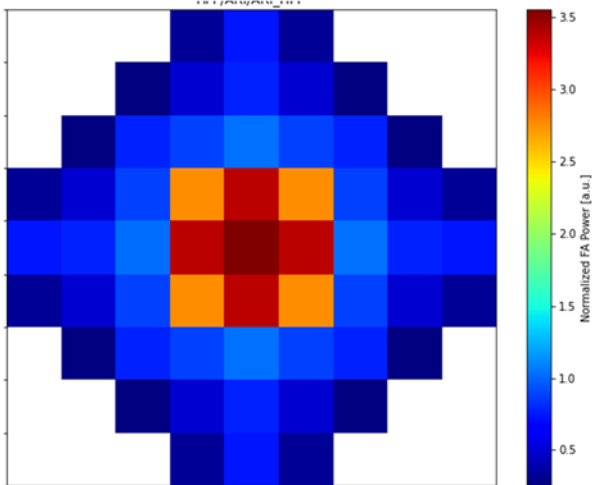


Figure 74 SERPENT2 axially integrated FA normalized radial power for HFP ARI.

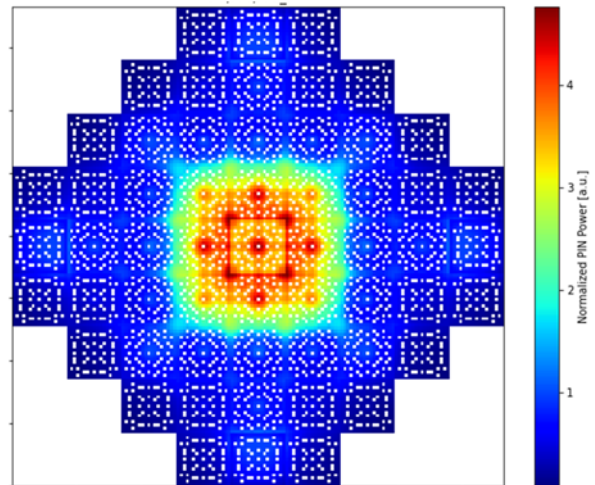


Figure 75 SERPENT2 axially integrated pin normalized radial power for HFP ARI.

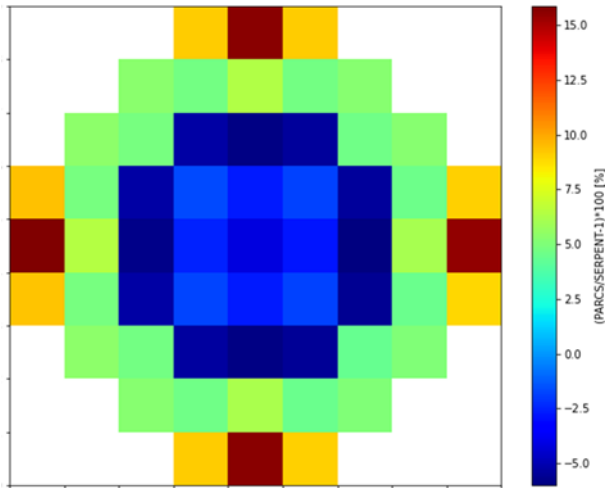


Figure 76 PARCS-ICoCo -SERPENT2 axially integrated FA normalized radial power relative difference for HFP ARO. Infinite leakage model with DFs, CDFs and TRC.

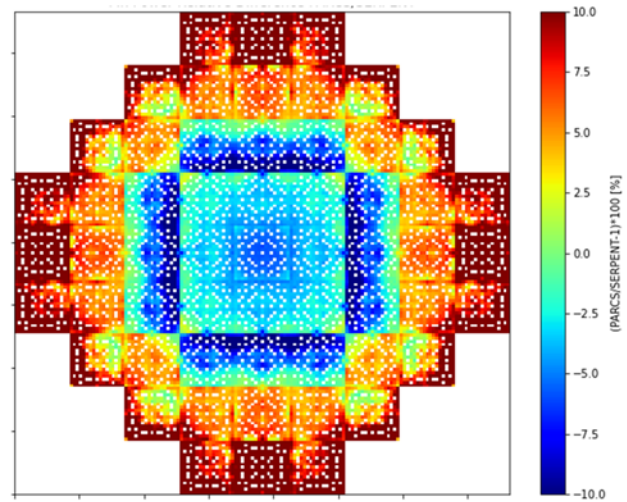


Figure 77 PARCS-ICoCo -SERPENT2 axially integrated pin normalized radial power relative difference for HFP ARI. Infinite leakage model with DFs, CDFs and TRC. Values are truncated in the interval [-10; 10] %

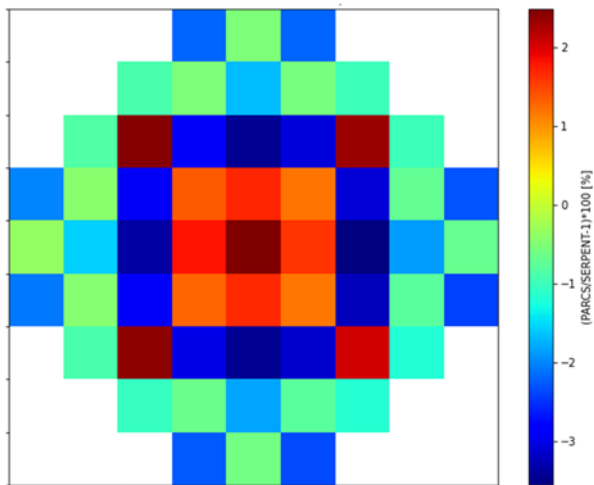


Figure 78 PARCS-ICoCo -SERPENT2 axially integrated FA normalized radial power relative difference for HFP ARI. FM CMM leakage model with DFs, CDFs and TRC.

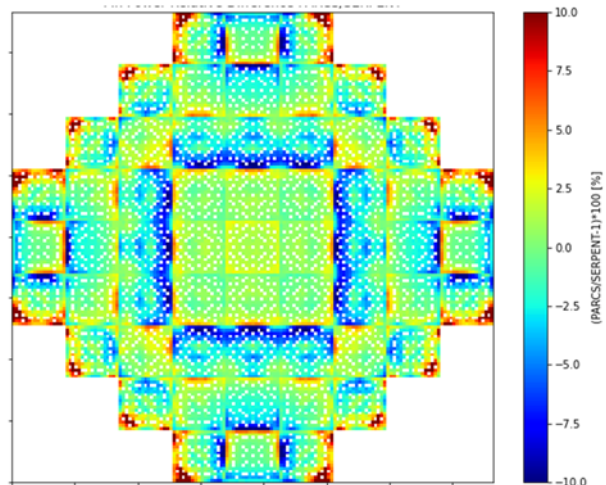


Figure 79 PARCS-ICoCo -SERPENT2 axially integrated pin normalized radial power relative difference for HFP ARI. FM CMM leakage model with DFs, CDFs and TRC. Values are truncated in the interval [-10; 10] %